TP9658E

Feasibility Study
Final Report

PREPARED FOR
Transportation
Development Centre
Transport Canada

BY
Spar Aerospace Limited

DATE
March 1989

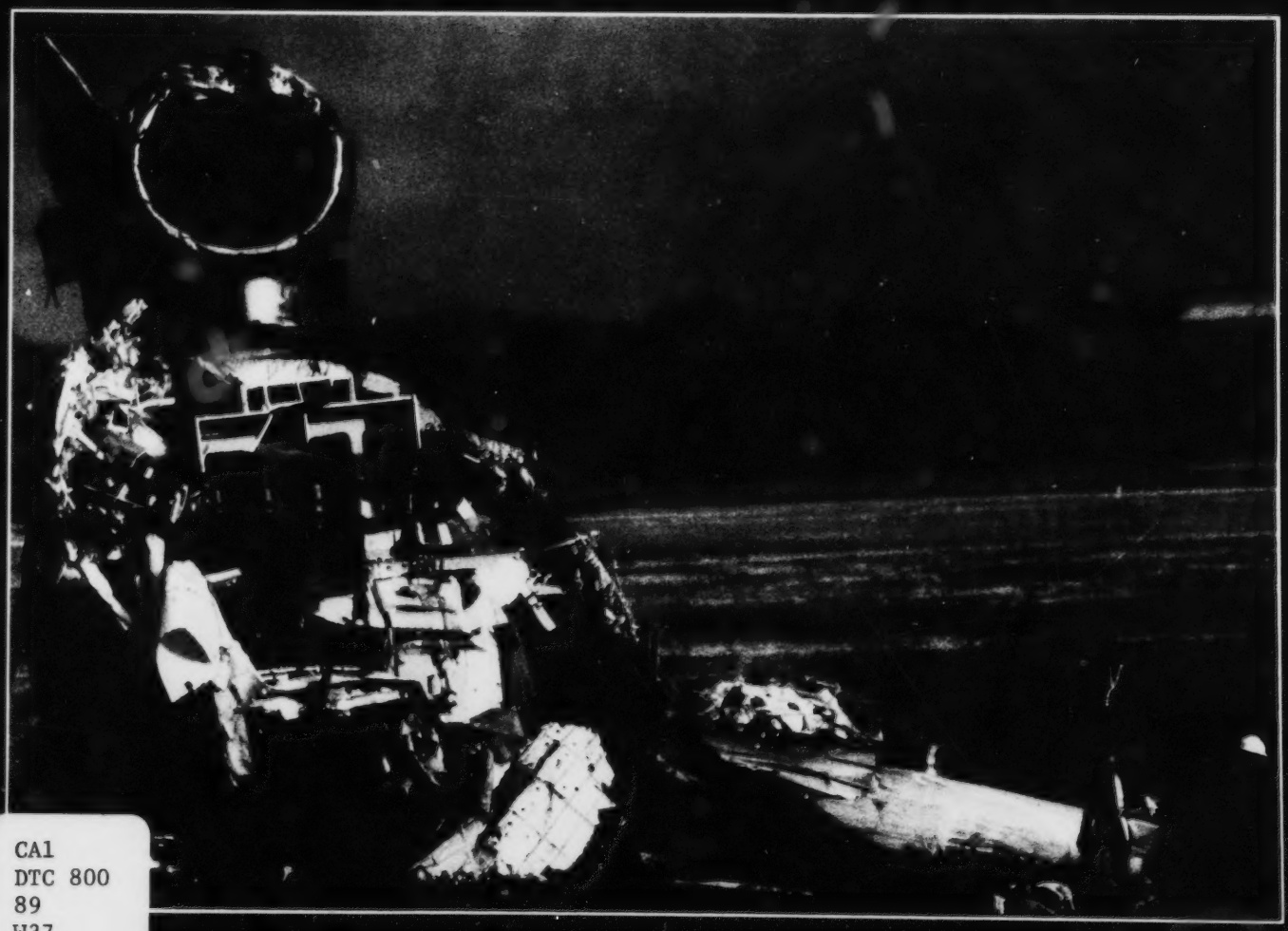

CA1
DTC 800
89
W37

SPAR

Date Due

APR AVR	8 1990		

TP 9658E

CA1
DTC800-
89
W37

415739

41.D

WIND SHEAR FEASIBILITY STUDY

FINAL REPORT

Prepared for the
Transportation Development Centre
Policy and Coordination Group
Transport Canada

by

Ivor C. Barnard

Spar Aerospace Limited

March 1989

Library and Information Centre
Centre de Documentation (GSC)
RECEIVED - REÇU LE
JAN 9 1990
Transport Canada / Transports Canada

DDN 415737

"The contents of this report reflect the views of Spar Aerospace Ltd. and their subcontractor McMaster University and not necessarily the official view or opinions of the Transportation Development Centre of Transport Canada."

"Un sommaire en français de ce rapport est inclus avant la Table des matières."

Transport Canada / Transports Canada

PUBLICATION DATA FORM

1. Transport Canada Publication No.	2. Project No.	3. Recipient's Catalogue No.
TP 9658E	6792	

4. Title and Subtitle

WIND SHEAR FEASIBILITY STUDY
FINAL REPORT

5. Publication Date
March, 1989

6. Performing Organization Document No.
RML-009-88-113

7. Author(s)
I. Barnard

8. Transport Canada File No.
D1455-186

9. Performing Organization Name and Address
Spar Aerospace Limited
Satellite & Communications Systems Division
21025 Trans-Canada Highway,
Ste-Anne-de-Bellevue, Quebec H9X 3R2

10. DSS File No.
11SD.T8200-6-6547-B

11. DSS or Transport Canada Contract No.
T8200-6-6547/01-SD

12. Sponsoring Agency Name and Address
Transportation Development Centre (TDC)
200 Réné Lévesque Blvd. West
West Tower, Suite 601
Montreal, Quebec H2Z 1X4

13. Type of Publication and Period Covered
Final

14. Project Officer
H. POSLUNS

15. Supplementary Notes (Funding programs, titles of related publications, etc.)

16. Abstract

This report details the work carried out by Spar Aerospace Limited and their subcontractor McMaster University for Transport Canada on the Wind Shear Feasibility Study during a one year period ending in December 1988.

The user requirements are defined for a sensor system suited for detecting wind shear activity in and around Canadian airports. Further, a thorough meteorological review of wind shear phenomena is presented and the salient parameters of the physical nature of microbursts are highlighted. Various technologies/systems are examined for their suitability to the wind shear detection problem; the most promising of which are ground-based radar and anemometers. These sensors are assessed in depth and conceptual system designs and estimated order of magnitude costs outlined.

Recommendations include a dedicated measurement program to gather wind shear data close to, for example, Calgary and Toronto airports. This data and subsequent processing and interpretation would be used to help estimate the wind shear "risk" in Canada.

17. Key Words	18. Distribution Statement
Wind Shear, Aviation Airports, Microbursts	Limited number of copies available on request from the Transportation Development Centre.

19. Security Classification (of this publication)	20. Security Classification (of this page)	21. Declassification (date)	22. No. of Pages	23. Price
Unclassified	Unclassified		225	

TDC/CDT 79-005
Rev 88

Canada

Transports Canada | Transport Canada

FORMULE DE DONNÉES POUR PUBLICATION

1. N° de la publication de Transports Canada	2. N° de l'étude	3. N° de catalogue du destinataire
TP 9658E	6792	

4. Titre et sous-titre	5. Date de la publication
WIND SHEAR FEASIBILITY STUDY FINAL REPORT	mars, 1989
	6. N° du document de l'organisme exécutant RML-009-88-113

7. Auteur(s)	8. N° de dossier — Transports Canada
I. Barnard	D1455-186

9. Nom et adresse de l'organisme exécutant	10 N° de dossier — ASC
Spar Aérospatiale Limitée Division des systèmes de satellite et de communications 21025 route Trans-Canada Ste-Anne-de-Bellevue, Québec H9X 3R2	11SD.T8200-6-6547-B
	11. N° de contrat — ASC ou Transports Canada T8200-6-6547/01-SD

12. Nom et adresse de l'organisme parrain	13. Genre de publication et période visée
Centre de développement des transports (CDT) 200 ouest, boulevard René-Lévesque Tour ouest, suite 601 Montréal, Québec H2Z 1X4	Finale
	14. Agent de projet H. Posluns

15. Remarques additionnelles (Programmes de financement, titres de publications connexes, etc.)

16. Résumé

Ce rapport décrit le travail accompli par Spar Aérospatiale Limitée, et son sous-traitant l'université McMaster, dans le cadre de l'étude de faisabilité relative au cisaillement du vent, mené pour Transports Canada, au cours de la période d'un an qui s'est terminée en décembre 1988.

Les exigences de l'utilisateur portent sur un système de détection approprié, capable de détecter les activités de cisaillement du vent dans les aéroports canadiens ou aux alentours. De plus, une étude météorologique complète du phénomène de cisaillement du vent est présentée, et les paramètres caractérisant la nature physique des micro-rafales sont mis en vedette. Diverses technologies et systèmes sont examinés pour faire le jour sur la validité de leur utilisation, afin de régler le problème de détection du cisaillement du vent; les plus prometteurs sont le radar au sol et les anémomètres. Ces détecteurs sont évalués en profondeur, et les études conceptuelles du système ainsi que l'ampleur des coûts anticipés sont donnés dans ce rapport.

Les recommandations énoncées couvrent un programme de mesure voué à recueillir des données sur le cisaillement du vent proche, par exemple, des aéroports de Calgary et Toronto. Les données, leur traitement et interprétation ultérieurs serviront à évaluer le "risque" du cisaillement du vent au Canada.

17. Mots clés	18. Diffusion
Cisaillement du vent, Aérienne, Aeroports, Micro-rafales	Le Centre de développement des transport dispose d'une nombre limité d'exemplaires.

19. Classification de sécurité (de cette publication)	20. Classification de sécurité (de cette page)	21. Déclassification (date)	22. Nombre de pages	23. Prix
non-classifiée	non-classifiée		225	

CDT/TDC 79-005
Rev 88

Canada

EXECUTIVE SUMMARY

User Requirements

Recent wind shear related incidents in and around airports have caused an increased awareness within the air transportation community of the hazards related to wind shear phenomena. A pressing safety related need has therefore developed for the capability to detect and alert users regarding wind shear conditions, in particular, microbursts.

The user requirements for a system to detect low level wind shear conditions in and around Canadian airports, are to detect, with a high degree of confidence, and locate wind shear events out to 15 km from the centre of the airport. Also, the system should provide sufficient warning for the pilots to operate their aircraft safely.

The Phenomenon

A wind shear is a meteorological phenomenon which is characterized by changes in wind speed and/or direction that takes place over small distances. When an aircraft flies through a wind change of this kind, especially when at low altitude, the pilot must adjust for it quickly to maintain course and altitude. Most wind shears pose little danger unless they occur over a distance as short as 1 to 3 km at low level. In such circumstances, a pilot may have only a matter of 30 seconds to recover safely from its effects.

Examples of meteorological conditions and phenomena which cause low level wind shear are:

- wind flow in the friction layer,
- wind flow associated with Frontal Surface,
- thunderstorms,
- gust front,
- microbursts/macrobursts.

Figure 1 is a pictorial representation of a microburst. It demonstrates the physical extent of the event, superimposed is the path of an airliner, with its initial position at 900 ft. altitude (to the left of the picture) and finally at 0 ft. and 5 km to the right.

As can be seen from the last figure microbursts are intense downdrafts, sometimes wet (precipitation reaches the surface) and sometimes dry (precipitation does not reach the surface). Virga, one origin of microbursts, is downflow precipitation from convective cloud that cools the air through which it passes, evaporating before reaching the surface.

THIS PAGE INTENTIONALLY LEFT BLANK

FIGURE 1: MICROBURST AROUND AIRPORT WITH AN AIRCRAFT ON FINAL DESCENT

THIS PAGE INTENTIONALLY LEFT BLANK

EXECUTIVE SUMMARY (cont'd)

The Phenomenon (cont'd)

A number of research programs have been carried out in the U.S. to investigate microbursts and associated phenomena:

- Northern Illinois Meteorological Research on Downbursts (1978 University of Chicago), NIMROD
- Joint Airport Weather Studies (1982 University of Chicago and National Center of Atmospheric Research), JAWS
- Classify, Locate and Avoidance Wind Shear (1984 NCAR), CLAWS
- Convection Initiation and Downburst Experiment (1987 NCAR, NOAA, University of North Dakota, Colorado State University, MIT). CINDE.

These programs have produced a wealth of data and knowledge for wind shear phenomena close to Denver, Colorado and Chicago; but what is known of such wind shear activity in Canada? Can the U.S. data be extrapolated to Canadian airports?

Documented evidence (Canadian Aviation Safety Board) of the effects of wind shear on aircraft in Canada for the period 1976-1983 details:

- B737-200 (commercial sized aircraft) at Sault Ste. Marie, Ontario, January 2, 1982 at 2138 EST. A "hot landing" was reported but no injuries occurred.
- 29 cases involving light aircraft and helicopters.

To date, no detailed measurement programs have been carried out to estimate the frequency of occurrence of microbursts in Canada.

It is possible that there is a relationship between tornadoes and microbursts, if so, then the worst months for microbursts in Canada would be June, July and August (based on tornado data for Western Canada, 1890-1958). This is the same conclusion that was reached by looking at the incidence of thunderstorms in Canada. Data indicates that southwest Ontario and southeast Manitoba are areas of maximum tornado activity. Secondary maxima appear over extreme southeastern Quebec, Alberta and southern interior of British Columbia. This data is based on the formulation for incidence $I = n/bAt$ where n is the number of tornadoes, A is the area, t is the time and b is a population weighting factor.

Of considerable interest in this figure is the fact that the value of I for Denver, Colorado is similar to that for the regions in Canada defined as the Alberta Maximum, the Great Lakes Minimum and the Northern Maximum. The results of the JAWS, CLAWS and CINDE field trials have conclusively shown Denver to have a high incidence of

EXECUTIVE SUMMARY (cont'd)

microbursts. Based on: (1) the close physical relationship between microbursts and tornados, and (2) the fact that the probability of incidence of tornadoes is as high in some parts of Canada as in an area of the USA, where microburst have been detected, it follows that the likelihood of the occurrence of microbursts in parts of Canada is high.

Technologies

Three groundbased technologies were identified as prime candidates for further investigation: radar, sodar and anemometers.

Radar and its application to wind shear detection received a most detailed examination in the study. Anemometers, important as they are, received less attention since there is not that much new that can be promoted. They are, fortunately, simple and reliable devices that require a small amount of control and are routinely used for air speed sensing in airports all over the world. They are already used as part of a Low Level Wind Shear Alert system, LLWAS. With further development of sodar technology, sodars may be able to usefully supplement other wind shear detection devices but with their current technology their usefulness for detection is limited to a few kilometers up the glide slopes.

The LLWAS system, as installed in many U.S. airports, has several limitations with regard to the detection of small scale low level wind shear. These limitations include:

- the system cannot measure winds above the sensors on the ground,
- temporal and spatial resolution is too course,
- detection of wind shear is restricted to the airport perimeter,
- vertical wind motions are not sensed directly,
- wind along flight paths is not measured.

A system of anemometers with improved resolution and sensitivity could be used to provide small scale wind shear detection.

The second candidate technology is ground based pulse Doppler radar. There is a significant amount of evidence to demonstrate that Doppler radar can reliably detect and give early warning to both large and small scale wind shear events. The most recent data coming from the pulse Doppler Terminal Doppler Weather Radar system under test at Stapleton International Airport.

A Doppler radar which possesses suitable characteristics will detect wind shear events in and around Canadian airports. The general key characteristics the radar requires are as follows:

EXECUTIVE SUMMARY (cont'd)

Technologies (cont'd)

- coherence,
- fine resolution,
- low antenna sidelobes,
- azimuth and elevation coverage,
- tuned algorithms,
- advanced user interface.

All of these characteristics are realizable and can be implemented into several radar concepts or configurations.

Conceptual Designs and Costs

- a network of anemometers for low-density airports,
- a network of anemometers combined with a single pulse-Doppler radar.

a) Anemometer System

i) Suited to a low traffic density airport.

ii) Provides data on event as it occurs.

n.b. Although the use of pressure sensors may help to give a few seconds of advanced warning.

iii) Detection limited to the area enclosed by the anemometer stations.

iv) Needs algorithm development and be tuned for local features.

v) Spatial resolution to be better than 2 1/2 km.

vi) Relatively cheap - $750K Cdn (including algorithm development).

vii) Reliable.

b) Pulse Doppler Radar

i) Suited to a high traffic density airport e.g., Calgary and Toronto.

ii) Could usefully be integrated with an anemometer system (e.g., a) above).

EXECUTIVE SUMMARY (cont'd)

Conceptual Designs and Costs (cont'd)

b) Pulse Doppler Radar (cont'd)

iii) Provides advanced detection and warning.

iv) Long detection ranges (~15 km).

v) High resolution.

vi) Requires automatic recognition resulting in the need for:

- artificial intelligence to replace the role only meteorologists can currently perform.

vii) Fusion of radar and anemometer data needs investigation.

viii) Three possible radar solutions, see table below.

For ease of presentation, risks and order of magnitude costs for the recommended Doppler technology are given in the Table below.

RADAR OPTION	TECHNICAL RISK	COST	FIGURE OF MERIT*
TDWR	Low for radar hardware	High $5M	4
Enterprise		Low	
- modified[3]	Medium	$2M Cdn	3
- revised[2]	Very low	$1M Cdn	1
- existing[1]	Very low	$1M Cdn	2
New design	High	High	5

* A low Figure of Merit represents a preferred option.

1: As per current King City installation, Toronto (Atmospheric Environment Service).

2: As per 1 with optimized range.

3: As per 2 with fully coherent source.

TDWR: Terminal Doppler Weather Radar.

The costs are based on figures supplied by Enterprise Electronics Corporation and the TDWR project office. Spar does not commit to build or supply these radars at the quoted prices.

EXECUTIVE SUMMARY (cont'd)

The figure of merit is traded by that information supplied in the table and radar performance expectations such as spectral purity.

To achieve robust automatic recognition of low-altitude wind shear, much work is required on pattern recognition. The fundamental pre-requisite for the development of pattern recognition techniques, e.g., feature extraction, is real data. For it to be applicable it must be representative of the weather phenomenon, i e., Canadian data.

Measurement Program

The major objectives of a measurement program must be to answer some of the most fundamental questions concerning microbursts in Canada.

- Do they occur?
- What is the likelihood of their occurrence at Canadian airports?

Assuming they occur:

- What are the processes involved in the initiation of microbursts?
- What is their fine structure?
- How applicable are the Stapleton results to Canada?

To answer these and other questions there is a overwhelming need for Doppler radar measurements. Doppler radar is an essential, although not the sole component of the wind shear measurement system. It is a fact that it can detect both large and small scale wind shear events.

Two locations for a measurement program could form the kernel of a future program. The Atmospheric and Environment Services facility at King City near Toronto could be one location, utilizing the existing radar equipment. It is expected that for microburst detection the radar software would need to be modified to provide finer range resolution (~75m). This radar is not fully coherent and may prevent the detection of some microburst activity - as yet this is unknown and needs study. Such a study should be carried out as soon as possible in collaboration with King City.

A new facility could be set up at or close to Calgary airport. Being a new facility a fully coherent radar would be preferred for ensuring the best possible target sensitivity. The choice of Calgary is commensurate with the Alberta maximum for the incidence of tornadoes which are suspected to having some relationship to microburst activity. Further the experience of the Alberta Hail project suggests that microbursts occur in central and southern Alberta.

EXECUTIVE SUMMARY (cont'd)

Measurement Program (cont'd)

Also, the data and wealth of knowledge residing in the U.S. must not be ignored. Indeed it should be reviewed further to see how it can complement a Canadian measurement program. Also expertise should be built up in Canada on developing software for the recognition of wind shear, particularly microbursts. This is important since conditions from one airport to another are not alike and a good understanding of all aspects of the wind shear problem is essential.

In conclusion, it is the opinion of the authors that

- microbursts are likely to occur in Canada,
- there is a danger to aviation due to wind shear at Canadian airports,
- pulse Doppler radar will provide detection of wind shear events, particularly microbursts,
- much more information is needed on microbursts in Canada,
- a measurement program is required, using existing or modified facilities at AES King City and/or a new facility in Alberta,
- a follow on stage to the current study is required to define detailed objectives and scope of the measurement program.

SOMMAIRE EXECUTIF

Besoins des utilisateurs

Les derniers incidents reliés au cisaillement du vent, survenus dans et autour des aéroports, ont suscité une prise de conscience au sein de la communauté du transport aérien quant aux dangers que pose le phénomène du cisaillement du vent. Un besoin pressant relatif à la sécurité se fait donc sentir et fait appel à une capacité de détection et d'alerte des utilisateurs sur les conditions de cisaillement du vent, en particulier, les micro-rafales.

Les besoins des utilisateurs pour un système de détection des conditions de cisaillement du vent à basse altitude, dans les aéroports canadiens et aux alentours, portent sur la capacité de détecter avec un haut degré de fiabilité et de localiser les événements de cisaillement du vent sur une distance de 15 km, à partir du centre de l'aéroport. Ce système devrait aussi fournir une alerte avancée pour permettre aux pilotes de manoeuvrer leurs avions de façon sécuritaire.

Le phènomène

Le cisaillement du vent est un phénomène météorologique qui est caractérisé par des changements dans la vitesse et/ou la direction du vent, se produisant sur de petites distances. Lorsqu'un avion vole à travers un changement de vent de ce genre, surtout à de basses altitudes, le pilote doit ajuster sa manoeuvre rapidement pour maintenir sa trajectoire et son altitude. La plupart des cisaillements de vent posent peu de danger, à moins qu'ils ne surviennent sur une distance aussi petite que 1 à 3 km, à basse altitude. Dans de telles circonstances, le pilote ne dispose que de 30 secondes pour se remettre sain et sauf (sans accident) de ses effets.

Voici quelques exemples de conditions météorologiques et des phénomènes qui causent le cisaillement du vent à basse altitude:

- direction du vent dans les couches de frottement
- direction du vent accompagnée de surface frontale
- orages
- front de rafales
- micro-rafales/macro-rafales.

La figure 1 repésente une image d'une micro-rafale. Elle illustre l'étendue physique de l'événement; en superposition, on voit la trajectoire d'un avion ayant sa position initiale à 900 pieds d'altitude (à gauche de la photo) et sa position finale à 0 pied et à 5 km vers la droite.

CETTE PAGE LAISSÉE EN BLANC AVEC INTENTION

Figure 1: Microsursaut autour d'un aéroport pendant la descente finale d'un avion

CETTE PAGE LAISSÉE EN BLANC AVEC INTENTION

Comme le montre la dernière figure, les micro-rafales sont des courants d'air descendants intenses, parfois humides (les précipitations atteignent la surface) et parfois secs (les précipitations n'atteignent pas la surface). Virga, une des sources des micro-rafales, est une précipitation verticale provenant de nuages de convection qui refroidissent l'air dans lequel ils passent, s'évaporant avant d'atteindre la surface.

Plusieurs programmes de recherche ont été menés aux États-Unis dans le but d'étudier les micro-rafales et les phénomènes connexes:

- Recherche météorologique du Nord de l'Illinois sur les vents descendants (1978, Université de Chicago), NIMROD.

- Études conjointes sur la météorologie des aéroports (1982, Université de Chicago et Centre national de recherche atmosphérique), JAWS.

- Classifier, localiser et éviter le cisaillement du vent (1984, NCAR), CLAWS.

- Initiation de la convection et expérience sur les vents descendants (1987, NCAR, NOAA, Université du Dakota du Nord, Université du Colorado, MIT), CINDE.

Ces programmes ont généré une abondance de données et de connaissances sur les phénomènes de cisaillement du vent proche de Denver, (Colorado) et Chicago; mais que connait-on d'une telle activité de cisaillement du vent au Canada? Pourrait-on extrapoler les données des États-Unis pour les aéroports canadiens?

Des preuves documentées (Bureau canadien de la sécurité aérienne) des effets du cisaillement du vent sur les avions au Canada, au cours de la période 1976-1983, révèlent les détails suivants:

- B737-200 (avion commercial) à Sault Ste-Marie, Ontario, le 2 janvier 1982, à 2138 EST. Un "atterissage dangereux" a été signalé, mais il n'y a pas eu de blessés.

- Vingt-neuf cas comprenant des avions légers et des hélicoptères.

Il se peut qu'un lien existe entre les tornades et les micro-rafales et, si c'est le cas, les pires mois pour les micro-rafales au Canada seraient donc juin, juillet et août (fondé sur les données recueillies sur les tornades dans l'ouest canadien, 1890-1958). Cette conclusion est la même que celle obtenue lorsqu'on a examiné la fréquence des orages au Canada. Les données indiquent que le sud-ouest de l'Ontario et le sud-est du Manitoba sont des régions d'activité maximale pour les tornades. Des maximums secondaires apparaissent au-dessus de l'extrême sud-est du Québec, de l'Alberta et du sud intérieur de la Colombie Britannique. Ces données reposent sur la formule suivante: Incidence I=n/bAT, selon laquelle n représente le nombre de tornades, A la zone, T le temps et b le facteur pondéré de la population.

Le plus grand intérêt que suscite cette équation réside dans le fait que la valeur de I pour Denver (Colorado) est la même que pour ces régions canadiennes connues comme "Alberta Maximum", "Great Lakes Minimum" et "Northern Maximum". Les résultats des essais en chantier de JAWS, CLAWS et CINDE indiquent d'une manière concluante qu'il existe à Denver une fréquence élevée de micro-rafales. Compte tenu des deux facteurs suivants: (1) le rapport étroit entre les micro-rafales et les tornades, et (2) la forte probabilité d'avoir une fréquence de tornades aussi élevée dans certaines régions canadiennes que dans une région des Etats-Unis, où des micro-rafales ont été détectées, il s'en suit que la possibilité d'occurence des micro-rafales dans certaines régions canadiennes est élevée.

Technologies

Trois technologies au sol ont été identifiées pour faire l'objet d'une étude plus poussée: le radar, le "Sodar" et les anémomètres.

Le radar, et son application à la détection du cisaillement du vent, a été examiné en détails dans cette étude. Les anémomètres, aussi importants qu'ils soient, ont reçu moins d'attention étant donné qu'il n'y a presque rien de nouveau à développer là-dessus. Ces dispositifs sont, heureusement, simples et fiables, ne nécessitent que très peu de contrôle et sont utilisés régulièrement dans les aéroports autour du monde pour la détection de la vélocité de l'air. Ils font déjà partie du système de détection du cisaillement du vent à basse altitude "LLWAS". En développant la technologie des "sodars", ceux-ci pourraient être utilisés pour compléter les autres dispositifs de détection du cisaillement du vent; mais, à l'état actuel de leur technologie, leur capacité de détection est limitée à quelques kilomètres au-dessus des trajectoires de descente.

Le système LLWAS , tel qu'il existe actuellement dans plusieurs aéroports américains, a plusieurs limitations quant à la détection du cisaillement du vent à basse altitude sur une petite échelle. Ces restrictions sont les suivantes:

- le système ne peut mesurer les vents au-dessus des détecteurs au sol,
- la résolution spatiale et temporelle est trop rudimentaire,
- la détection du cisaillement du vent est limitée au périmètre de l'aéroport,
- les mouvements verticaux du vent ne sont pas détectés directement,
- le vent n'est pas mesuré le long des trajectoires de vol.

Un système d'anémomètres ayant une meilleure résolution et une meilleure sensibilité peut être utilisé pour la détection du cisaillement du vent sur une petite échelle.

La deuxième technologie à développer serait le radar au sol à effets Doppler. Il y a suffisamment de faits prouvant que le radar Doppler peut détecter de façon fiable et donner un avertissement avancé des événements de cisaillement du vent à grande et à petite échelle. Les données les plus récentes proviennent du système de radar météorologique Doppler terminal (anti-brouilleur), présentement à l'essai à l'aéroport international de Stapleton.

Un radar Doppler qui possède les caractéristiques appropriées peut détecter les événements de cisaillement du vent dans et autour des aéroports canadiens. Les principales caractéristiques générales qu'exige le radar sont:

- cohérence
- fine résolution
- antenne à lobe latéral basse
- couverture en azimuth ou élévation
- algorithmes accordés
- interface d'utilisateur avancée.

Toutes ces caractéristiques sont réalisables et peuvent être incorporées à plusieurs concepts ou configurations de radar.

Études conceptuelles et coûts

- un réseau d'anémomètres pour les aéroports à faible densité de trafic
- un réseau d'anémomètres combiné à un radar simple anti-brouilleur.

a) Système d'anémomètres

i) Approprié pour un aéroport à faible densité de trafic.

ii) Fournit des données sur les événements à mesure qu'ils se produisent.

n.b. Malgré que l'utilisation des détecteurs de pression peut aider à donner un avertissement avancé de quelques secondes.

iii) La détection est limitée à la zone entourée par les postes d'anémomètres.

iv) Nécessite la mise au point d'algorithmes, et accorder ceux-ci aux caractéristiques locales.

v) La résolution spatiale doit être supérieure à 2.5 km.

vi) Coûts raisonnables - 750 000 $ Can. (y compris la mise au point des algorithmes).

vii) Fiable.

b) Radar anti-brouilleur

i) Approprié aux aéroports à trafic intense comme ceux de Calgary et de Toronto.

ii) Peut facilement être intégré à un système d'anémomètres (par ex. celui cité en a).

iii) Fournit une détection et un avertissement avancé.

iv) Vastes gammes de détection (≈ 15 km).

v) Haute résolution.

vi) Exige une reconnaissance automatique, ce qui nécessite:

- une intelligence artificielle pour remplacer le rôle que seuls les météorologues peuvent remplir actuellement.

vii) La fusion des données du radar et des anémomètres doit être étudiée plus profondément.

viii) Trois solutions possibles de radar, voir le tableau ci-dessous.

Pour faciliter la présentation, les risques et l'amplitude des coûts de la technologie Doppler recommandée sont donnés dans le tableau suivant:

OPTION DE RADAR	RISQUE TECHNIQUE	COÛT	MÉRITE*
TDWR	Faible pour l'équipement radar	Élevé 5M$	4
Enterprise		Faible	
- modifié[3]	Moyen	2M$Can	3
- révisé[2]	Très faible	1M$Can	1
- actuel[1]	Très faible	1M$Can	2
Nouvelle conception	Élevé	Élevé	5

* Un chiffre inférieur indique une option préférée.
1: Comme l'installation actuelle à King City, Toronto
2: Comme 1, mais avec gamme optimalisée
3: Comme 2, mais avec une source entièrement cohérente.
TDWR: radar météorologique à effet Doppler

Ces coûts sont basés sur les chiffres qui nous ont été fournis par Enterprise Electronics Corporation et par le bureau du projet TDWR. Spar ne s'engage nullement à construire ou fournir ces radars aux prix fixés dans la présentre.

Le chiffre de mérite est basé sur l'information fournie dans le tableau et la performance du radar anticipée, telle la pureté spectrale.

Afin de réaliser une forte reconnaissance automatique du cisaillement du vent à basse altitude, un long travail doit être fait sur la reconnaissance des configurations. Les prérequis de base pour la mise au point de techniques de reconnaissance des configurations, comme par exemple l'extraction des motifs, sont les données réelles. Pour qu'elles soient applicables, celles-ci doivent être représentatives du phénomène météorologique, c.-à-d. les données canadiennes.

Programme de mesure

Le but principal d'un programme de mesure devrait être de trouver des réponses aux questions les plus fondamentales concernant les micro-rafales au Canada.

- Se produisent-elles au Canada?
- Quelles sont les probabilités de leur fréquence aux aéroports canadiens?

En supposant qu'elles se produisent:

- Quels sont les phénomènes à l'origine des micro-rafales?
- Quelle est leur fine structure?
- A quel point s'appliquent les résultats de Stapleton au Canada?

Pour répondre à ces questions et bien d'autres, il existe un besoin pressant d'avoir des mesures de radar Doppler. Le radar Doppler est essentiel, malgré qu'il n'est pas le seul élément du système de mesure du cisaillement du vent. C'est un fait établi qu'il peut détecter les événements de cisaillement du vent à petite et à grande échelle.

Deux sites pour un programme de mesure peuvent former éventuellement le noyau d'un programme futur. Les laboratoires d'"Atmospheric and Environmental Services" à King City, près de Toronto, pourraient être un des sites utilisant l'équipement de radar existant. Pour la détection des micro-rafales, le logiciel du radar devrait être modifié afin de fournir une résolution plus fine ($\approx$ 75m). Ce radar n'est pas entièrement cohérent et peut prévenir la détection de certaines activités des micro-rafales - encore inconnu à ce point et doit être étudié. Une telle étude devrait être menée aussitôt que possible en collaboration avec King City.

Une nouvelle installation pourrait être établie à l'aéroport de Calgary ou proche de là. Étant nouvelle, on pourrait l'équiper d'un radar entièrement cohérent afin d'assurer la meilleure sensibilité possible à la cible. Le choix de Calgary est en fonction des maximums de l'Alberta pour l'incidence des tornades qu'on soupçonne avoir un lien avec l'activité des micro-rafales. L'expérience du projet "Alberta Hail" suggère que les micro-rafales se produisent dans le centre et le sud de l'Alberta.

Les données et la richesse des connaissances déjà établies aux États-Unis ne devraient pas être ignorées. De fait, celles-ci devraient être examinées plus profondément pour voir comment elles peuvent compléter un programme canadien de mesure. Il faut aussi bâtir une expertise canadienne dans la conception de logiciels destinés à la reconnaissance du cisaillement du vent, surtout les micro-rafales. Ceci est important en raison des conditions qui diffèrent d'un aéroport à l'autre, et une bonne connaissance de tous les aspects du problème de cisaillement du vent est essentielle.

En conclusion, les auteurs sont d'avis que:

- des micro-rafales peuvent se produire au Canada,
- un danger existe aux aéroports canadiens en raison du cisaillement du vent,
- le radar anti-brouilleur permettra une détection des événements de cisaillement du vent, surtout les micro-rafales,
- de plus amples informations doivent être obtenues sur les micro-rafales au Canada,
- un programme de mesure est nécessaire, utilisant les installations existantes ou modifiées d'AES à King City et/ou une nouvelle installation en Alberta,
- une étape ultérieure à l'étude courante est nécessaire pour définir en détails les objectifs et la portée du programme de mesure.

TABLE OF CONTENTS

Section	Title	Page
1.0	GENERAL INTRODUCTION	1
	1.1 Report Structure	1
	1.2 Report Emphasis	2
	PART A: USER REQUIREMENTS AND TECHNICAL SPECIFICATIONS	3
1.0	INTRODUCTION	4
1.1	Scope	4
	1.2 General Background	5
2.0	USER REQUIREMENTS	7
	2.1 General Requirements	7
	2.1.1 Detection	7
	2.1.2 Identification	7
	2.1.3 Accident Prevention	7
	2.2 Transport Canada User Requirements	7
	2.2.1 Cost	7
	2.2.2 Range of Coverage	7
	2.2.3 Detection Parameters	7
	2.2.4 User Interface	8
	2.2.5 Detection Status	8
	2.2.6 Probability of Detection vs False Alarm Rate	8
	2.2.7 Technical and Environmental Constraints	8

TABLE OF CONTENTS (cont'd)

Section	Title	Page
	PART A: USER REQUIREMENTS AND TECHNICAL SPECIFICATIONS (cont'd)	
	2.3 Comments on Supplied User Requirements	10
	2.3.1 Detection	10
	2.3.2 Revisit Time	10
	2.3.3 User Alert Time	10
3.0	METEOROLOGICAL REVIEW	11
	3.1 Introduction	11
	3.2 Meteorological Conditions and Phenomena Which Cause Low Level Wind Shear	13
	3.2.1 Wind Profile in the Lower Levels of the Atmosphere	13
	3.2.2 Wind Flow Around Obstacles	15
	3.2.3 Wind Flow Associated with Frontal Surfaces	15
	3.2.4 Thunderstorms	16
	3.2.5 The Gust Front	18
	3.3 Physical Description of Microbursts	18
	3.3.1 In Brief, What are Microbursts?	18
	3.3.2 History of the Observation of Microbursts	24
	3.3.3 Observations of Microbursts	26
	3.3.4 Effects of Wind Shear Upon the Lift Force	31
	3.3.5 Types of Microbursts and Parent Clouds	35
	3.3.6 Classification of Parent Clouds	41
	3.3.7 Location of Microburst-related Accident Cases	46
	3.4 Detailed Characteristics of Microbursts	51
	3.4.1 Microburst Visual Characteristics	51
	3.4.2 The JAWS Project	51
	3.4.3 The Microburst Examined	56
	3.5 Canadian Wind Shear Assessment	71
	3.6 Future Needs	79

TABLE OF CONTENTS (cont'd)

Section	Title	Page
	PART A: USER REQUIREMENTS AND TECHNICAL SPECIFICATIONS (cont'd)	
4.0	**MICROBURST MODEL**	80
	4.1 Physical Extent	80
	4.1.1 Horizontal Dimensions	80
	4.1.2 Vertical Dimensions	81
	4.2 Event Duration	81
	4.3 Windspeed	81
	4.3.1 Horizontal Windspeeds	81
	4.3.2 Vertical Windspeeds	81
	4.4 Frequency of Occurrence	82
	4.5 Pressure	82
	4.6 Temperature	82
	4.7 Rain Rate	82
	4.8 Propagation Speeds	82
	4.9 Lapse Rates	82
	4.10 Diurnal Variations	82
	4.11 Seasonal Variations	83
5.0	**WIND SHEAR DETECTION TECHNOLOGY**	84
	5.1 Airborne Instruments	84
	5.2 Groundbased Instruments	87
	5.2.1 Cup Anemometry	87
	5.2.2 Sodar	88
	5.2.3 Radar	90
	5.2.4 Lidar	94
	5.2.5 Other Laser Devices	94
	5.2.6 Profiler	95

TABLE OF CONTENTS (cont'd)

Section	Title	Page
	PART A: USER REQUIREMENTS AND TECHNICAL SPECIFICATIONS (cont'd)	
6.0	SUMMARY & CONCLUSIONS	96
	BIBLIOGRAPHY	102
	GLOSSARY	113
	APPENDIX	115

TABLE OF CONTENTS (cont'd)

Section	Title	Page
	PART B: DOPPLER RADAR TECHNOLOGY ASSESSMENT	127
1.0	**INTRODUCTION**	129
	1.1 Uses of Radar in Meteorology	129
	1.2 Some Historical Notes on Microbursts	132
2.0	**MICROBURSTS AND GUST FRONTS**	136
	2.1 Microbursts	136
	2.2 Gust Fronts	139
	2.3 Laboratory and Numerical Models	142
3.0	**RADAR MEASUREMENTS AND REFLECTIVITY**	145
	3.1 Reflectivity	145
	3.2 Doppler Spectrum	146
	3.3 Doppler Interpretation	149
4.0	**DETECTION AND PATTERN RECOGNITION ALGORITHMS**	155
	4.1 Automatic Detection of Microbursts	155
	4.2 Automatic Detection of Gust Fronts	160
	4.3 Clutter Residue Map	161
	4.4 An Artificial Intelligence Approach to Microburst Precursor Recognition	162
5.0	**DATA UPDATE RATES AND LIMITATIONS**	165
	5.1 Pulse Repetition Frequency Selection	165
	5.2 Scanning Strategies	169
	5.3 Antenna Sidelobes	173

TABLE OF CONTENTS (cont'd)

Section	Title	Page
	PART B: DOPPLER RADAR TECHNOLOGY ASSESSMENT (cont'd)	
6.0	SUMMARY AND DISCUSSION	174
APPENDIX A	TERMINAL DOPPLER WEATHER RADAR	176
APPENDIX B	KING CITY WEATHER RADAR	183
REFERENCES		185

TABLE OF CONTENTS (cont'd)

Section	Title	Page
	PART C: CONCEPTUAL DESIGNS AND COST ESTIMATES	189
1.0	INTRODUCTION	190
2.0	ANEMOMETER SYSTEM	191
	2.1 LLWAS	191
	2.2 Anemometer Based System for Microburst Detection	195
	2.3 Technical and Environmental Constraints	195
	2.4 Technology Risk	197
2.5	Cost	197
3.0	RADAR SYSTEM	198
	3.1 Canadian Doppler Radar	198
	3.1.1 Options	199
	3.1.2 Technical and Environmental Constraints	200
3.2	Doppler Summary for Risks and Costs	202
	PART D: RECOMMENDATIONS	205

LIST OF FIGURES

PART A

Figure No.	Title
3.1-1	Basic features of a typical microburst.
3.1-2	Flight through a microburst.
3.2.4-1	Life cycle of a thunderstorm.
3.2.5-1	Cross section of typical gust front.
3.3.1-1	Innocent looking virga.
3.3.1-2	Dust clouds on 8 July, 1982.
3.3.1-3	Artist's concept of a microburst.
3.3.2-1	A sequence of photos of a wet microburst.
3.3.3-1	An intense microburst embedded inside one of the northern Wisconsin macrobursts on 4 July, 1977.
3.3.3-2	A sequence of telephoto pictures showing the curling features of the dust clouds behind the leading edge of a microburst outflow.
3.3.3-3	Simplified models of a vertical vortex in a tornado and a horizontal vortex in a microburst.
3.3.3-4	A ground view of a horizontal vortex of the Wichita, Kansas microburst on 1 July, 1978.
3.3.3-5	Various features of microburst-induced dust clouds beneath a decaying anvil cloud on 18 July, 1982 during the JAWS project.
3.3.4-1	Definition of the quantities used.
3.3.4-2	Lift coefficient of swept-wing aircraft with a 15° flap setting and gear-up configuration.
3.3.5-1	Schematic views of wet and dry microbursts.
3.3.5-2	The variation of airflow inside microbursts with different travelling speeds.

LIST OF FIGURES (Continued)

PART A

Figure No.	Title
3.3.5-3	A radial microburst characterized by the straight line outflow and a twisting microburst with curved streamlines.
3.3.5-4	Three stages of a descending microburst.
3.3.5-5	Outflow microbursts are the most commonly observed type of microbursts.
3.3.5-6	A schematic view of a surface microburst accompanied by a misocyclone aloft.
3.3.6-1	Schematic diagrams showing the formation of microbursts beneath an anvil cloud in dry areas.
3.3.6-2	Schematic diagram showing the shape of the bow echo and microbursts in formative and mature stages.
3.3.6-3	Freezing levels of type "I" showers, which vary from location to location and from season to season.
3.3.6-4	Three subclassifications of type "C" parent clouds.
3.3.7-1	Locations of microburst-related aircraft accidents/incidents around the world.
3.4.2-1	Map of JAWS project research network.
3.4.3-1	Velocity fields based on a dual Doppler analysis.
3.4.3-2	Number of JAWS microburst as a function of time of day.
3.4.3-3	Number of JAWS microburst as a function of maximum differential velocity.
3.4.3-4	Wind velocity data over Stapleton Airport, 1982.
3.4.3-5	Evolution of a microburst, vertical cross section.
3.4.3-6	Radar reflectivity against maximum velocity differential.
3.4.3-7	Wind vector change against rain rate.

LIST OF FIGURES (Continued)

PART A

Figure No.	Title
3.4.3-8	Pressure change as a function of temperature.
3.4.3-9	Wind vector change plotted against temperature.
3.4.3-10	Maximum wind speed change plotted against pressure change.
3.4.3-11	Maximum wind speed change as a function of pressure.
3.4.3-12	Processes possibly causing the variety of pressure disturbances for impacting microbursts.
3.4.3-13	Schematic of evolutionary microburst reflectivity.
3.5-1	Mean number of days per year with thunderstorms, 1951-1975.
3.5-2	Mean number of days per year with thunderstorms, 1941-1970.
3.5-3	Seasonal distribution of tornadoes in Western Canada.
3.5-4	Diurnal distribution of tornadoes in Western Canada.
5.2.2-1	Diagram of the operating principle of the new Megasodar.
5.2.3-1	Doppler measurement.
5.2.3-2	Multistatic example.

PART B

(i)	This spectacular photograph of a thunderhead was taken near Grand Forks, North Dakota.
1.	The unusual conditions which led to the Kano accident in 1956.
2.	Microburst situation similar to that present during the takeoff of PanAm Flight 759 in New Orleans on July 1982.
3.	Schematic views of wet and dry microbursts.
4.	A schematic view of a surface microburst accompanied by a misocyclone aloft.

LIST OF FIGURES (Continued)

PART B

Figure No.	Title
5.	Squall line thunderstorm outflow (schematic).
6.	Photo of submerged density current and an outflow propagation through a neutral boundary.
7.	Doppler radar viewing configuration.
8.	Plan view of (a) wind field and (b) corresponding Doppler velocity contours along an inverted conical surface with the radar at the apex.
9.	Single - Doppler radar signatures of a microburst.
10.	Gust front convergence signatures.
11.	Microburst outflow detection algorithm block diagram.
12.	Cases used for performance evaluation.
13.	WX1 System Design.
14.	Simultaneous unambiguous r_a and V_a intervals.
15.	System Functional relationships.
16.	Clutter suppression capability characterization for linear time invariant clutter filtering.

PART C

1.1	Locations of the five anemometers for Hong Kong low-level wind shear detection system.
1.2	Illustration of the LLWAS at Denver Stapleton International Airport.

LIST OF TABLES

Table No.	Title
	PART A
1.2-1	Aircraft Accidents and Incidents Related to Low-Altitude Wind Shear (1964-1982).
2.2.7-1	Operational Equipment.
3.3.4-1	Fractional (%) Loss of Lift Due to a One Knot Increase of the Tailwind or One Knot Increase of the Downflow.
	PART B
1.	1987 TDWR Scan Strategy.
A-1	Required Ground Clutter Suppression Capability.
2.	Basic Radar Parameters.
	PART C
2.1	Operational Equipment.
3.1	Operational Equipment.

1.0 GENERAL INTRODUCTION

This report details all technical work carried out on The Wind Shear Study, Contract No. 11SD.T8200-6-6547-B, and completes Task 5.8 of the Statement of Work: final reports.

1.1 Report Structure

For ease of presentation, this report has been structured into an Executive Summary and four main parts A, B, C and D: Parts A and B are fully self contained for any later dissemination purposes. Part A presents "The User Requirements and Specifications" and Part B "Doppler Radar Technology Assessment". Part C presents outline designs and estimated order of magnitude costs for the preferred technology solutions. Part D concludes the report with recommendations for future work.

Part A begins with the user requirements as defined by Transport Canada. This is followed by a thorough review into meteorological conditions and phenomena which cause low level wind shear. A physical description of microbursts is then given. This is followed with a general review of technology suited to the detection of low level windshear and the most promising technologies highlighted.

Part B is divided into six sections. Section 1 presents introductory material. Section 2 briefly reviews the description of microbursts and gust fronts, and their numerical modelling on a digital computer. Section 3 reviews the fundamentals of radar measurements and signatures with emphasis on pulse Doppler radar. In Section 4, a survey of algorithms for the detection and recognition of low-altitude wind shear is presented. Section 5 deals with data update rates and limitations of Doppler weather radar. Section 6 provides a summary plus a discussion on fruitful areas of research in the context of radar detection. Part B concludes with useful data on the Terminal Doppler Weather Radar (TDWR) and the Atmospheric Environmental Service weather radar at King City.

Part C presents possible conceptual designs for a low level wind shear detection system; technology risk and order of magnitude costs are given. The report finishes with Part D: Spar's recommendations and concluding remarks.

1.2 Report Emphasis

As described above the report is broken down into four parts; common to parts B, C and D is the firm belief that a ground based Doppler radar sensor is the best solution to the detection and recognition of low level wind shear events in and around Canadian airports. Other sensor/technology solutions have been investigated but have not compared favourably with Doppler radars.

For this reason the latter parts of the report are dedicated to discussions on Doppler radar. The only exception to this is that anemometers have been introduced as instruments worthy of inclusion to any detection system.

PART A:

USER REQUIREMENTS AND TECHNICAL SPECIFICATIONS

1.0 INTRODUCTION

1.1 Scope

Recent wind shear related incidents in and around airports have caused an increased awareness within the air transportation community of the hazards related to wind shear phenomena. A pressing safety related need has therefore developed for the capability to detect and alert users regarding wind shear conditions, in particular, microbursts.

In response to this need, Transport Canada tasked its research and development organizaton, the Transportation Development Centre (TDC), to undertake a feasibility study to determine possible technical approaches for the detection and analysis of wind shear conditions, specifically microbursts, in and around Canadian airports. In turn, TDC let two parallel study contracts to industry to investigate the feasibility of wind shear detection; one of these study contracts was given to Spar Aerospace Ltd. of Ste-Anne-de-Bellevue, Quebec, with their sub-contractor McMaster University, Hamilton, Ontario.

This report details the work carried out on Task 5.2: "User Requirements and Specifications" of the Statement of Work for the wind shear study, contract No. 11SD.T8200-6-6547-B.

Following a general introductory section the report, in Section 2, outlines User Requirements as supplied by The Air Navigation Systems Requirements Branch. Additional requirements and specifications, proposed by Spar, are also included for completeness.

Section 3 provides an in-depth review of meteorology and explains how it pertains to the microburst phenomenon. In some instances there is an overlap with the material presented in the next part of the report, Section 4:Wind shear Model. This is to be expected, since much of the data extracted to characterize a microburst originates in Section 3.

Section 5 presents a narrative on existing and possible future options for detection technologies. For convenience, this section has been split between airborne and groundbased equipments. The main body of the report concludes with a summary, Section 6.

1.2 General Background

From 1964 to 1982 twenty-four wind-shear-related accidents and three wind-shear-related incidents (US data from Elmore et al 1986, see Meteorology Review literature in the References Section) occurred at US airports. These involved large - gross weight greater than 5670 kg - transport aircraft and were identified from 19,332, US National Transportation Safety Board reports of accidents and incidents. These 24 accidents resulted in 491 fatalities and 206 injuries, accounting for nearly all the fatalities suffered by the air carrier industry in the United States. These accidents and incidents are detailed in Table 1.2-1 (McCarthy, 1984).

No fatalities can be attributed to wind shear conditions at Canadian airports. From information supplied in CANADA-AIDS, only one accident between 1976 and 1983 involved a commercial size aircraft at a Canadian airport. The captain reported a "hot landing" in a B737-200 at Sault Ste. Marie, Ontario on January 2 1982.

Microbursts were first recognized as an aircraft hazard by an Australian Bureau of Air Safety investigation of an accident that occurred at Bathurst, New South Wales, on 31 May 1974. A Fokker F-27 crashed as it attempted a "go-round" after experiencing difficulty during its approach. From the pilot's description, eyewitness accounts, and the very limited information from the flight Data Recorder (FDR) on board the aircraft, the bureau determined that the crash was caused by strong, diverging horizontal winds that resulted when a downdraft penetrated to the surface. Similar small-scale outflows had been identified 25 years previously during the Thunderstorm Project (Byers and Braham, 1949). However, the low-altitude wind shear hazard was not fully appreciated in the United States until the crash of Eastern Airlines (EAL) Flight 66 on approach to John F. Kennedy International Airport on 24 June 1975 (Fujita and Byers, 1977; Fujita, 1983). Inspection of the Table reveals that almost 90% of aircraft accidents/incidents occurred on landing. To some degree this can be explained by the pilot's "mind-set" to landing.

The lethality of small scale wind shear phenomenon is now well known although as yet not fully understood.

The following sections of this document present a summary of Spar's current understanding of microburst. The summary is not complete but is considered satisfactory as a precursor to a detailed examination into wind shear detection, recognition and alert.

TABLE 1.2-Aircraft Accidents and Incidents Related to Low-Altitude Wind Shear (1964-1982)

No	Year & Date	Time (LST)	Location	Airline Flt No (Aircraft type)	T/O or LDG (Runway)	Fat/Inj	Wind Shear Experienced	Weather Systems
1	1964 MAR 01	1129	Lake Tahoe NV	Paradise 901A (L-1049)	●LDG —	85/0	During climbout after a missed approach	Strong mountain lee wave during snowstorm
2	1964 JUL 01	2134	JFK New York NY	AA 64 (B-720B)	●LDG 31R	0/0	Windshift from headwind to crosswind	Thunderstorm with a sharp pressure rise
3	1965 MAR 17	1858	Kansas City MO	TWA 407 (B-727)	●LDG 36	0/0	Wind direction change on final, 310°-21kts to 280°-22kts	Unstable moist air
4	1968 JUN 08	1351	Salt Lake City UT	UAL 8327 (B-727)	●LDG 34L	0/1	260°-13kts at 1351 to 280°-12kts at 1354	Heavy thunderstorm with suspected gust front
5	1970 JUL 20	1136	Naha AB Okinawa	FFLY TIG 45 (DC-8)	●LDG 18	4/0	10kts tailwind near threshold	Heavy rainshower one mile in diameter
6	1970 DEC 10	1926	St Thomas VI	Carib-Atl (CV-640)	●LDG 09	NA	Landing in 080°-20kts wind	Lee side flow in rainshower
7	1971 JAN 04	1832	LGA New York NY	FAA N-7 (DC-3)	●LDG 04	0/2	Tailwind changed into headwind.	Frontal Shear
8	1972 MAY 18	1421	Ft Lauderdale FL	EAL 346 (DC-9)	●LDG 09L	0/3	180°-10kts at 1418 to 130°-12kts at 1426	Heavy thunderstorm
9	1972 JUL 26	1406	New Orleans LA	NA 32 (B-727)	●LDG 28	0/0	IAS dropped 162 to 122kts	Intense rainstorm and thunderstorm
10	1972 DEC 12	2256	JFK New York NY	TWA 669 (B-707)	●LDG 04R	0/0	42kts tailwind at 1500' to 5kts headwind at the surface	Frontal shear; Fog and drizzle
11	1973 MAR 03	1250	Wichita KS	TWA 315 (B-727)	●LDG 19R	0/0	100°-10kts at 1240:00 to 170°-10kts to 070°-10kts at 1249:10	Thunderstorm
12	1973 JUN 15	1403	ORD Chicago IL	Airlift 105 (DC-8)	●LDG 22R	0/0	Estimated downdraft 50fps at 3000', 15fps at 500' AGL	Heavy rainstorm
13	1973 JUL 23	1643	St Louis MO	OZ 809 (FH-227B)	●LDG 30L	38/6	Up- and downdrafts	Outflow shear; Thunderstorm, sharp pressure rise
14	1973 NOV 27	1851	Chattanooga TN	DL 516 (DC-9)	●LDG 20	0/42	Low-altitude wind shear	Outflow shear; Thunderstorm outflow
15	1973 DEC 17	1543	Boston MA	Iberia 933 (DC-10)	●LDG 33L	0/16	200°-24kts at 500', 260°-12kts at 200', 315°-08kts at surface	Frontal shear; Rain and fog
16	1974 JAN 30	2341	Pago Pago SAMOA	PAA 806 (B-707)	●LDG 05	96/5	Decreasing headwind and/or downdraft during the final 4 seconds	Outflow shear; Heavy rainshower
17	1975 JUN 24	1457	JFK New York NY	EAL 902 (L-1011)	○LDG 22L	—	8kts headwind to 6kts tailwind with 20fps downdraft	Small downburst or microburst; Strong thunderstorm
18	1975 JUN 24	1505	JFK New York NY	EAL 66 (B-727)	●LDG 22L	112/12	14kts headwind to 1kt headwind with 21fps downdraft	Small downburst or microburst; outflow shear, Strong thunderstorm
19	1975 AUG 07	1511	Denver CO	CO 426 (B-727)	●T/O 35L	0/15	IAS decreased 158 to 116kts in 5 seconds	Small downburst or microburst; Outflow shear; Thunderstorm
20	1975 NOV 12	2002	Raleigh NC	EAL 576 (B-727)	●LDG 23	0/1	10° windshift, gust up to 20kts	3 inch per hour rain fall rate
21	1975 DEC 31	1056	Greer SC	EAL (DC-9)	●LDG 03	0/0	200° change in wind direction	Light rain and fog
22	1976 JUN 23	1612	Philadelphia PA	AL 121 (DC-9)	●LDG 27R	0/87	65kts headwind to 20kts tailwind	Microburst; Outflow shear; Fast-moving thunderstorm
23	1976 DEC 12	2326	Cape May NJ	Atl City 977 (DHC-6)	●LDG 19	3/7	Gust to 50kts	Frontal shear
24	1977 JUN 03	1258	Tucson AZ	CO 63 (B-727)	●T/O 21	0/0	30kts headwind to 30kts tailwind	Microburst; Outflow shear; Downdraft in thunderstorm
25	1979 AUG 22	1412	Atlanta GA	EAL 693 (B727)	○LDG 27L	—	strong downdraft and headwind	Microburst; Thunderstorm rainshower
26	1982 JUL 09	1509	New Orleans LA	PAA 759 (B-727)	●T/O 10	153/9	Headwind tailwind and downdraft shear	Microburst with heavy rain
27	1982 JUL 28	1521	LGA New York NY	TWA 524 (B-727)	○LDG 22		Severe wind shear at 20-100' AGL	Strong thunderstorm with gusty winds

TOTAL: ● 24 Accidents; ○ 3 Incidents; 491 Fatalities / 206 Injuries

2.0 USER REQUIREMENTS

2.1 General Requirements

2.1.1 Detection

Detect wind shear conditions, in particular, microburst, in and around Canadian airports.

2.1.2 Identification

Identify the existence of wind shear conditions from the gathered meteorological data.

2.1.3 Accident Prevention

Issue warning to users in time to prevent hazardous flying conditions.

2.2 Transport Canada User Requirements

These requirements have been supplied by the Aviation Group of Transport Canada, specifically the Air Navigation Systems Requirements and Facility Engineering and Systems Development Branches.

2.2.1 Cost

The cost for an installed wind shear/microburst detection system should not exceed an order of magnitude $1,000,000 Canadian per airport.

2.2.2 Range of Coverage

The wind shear/microburst detection system should be capable of detecting and reporting wind shear/microburst events out to fifteen (15) kilometres from the centre of the airport and to an altitude of one (1) kilometre.

2.2.3 Detection Parameters

The wind shear/microburst detection system should be able to detect wind shear/microburst and provide, as a minimum the location of any wind shear/microburst detected.

2.2.4 User Interface

The wind shear/microburst detection system should provide sufficient warning, of wind shear/microburst, such that,

pilots are able to effectively utilize this information to operate their aircraft in a safe manner.

Air Traffic Controllers are able to effectively utilize this information in the provision of advisories and the management of their control area

2.2.5 Detection Status

The detection system must provide "positive" or "negative" status

Positive means: A hazardous wind shear/microburst condition is present within the area of coverage.

Negative means: A hazardous wind shear/microburst is NOT present within the area of coverage.

2.2.6 Probability of Detection vs False Alarm Rate

The design of the wind shear/microburst detection system should give the best possible balance between a high probability of detection and false alarm rate.

Note: It is desirable that the wind shear/microburst system be able to provide its information to a possible future wind shear/microburst forecasting system.

2.2.7 Technical and Environmental Constraints

Any installation must conform to the requirements and standards detailed in "General Specification for Procurement of Electronic Equipment", DFS 1000 (TP3131) supplied by Transport Canada).

Further, any operating equipment must not interfere with other airport/aircraft equipment. Table 2.2.7-1, supplied by Aviation Group of Transport Canada:Facility Engineering and Systems Development Branch, presents the equipments and their respective frequency bands of operation. Also, any installed airport equipment must conform to zoning requirements as detailed in the Transport Canada publication T.P.1247 "Land Use in the Vicinity of Airports".

TABLE 2.2.7-1 OPERATIONAL EQUIPMENT

9 - 14 kHz	Omega
90 - 110 kHz	Loran-C
190 - 1750 kHz	Automatic Direction Finder (ADF)
2850 - 3025 kHz	H.F. Air Ground Communications
3400 - 3500 kHz	H.F. Air Ground Communications
4650 - 4700 kHz	H.F. Air Ground Communications
5450 - 5680 kHz	H.F. Air Ground Communications
6525 - 6685 kHz	H.F. Air Ground Communications
8815 - 8965 kHz	H.F. Air Ground Communications
10005 - 10100 kHz	H.F. Air Ground Communications
11275 - 11400 kHz	H.F. Air Ground Communications
13260 - 13560 kHz	H.F. Air Ground Communications
17900 - 17970 kHz	H.F. Air Ground Communications
75 MHz	ILS - Marker Beacon
108 - 118 MHz	ILS - Localizer, VOR
118 - 137 MHz	VHF Air Ground Communications
121.5 MHz, 243 MHz	ELT
328.6 - 335.6 MHz	ILS - Glide Path
406 - 406.1 MHz	Possible new band for ELT
890 - 902 MHz	Airphone - airborne telephone
942 - 960 MHz	Airphone - airborne telephone
960 - 1215 MHz	DME, TACAN
1030 MHz, Rx; 1090 MHz Tx	SSR Transponder
1215 - 1240 MHz	Future Band for Navstar Satellite System
1250 - 1350 MHz	Ground Based Primary Radar
1545 - 1559 MHz	Future Aeronautical Mobile Satellite (space to earth)
1559 - 1610 MHz	Future band for Navstar Satellite System
1610 - 1626.5 MHz	Proposed for Radio Determination Satellite System (earth to space)
1646.5 - 1660.5 MHz	Future Aeronautical Mobile Satellite (earth to space)
2483.5 - 2500 MHz	Proposed for Radio Determination Satellite System (space to earth)
2700 - 2850 MHz	Ground Based Primary Radar
4200 - 4400 MHz	Radio Altimeter
5030 - 5090.7 MHz	MLS
5350 - 5460 MHz	Airborne Weather Radar
8750 - 8850 MHz	Airborne Doppler Navigator
9300 - 9500 MHz	Airborne Weather Radar
13.25 - 13.4 GHz	Airborne Doppler Navigator
15.4 - 15.7 GHz	National MLS
15.7 - 16.6 GHz	Ground Based Airport Surface Detection Equipment
24.25 - 25.25 GHz	Ground Based Airport Surface Detection Equipment

2.3 Comments on Supplied User Requirements

The following sub-sections contain Spar's comments/ideas on User requirements.

2.3.1 Detection

Currently, no specific values have been attributed to Pd although it is reasonable to assume it must be fairly high. It is understood that the current requirements of the FAA are for a P_d=0.9 and a 10% false alarm rate. It should be noted however that higher required detection probabilities translate into higher signal to noise ratios thus increasing system cost.

Also, it is important to realize that multiple microburst events can occur in close proximity. Ideally, when such a multiple event occurs the detection system should be capable of: -

detecting each microburst
recognizing there are multiple microbursts
tracking each microburst whilst in sensor range

2.3.2 Revisit Time

Due to the short temporal extent of microbursts, the revisit time of the sensor should not be too long. A revisit time of between 1 and 2 minutes seems reasonable.

2.3.3 User Alert Time

Any advance warning of severe wind shear conditions given to the pilot is valuable, no matter how short. However, warning times of not less than than 30 seconds appear a reasonable goal to strive for.

3.0 METEOROLOGICAL REVIEW

3.1 Introduction

Wind shears have been identified by the US National Transportation Board as the cause of twenty-four of the 19,332 air accidents which occurred in the United States between 1964 to 1982 (Elmore et al 1986). All of these occurred at airports and involved large (gross weight greater than 5670 kg) transport aircraft. These 24 accidents resulted in 491 fatalities and 206 injuries, accounting for nearly all the fatalities suffered by the air carrier industry in the United States. These 24 accidents and 3 incidents were detailed in Table 1.2-1 (McCarthy, 1984). In Canada it is found, from information made available by the Aviation Safety Board, that only one accident involving commercial-sized aircraft at Canadian airports during all landings and takeoffs could be related to wind shear. This accident involved a B737-200 and occurred at Sault Ste. Marie, Ontario, on January 2, 1982 at 2138 EST.

Microbursts were first recognized as an aircraft hazard by an Australian Bureau of Air Safety investigation of an accident that occurred at Bathurst, New South Wales, on 31 May 1974. A Fokker F-27 crashed as it attempted a go-round after experiencing difficulty during its approach. From the pilot's description, eyewitness accounts, and the very limited information from the Flight Data Recorder (FDR) on board the aircraft, the bureau determined that the crash was caused by strong, diverging horizontal winds that resulted when a downdraft penetrated to the surface. Similar small-scale out-flows had been identified 25 years previously during the Thunderstorm Project (Byers and Braham, 1949). However, the low-altitude wind shear hazard was not fully appreciated in the United States until the crash of Eastern Airlines (EAL) Flight 66 on approach to John F. Kennedy International Airport on 24 June 1975 (Fujita and Beyers, 1977; Fujita, 1983).

A wind shear is a meteorological phenomenon which is characterized by changes in wind speed and/or direction that take place over small distances. When an aircraft flies through a wind change of this kind, especially when at low altitude, the pilot must adjust for it quickly to maintain course and altitude. Usually a wind shear poses little danger. But should it occur over a distance as short as about 1 to 3 km, a pilot may have only a matter of 30 seconds to recover safely from its effects.

For our purposes a microburst is an intense wind shear condition which is defined as a downdraft-induced, diverging horizontal flow of air near the Earth's surface which has an initial horizontal dimension of less than 4 kilometers (km) and a differential velocity of greater that 10 meters per second (m/s). Figure 3.1-1 gives the basic features of a microburst. We see the microburst originating from the base of a

FIGURE 3.1-1 BASIC FEATURES OF A TYPICAL MICROBURST

3.1 Introduction (cont'd)

cloud, the presence of virga and the outflow front at the perimeter of the base of the microburst. Of particular importance, the scale size is seen to be about 12.5 kft (approx. 4km).

When an aircraft flies through a microburst (McCarthy and Serafin, 1984) the encounter can be lethal. It is not difficult to understand why. In Figure 3.1-2 is shown a vertical cross section of a microburst, with the flight track of an aircraft penetrating it shortly after takeoff. At position (1) in the diagram, the aircraft first encounters a headwind component from the microburst outflow, which increases lift by increasing the relative airflow over the wing. The plane may then pitch up, and the pilot may try to compensate by leveling off. But only a matter of seconds later (2) the plane encounters a decreasing headwind, then a downdraft (3), and then a strong tailwind (4). By that time the aeroplane has lost lift and the pilot could be flying too low and with insufficient air speed to avoid a crash (5).

Two research programs have been carried out in recent years to study the microburst phenomenon. The Northern Illinois Meteorological Research on Downbursts (NIMROD) Experiment, directed by University of Chicago Professors Fujita and Srivastava, was conducted near Chicago in the spring of 1978. In the summer of 1982, the Joint Airport Weather Studies (JAWS) Project, directed by John McCarthy and James Wilson of the National Centre for Atmospheric Research (NCAR), in collaboration with Fujita, was conducted at Denver's Stapleton International Airport. The results of both these programs have provided further insight into the airflow characteristics of microbursts, as well as new understanding of aircraft performance in microbursts, and have pointed to a need for adequate detection and warning of the event in the context of aviation safety.

3.2 Meteorological Conditions and Phenomena which Cause Low-Level Wind Shear

3.2.1 Wind Profile in the Lower Levels of the Atmosphere

It is a well known fact (ICAO Circular 186-AN/122) that, even outside the influence of the specific wind shear-causing meteorological phenomena, wind shear is always present in the atmosphere, although under normal circumstances such wind shear does not cause difficulty for a pilot. It is especially noticeable below 600 m (2,000 ft) where frictional drag on the air closest to the Earth's surface causes changes in both wind speed and direction with height. This layer is generally referred to as the "friction layer" which can be further sub-divided as follows into:

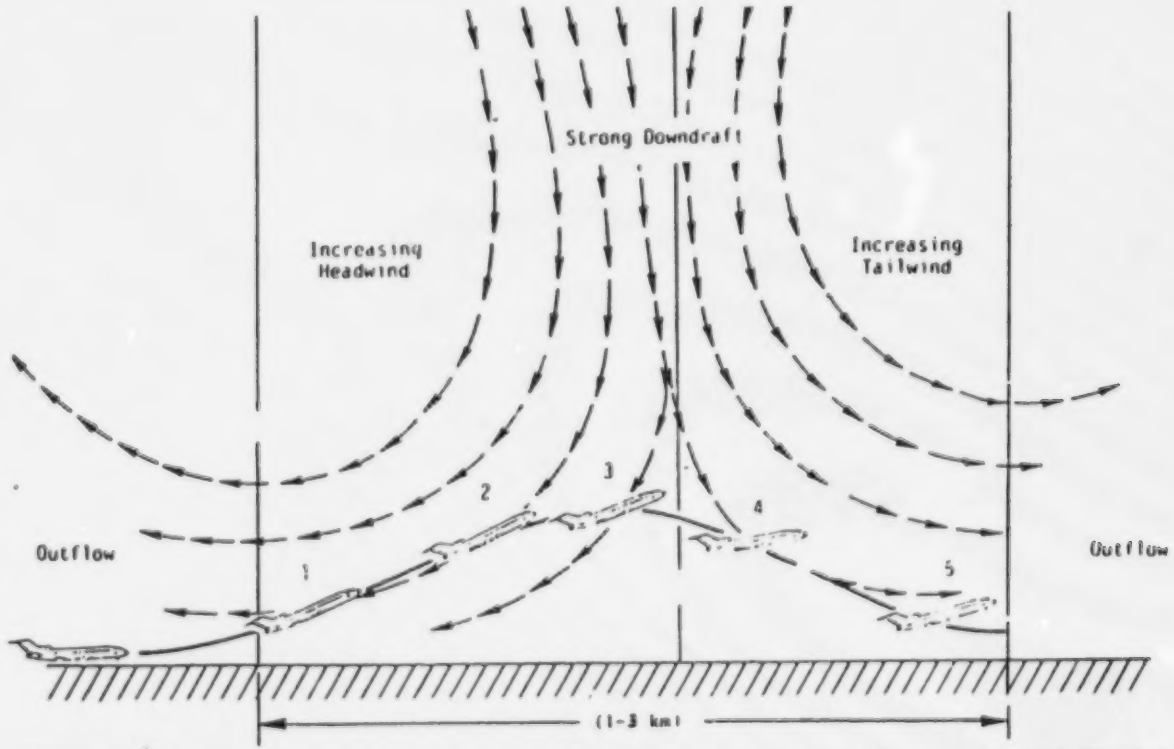

***MICROBURST SITUATION** similar to that present during the takeoff of Pan Am Flight 759 in New Orleans in July 1982. The airplane first encounters a headwind and experiences increasing performance (1); this is followed in short succession by a decreasing headwind component (2), a downdraft (3), and finally a strong tailwind (4), where 2 through 5 all result in decreasing performance of the airplane. Position (5) represents an extreme situation just prior to impact. Figure courtesy of Walter Frost, FWG Associates, Inc., Tullahoma, Tennessee.*

FIGURE 3.1-2 FLIGHT THROUGH A MICROBURST

3.2.1 Wind Profile in the Lower Levels of the Atmosphere (cont'd)

a) the "surface boundary layer" from the Earth's surface up to about 100 m (330 ft) in which air motion is controlled predominantly by friction with the Earth's surface; and

b) the "Ekman layer" from about 100 m (330 ft) up to at least 600 m (2,000 ft) in which the effect of friction, whilst still significant, diminishes progressively with increasing height, and other controlling factors, such as the Coriolis force and horizontal pressure gradient force, become increasingly important.

In the friction layer the wind speed tends to increase with height throughout, with the largest change occurring immediately above the Earth's surface in the surface boundary layer. The wind direction tends to remain constant with height in the surface boundary layer, but to veer (back) with height in the northern (southern) hemisphere throughout the Ekman layer.

3.2.2 Wind Flow Around Obstacles

A combination of strong surface winds and obstacles to the prevailing wind flow situated upwind of the approach or departure path, such as large buildings, low hills or close-planted stands of tall trees, can create localized areas of low-level wind shear. In these circumstances the wind shear is usually accompanied by clear-air turbulence. The effect that the obstacles have on the prevailing wind flow depends on a number of factors, the most important of which is the speed of the wind and its orientation relative to the obstacle and the scale of the obstacle in relation to the runway dimensions.

3.2.3 Wind Flow Associated with Frontal Surfaces

Frontal surfaces are transition zones separating air masses of different temperature and hence of different density. When two such air masses come into contact, equilibrium is attained so that the colder and more dense air lies as a wedge below the warmer and less dense air with the boundary between them inclined at a small angle to the horizontal. The inclination of the frontal surface is due to the earth's rotation, but the extent of the inclination also depends on the contrast in the distribution of temperature and wind along the boundary between the two air masses - the greater the contrast the steeper the slope. The dynamics of frontal surfaces dictate that there is a discontinuity in the wind velocity across the surface, particularly in the lower levels of the atmosphere; a frontal surface is thus, by its very nature, a wind shear zone.

3.2.4 Thunderstorms

The name "thunderstorm" is an all-embracing term which can include a number of phenomena produced by mature cumulonimbus clouds, such as thunder and lightning, torrential rain, hail, strong winds and tornadoes, etc. Most of these phenomena present great danger to aircraft.

Thunderstorms are usually composed of a cluster of several cells, each of which behaves as a unit of convective circulation, including both updrafts and downdrafts. Each cell goes through its own life cycle in a period of from one-half to one hour; these life cycles can be divided naturally into three stages (see Figure 3.2.4-1) depending upon the direction and magnitude of the predominating vertical air flow in the cell as follows:

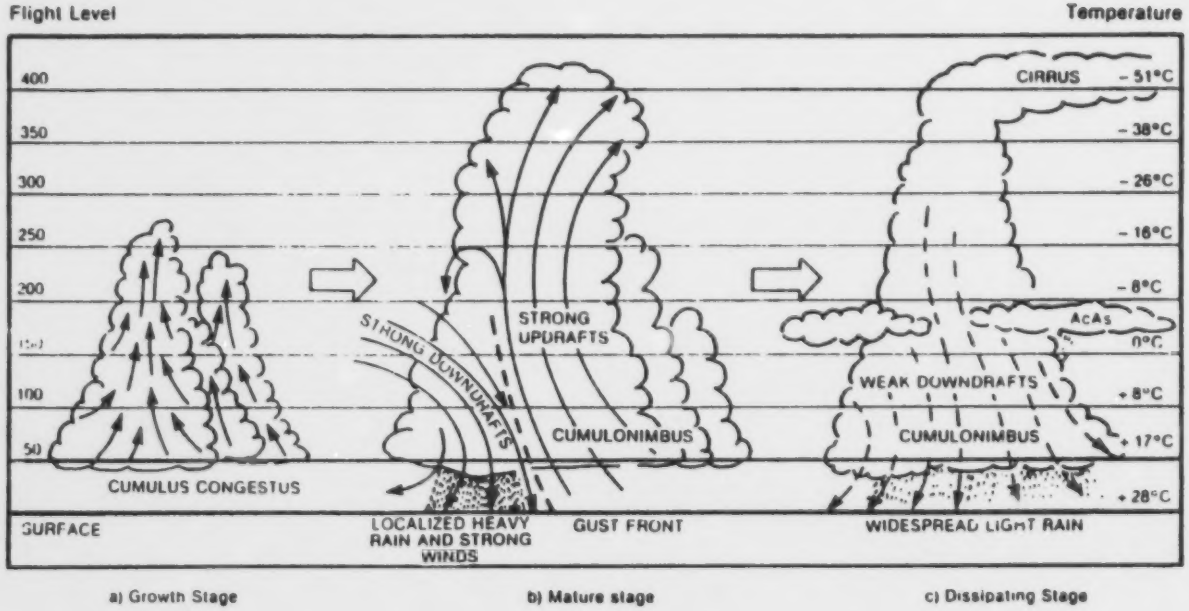

FIGURE 3.2.4-1 LIFE CYCLE OF A THUNDERSTORM

3.2.4 Thunderstorms (Cont'd)

a) cumulus or growing stage characterized by updrafts throughout the cell;

b) mature stage characterized by the presence of both updrafts and downdrafts; and

c) dissipating stage characterized by weak downdrafts throughout the cell.

3.2.5 The Gust Front

The gust front is the leading edge of the cold, dense air from a thunderstorm downdraft which reaches the ground and spreads out in all directions, undercutting the surrounding warmer and less dense air (see Figure 3.2.5-1). In this respect it resembles a shallow cold front except that the associated wind speeds, wind shear and turbulence are generally far higher in the gust front.

3.3 Physical Description of Microbursts

(From: Fujita, 1985)

3.3.1 In Brief, What Are Microbursts?

Microbursts are intense downdrafts, sometimes wet (precipitation reaches the surface) and sometimes dry (precipitation does not reach the surface). Virga, one origin of microbursts, is downflow precipitation from convective cloud that cools the air through which it passes, evaporating before reaching the surface. A good example is Figure 3.3.1-1a) and b), showing virga over Stapleton International Airport. As the precipitation evaporates, the air is cooled and becomes dense, descending at rates up to 20 m/s (4,000 feet per minute).

As the column of cold/dense air reaches the surface, it diverges in all directions producing gust front conditions up to three times the core diameter of about 2.5 km (1.5 miles). Although smaller than downbursts, microbursts develop tremendous energy and, therefore, are similarly hazardous. In areas like Denver, virga is the most common visual cue to a potential microburst. In semi-arid climates, common visual evidence of an active microburst is a ring of dust as pictured in Figure 3.3.1-2. The ring of dust results from the motion phenomenon illustrated in Figure 3.3.1-3, which is an artist's conception of a microburst. Figure 3.3.1-3 depicts a microburst in three dimensions, showing the region of downflow, the circular region of outflow and a stagnation zone.

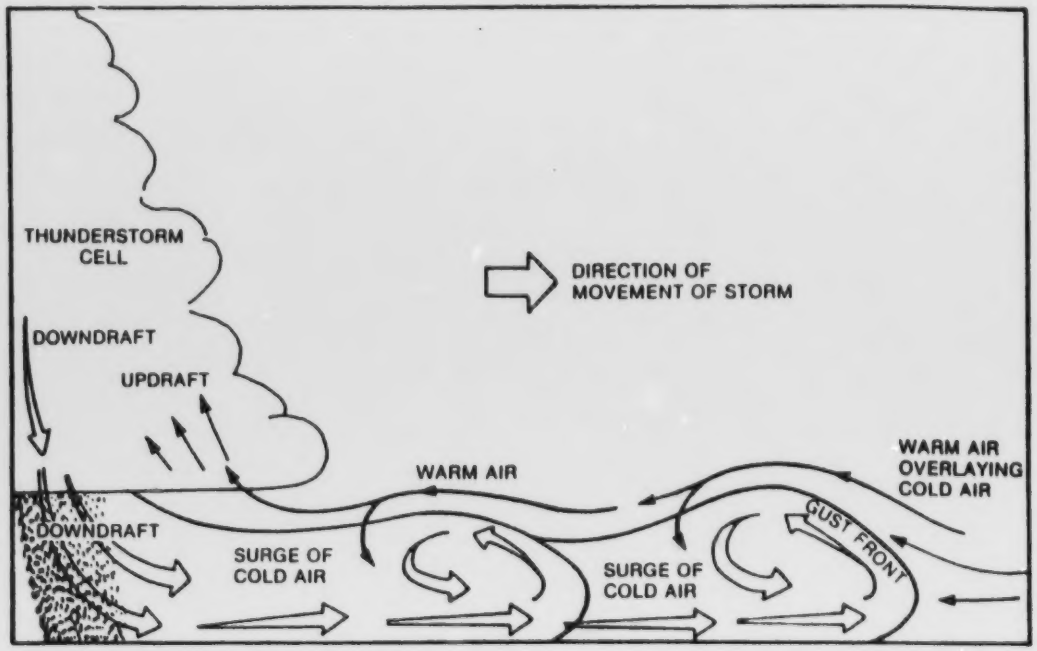

FIGURE 3.2.5-1 CROSS SECTION OF TYPICAL GUST FRONT (AFTER ICAO "GUST FRONT TURBULENCE AND WIND SHEAR" POSTER No.P621)

FIGURE 3.3.1-1 a) INNOCENT-LOOKING VIRGA ABOVE RUNWAY 35R OF STAPLETON AIRPORT AT DENVER, COLORADO ON 14 JULY, 1982.

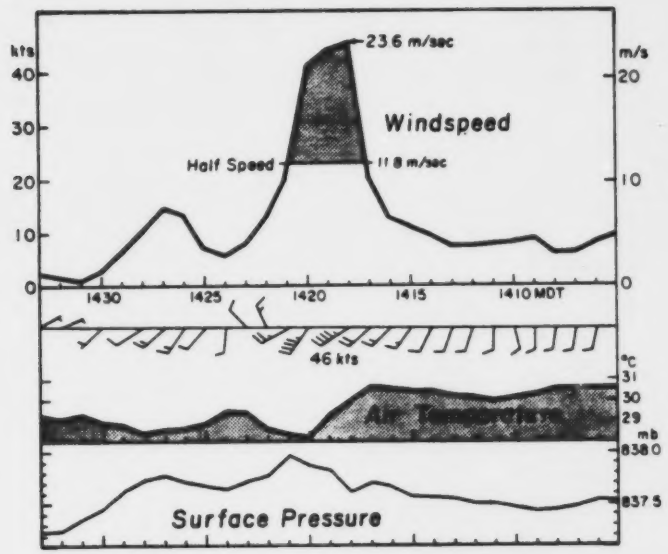

FIGURE 3.3.1-1 b) THE VIRGA IN a) INDUCED A MICROBURST WITH A PEAK WIND LASTING ONLY 3 MINUTES. TEMPERATURE DROPPED 2.5° C AND PRESSURE ROSE 0.3-0.4 mb.

PHOTO BY FUJITA.

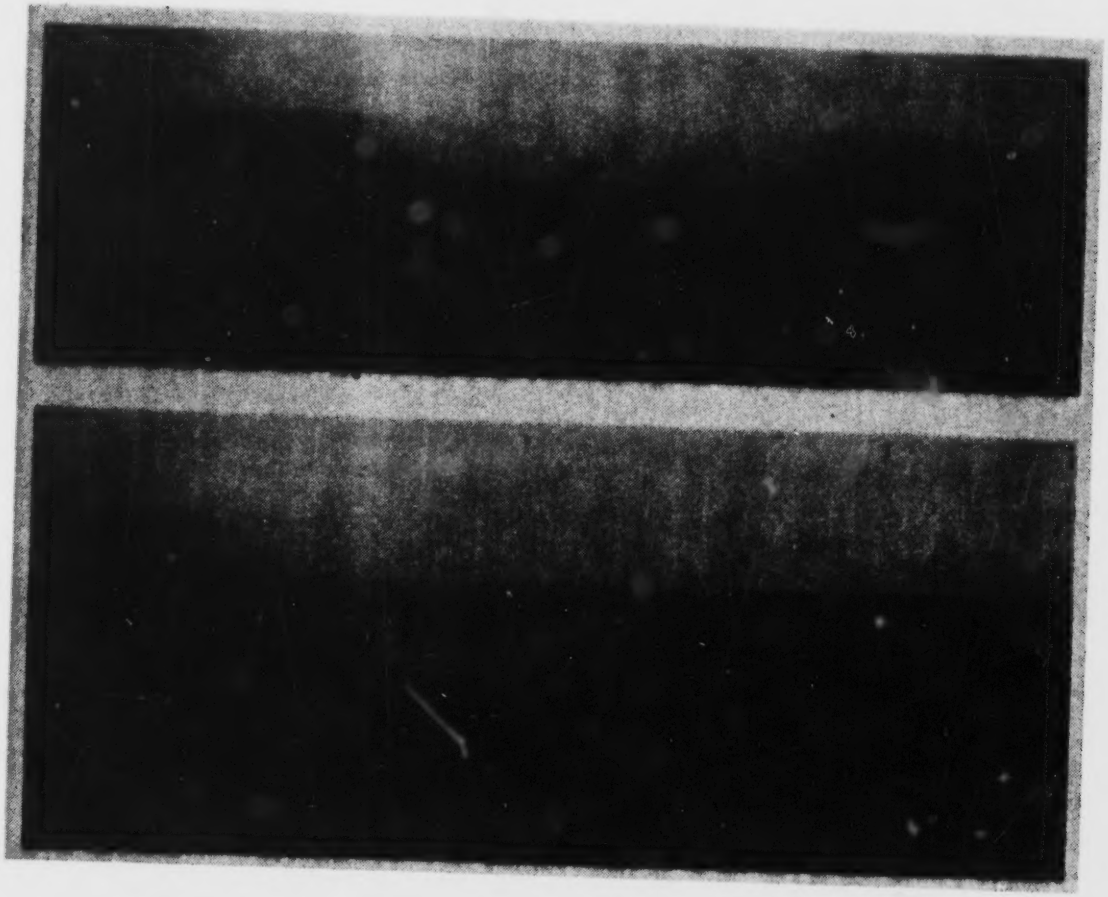

FIGURE 3.3.1-2 DUST CLOUDS ON 8 JULY, 1982. APPROACHING THE CP-3 DOPPLER RADAR SITE. THE UPPER PICTURE WAS TAKEN AT 1343:30 MDT, LOOKING WEST, SHORTLY BEFORE THE PAM STATION IN THE PICTURE RECORDED AN 18 m/sec (40 mph) PEAK WIND. THE LOWER PICTURE WAS TAKEN A FEW SECONDS BEFORE THE DUST CLOUD HIT THE CP-3 SITE. PHOTO BY FUJITA AT CP-3 SITE

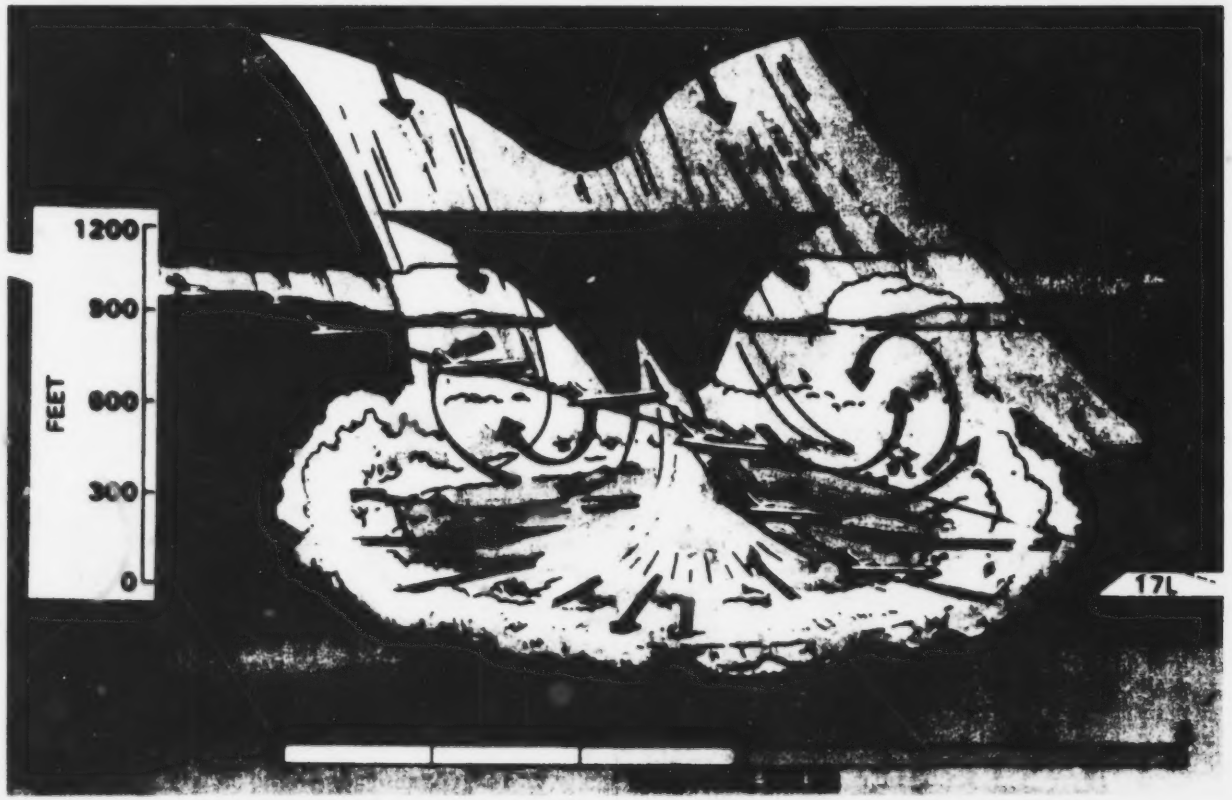

FIGURE 3.3.1-3 ARTIST'S CONCEPT OF A MICROBURST

3.3.2 History of the Observations of Microbursts

In about 1975 Fujita, during an aerial survey of the damage left behind by the super outbreak of 148 tornadoes on 3-4 April 1974, found a strange pattern of tree damage. Unlike the swirling patterns of fallen trees, commonly seen from the air in the wake of tornadoes, hundreds of trees, were blown down outward in a starburst pattern. Both aerial and ground photographs taken at the dead center of a downburst show the change in the airflow direction, from vertical to horizontal, upon hitting the ground surface or a ground object. For example, cornstalks near the dead center of a downburst were either cut or broken by strong straight-line winds outbursting from a single spot in the corn field.

The first field program on downbursts, called NIMROD (Northern Illinois Meteorological Research On Downburst), was conducted in 1978 by the University of Chicago. The project network, located in the western suburbs of Chicago, Illinois, was designed to depict the structure of downbursts in general by using three Doppler radars and 27 PAM (Portable Automated Mesonet) stations.

The second experiment in 1982, called JAWS (Joint Airport Weather Studies) was conducted jointly by the University of Chicago and the National Center for Atmospheric Research. The JAWS Network, located in the northern suburbs of Denver, Colorado was designed to depict microbursts, rather than macrobursts(see Section 3.3), because of a number of microburst-related accidents and incidents kept occurring in various parts of the world.

Of the 50 microbursts detected in the NIMROD network, 64% were accompanied by measurable rain (0.01" or more) while the other 36% had no measurable rain on the ground. It is important to note that 83% of JAWS microbursts were dry, occurring mostly beneath innocuous virga. An example of a dry microburst photographed over Stapleton Airport during JAWS is no more that an innocent-looking virga. Although no pictures of wet microburst during NIMROD were available, a photo sequence of a wet microburst to the west of Wichita, Kansas shows a remarkable difference between the appearance of wet and dry microbursts, Figure 3.3.2-1. The figure shows a sequence of photographs of a wet microburst on 1 July 1978 at 10 - 60 seconds intervals. A curling motion showing a vortex with a horizontal axis is visible near the left(west) edge of the outburst flow.

It is found that damaging microburst winds in the United States occur predominantly during the spring and summer months. As well, with the exception of the NIMROD and JAWS operations, Doppler radars located in various parts of the country rarely have detected microburst winds operationally. This is because microbursts are small and short lived. Furthermore, their maximum winds are very close to the ground where radar echoes are contaminated severely by ground clutter.

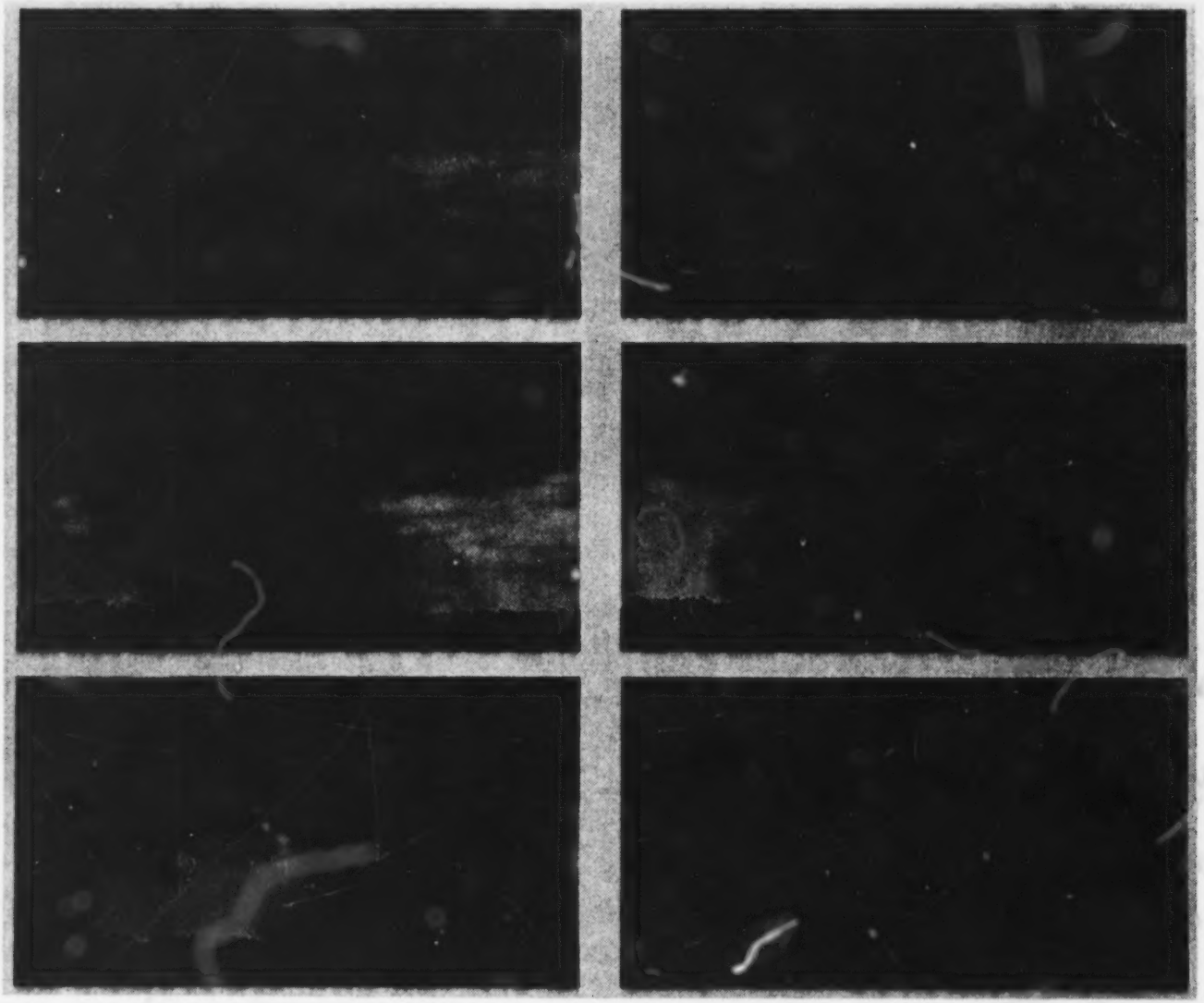

FIGURE 3.3.2-1 A SEQUENCE OF PHOTOS OF A WET MICROBURST. COPYRIGHTED PHOTOS BY MIKE SMITH

3.3.3 Observations of Microbursts

A downburst is a strong downdraft which induces an outburst of damaging winds on or near the ground. Damaging winds, either straight or curved, are highly divergent. The sizes of downbursts vary from less than one kilometer to tens of kilometers. Downbursts are subdivided into macrobursts and microbursts according to their horizontal scale of damaging winds.

Macroburst: A large downburst with its outburst winds extending in excess of 4 km (2.5 miles) in horizontal dimension. An intense macroburst often causes widespread, tornado-like damage. Damaging winds, lasting 5 to 30 minutes, could be as high as 60 m/s (134 mph).

Microburst: A small downburst with its outburst (damaging winds) extending only 4 km (2.5 miles) or less. In spite of its small horizontal scale, an intense microburst could induce damaging winds as high as 75 m/s (168 mph).

By virtue of its small size and its short life of less than 10 minutes, a microburst often escapes detection by non-Doppler radars or ground-based anemometers. Consequently, an aircraft at low altitude could encounter a microburst unexpectedly. A similar encounter could be experienced by cars and trucks on highways or by boats and ships on rivers, bays, and oceans.

3.3.3.1 Appearance of Microbursts

A small but very strong microburst often causes a starburst-shaped tree damage. If we assume a 25 m/s (56 mph) outburst wind along a circle of 100 m (330 ft) radius from the microburst center, the mean divergence inside the circle is as large as 0.5 per second. In order to induce such a large divergence at the near- ground level, the downflow speed will have to be 5 m/s (16 fps) at 10 m (33 ft) AGL and 10 m/s (33 fps) at 20 m (66 ft) AGL. In other words, the downdraft current at the starburst center is very strong even at the tree-top level Figure 3.3.3-1.

Photographic evidence of the microburst winds made visible by flying dust often shows a vortex with a horizontal axis. Winds beneath the vortex ring are accelerated continuously as the ring expands and stretches (Figures 3.3.3-2 and 3.3.3-3).

The horizontal roll of a microburst is illustrated by the Figure 3.3.3-4. This picture shows clearly an awesome feature of a roll vortex located along the leading edge of a wet microburst. In this case, the vortex was made visible by the raindrops blown out of a wet microburst.

FIGURE 3.3.3-1 AN INTENSE MICROBURST EMBEDDED INSIDE ONE OF THE NORTHERN WISCONSIN MACROBURSTS ON 4 JULY, 1977. THIS PICTURE IMPLIES THAT A DOWNFLOW DESCENDED ALMOST TO THE TREE-TOP HEIGHT BEFORE SPREADING.

PHOTO BY FUJITA.

PHOTOS BY BRIAN WARANAUSKAS

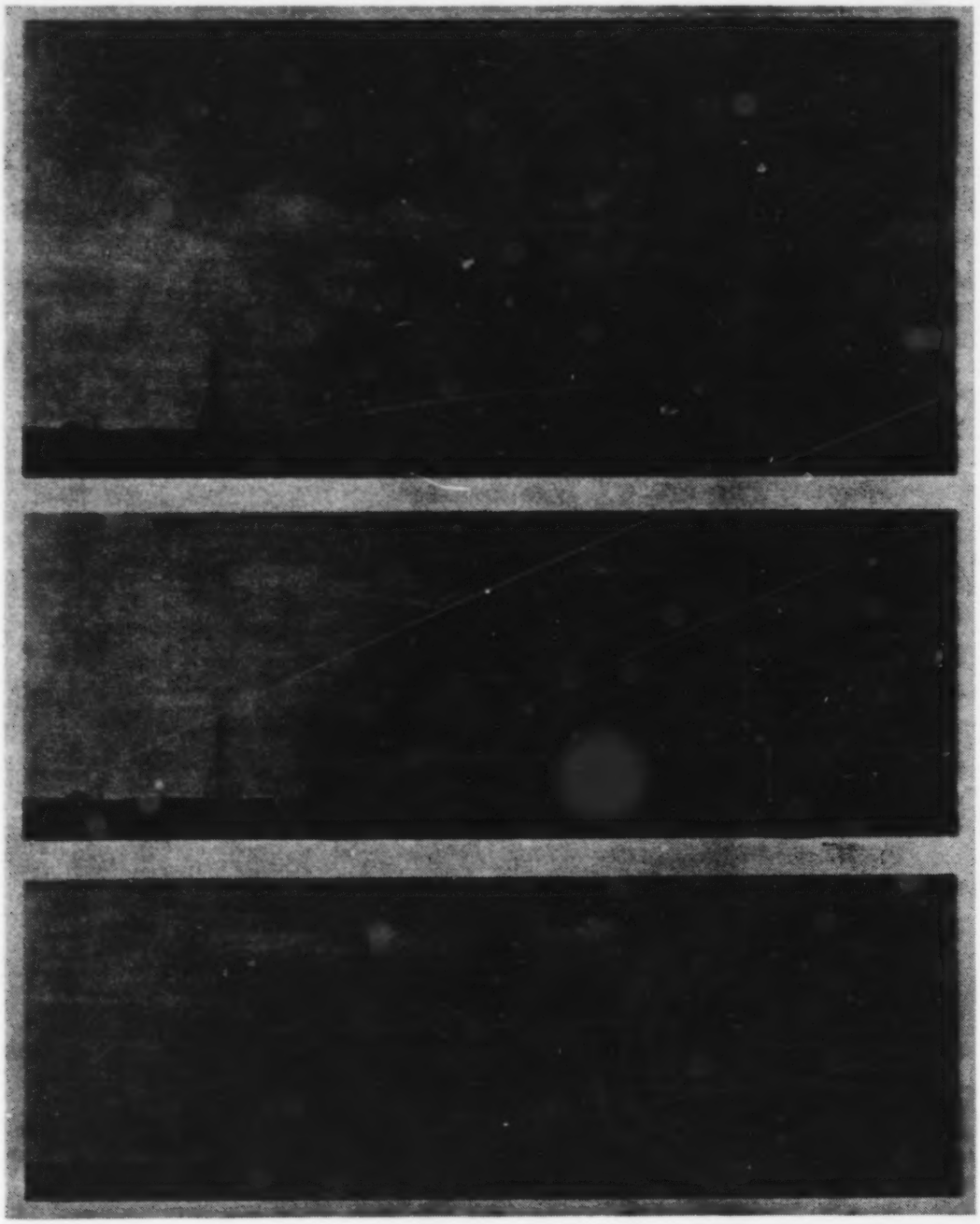

FIGURE 3.3.3-2 A SEQUENCE OF TELEPHOTO PICTURES SHOWING THE CURLING FEATURES OF THE DUST CLOUDS BEHIND THE LEADING EDGE OF A MICROBURST OUTFLOW. PICTURES WERE TAKEN LOOKING SOUTH FROM THE CP-3 SITE ON 15 JULY 1982 DURING THE JAWS FIELD OPERATION.

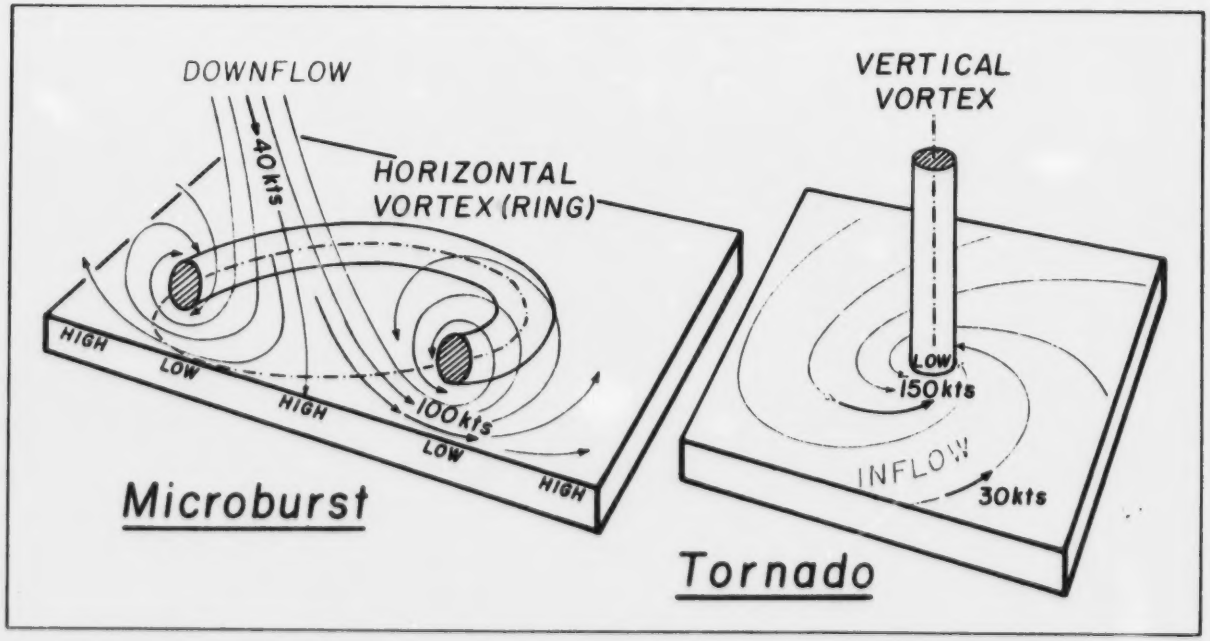

FIGURE 3.3.3-3 SIMPLIFIED MODELS OF A VERTICAL VORTEX IN A TORNADO AND A HORIZONTAL VORTEX IN A MICROBURST.

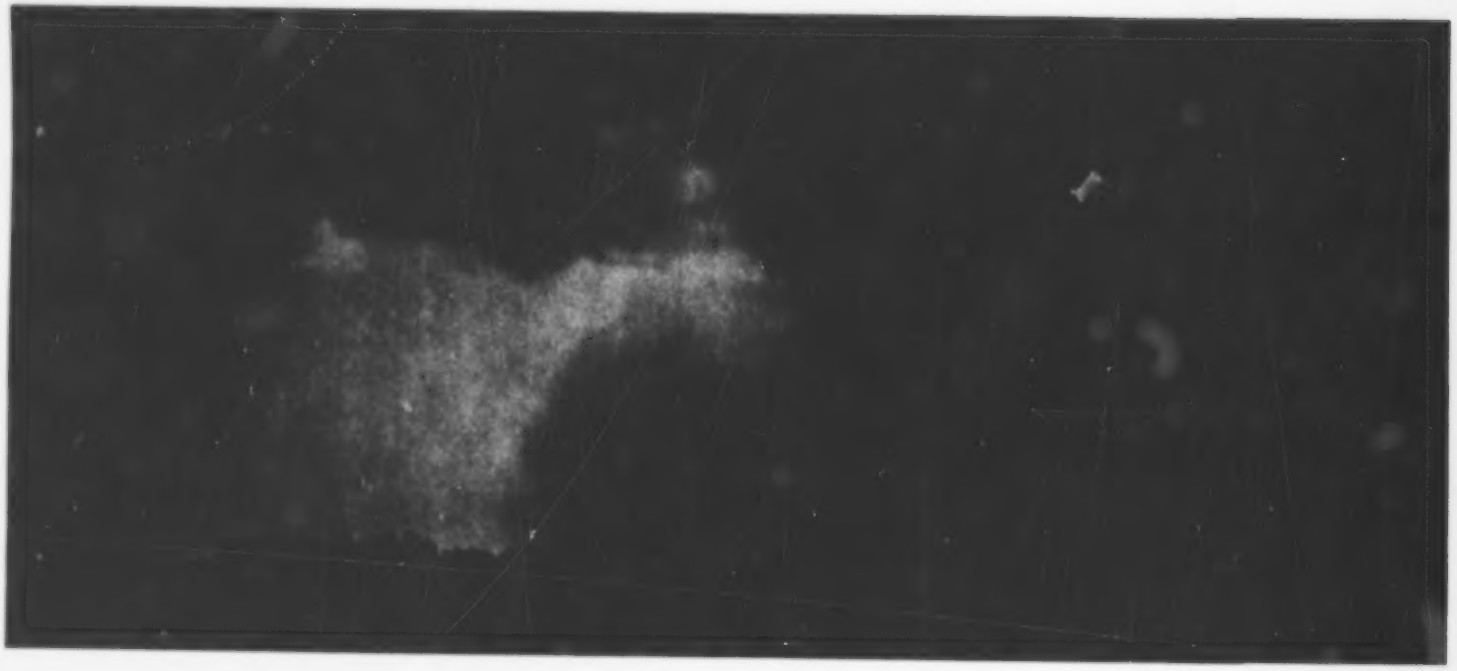

FIGURE 3.3.3-4 A GROUND VIEW OF A HORIZONTAL VORTEX OF THE WICHITA, KANSAS MICROBURST ON 1 JULY, 1978. THIS PHOTO IS AN ENLARGEMENT OF ONE OF THE COPYRIGHTED PHOTOS IN FIGURE 3.3.2-1 TAKEN BY MIKE SMITH

(FUJITA, 1985)

3.3.3.1 Appearance of Microbursts (cont'd)

Figure 3.3.3-5 shows a cloud of blowing dust which turns into a vortex with a horizontal axis. Three pictures on the left depict a strange process in which a horizontal vortex redevelops into a vertical vortex, somewhat like a giant dustdevil or a dusty tornado topped by an umbrella of thin dust.

3.3.4 Effects of Wind Shear upon the Lift Force

The airflow patterns which affect the aircraft's operations are grossly divided into "turbulence" and "wind shear". An aircraft in turbulent flow exhibits irregular and random motions while, more or less, maintaining its intended flight path. Wind shear, with or without turbulence, alters the lift force acting on an aircraft, resulting in a significant sinking or rising motion.

In meteorology, wind shear is the local variation of wind velocity in a given direction. The three components of wind shear can be described by expressing the wind velocity W by

$$W = iu + jv + kw \qquad (1)$$

where i, j, k are unit vectors pointing toward the x, y, z directions and u, v, w are the x, y, z components of the wind velocity.

Wind shear, in aviation, is the time variation of wind velocity along the path of a given aircraft, which can be written as

$$\frac{\Delta W}{\Delta t} = G \quad \frac{\delta W}{\delta L} + \frac{\delta W}{\delta t} \qquad (2)$$

where L is the distance measured along the flight path. The second term on the right side of this equation denotes the local variation of the winds caused by the formation or the development of a wind system penetrated by an aircraft. That is to say, the second term may not exist prior to the penetration. Whereas, the first term denotes the change of the winds as an aircraft flies into an existing wind-shear system.

Noting that the flight path is included in the x-z plane in Figure 3.3.4-1, we define the shear of the three component winds u, v, w by

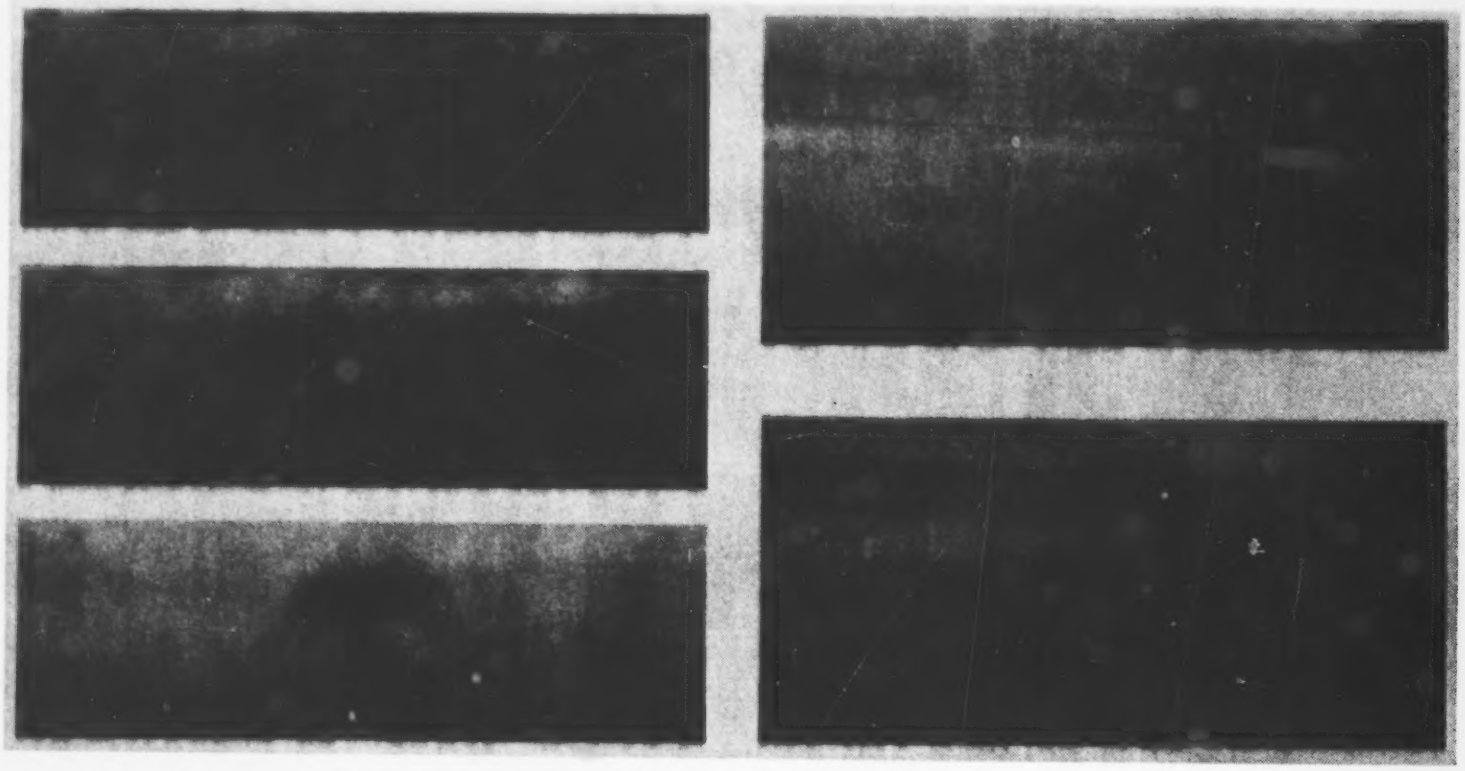

FIGURE 3.3.3-5 VARIOUS FEATURES OF MICROBURST-INDUCED DUST CLOUDS BENEATH A DECAYING ANVIL CLOUD ON 18 JULY, 1982 DURING THE JAWS PROJECT. LEFT PHOTOS: LOOKING NNE AT 1744:35 (TOP), 1745:45, and 1745:55 MDT. RIGHT PHOTOS: LOOKING ENE AT 1758:30 (TOP) and 1758:55 MDT.

PHOTOS BY JOE GOLDEN

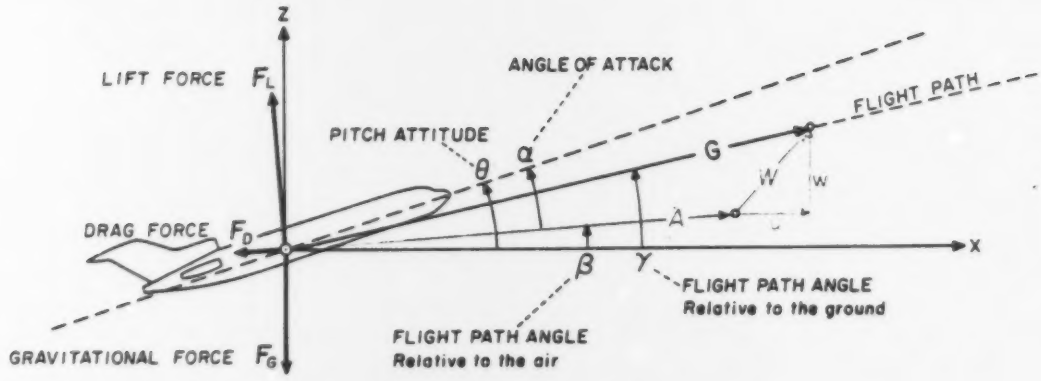

FIGURE 3.3.4-1 DEFINITION OF THE QUANTITIES USED: F_L-- LIFT FORCE, F_G-- GRAVITATIONAL FORCE, F_D-- DRAG FORCE, α -- ANGLE OF ATTACK, β -- FLIGHT PATH ANGLE RELATIVE TO THE AIR, γ --FLIGHT PATH ANGLE RELATIVE TO THE GROUND, θ -- PITCH ATTITUDE, W-- WIND VECTOR, u,v,w--x,y,z COMPONENTS OF WIND VECTOR, A-- TRUE AIRSPEED, AND G-- GROUND SPEED.

3.3.4 Effects of Wind Shear Upon the Lift Force (cont'd)

$-\frac{\Delta u}{\Delta t}$ = Headwind shear (+ headwind; - tailwind) (3)

$\frac{\Delta v}{\Delta t}$ = Crosswind shear (+ from the right; - from the left) (4)

$\frac{\Delta w}{\Delta t}$ = Vertical wind shear (+ upward; - downward) (5)

An aircraft with true airspeed A, flying inside a three-dimensional wind W, moves with the ground-relative velocity G. The lift force acting on the aircraft is perpendicular to vector A, and the drag force points opposite to vector A. Using the symbols in Figure 3.3.4-1, the lift force can be expressed by

$$F = \tfrac{1}{2} \rho A^2 C_L S \quad (6)$$

where ρ is the density of the air, C_L the lift coefficient, and S the cross-sectional area of the lift force acting on the aircraft. Since ß is small and both Θ and G do not vary with time as fast as the winds do, we are able to approximate the ground speed and the angle of attack as

$$G = A + u \quad \text{or} \quad 0 = \frac{\Delta R}{\Delta U} + I \quad (7)$$

$$\alpha = \theta - \gamma + \frac{W}{G} \quad \text{or} \quad \frac{\delta \alpha}{\delta W} = 0 - 0 + \frac{1}{G} \quad (8)$$

The increment of the lift force due to the variation of u and w is computed by differentiating Equation 6 as

$$\Delta F_L = \tfrac{1}{2}\rho C_L A^2 S \left(\frac{2}{A} \frac{\delta A}{\delta U} + \frac{1}{C_L} \frac{\delta C_L}{\delta \alpha} \right) \frac{\delta \alpha}{\delta W} \Delta W \quad (9)$$

Using Equations 7 and 8, we simplify Equation 9 into

$$\frac{\Delta F_L}{F_L} = -\frac{2}{A} \Delta U + \frac{K}{G} \Delta W \quad (10)$$

where $k = \frac{1}{C_L} \frac{\delta C_L}{\delta \alpha}$ (radians) $= \frac{180}{\pi C_L} \frac{\delta C_L}{\delta \alpha}$ (degrees) (11)

3.3.4 Effects of Wind Shear Upon the Lift Force (cont'd)

is determined by the characteristics of the lift coefficient during a wind shear penetration. This equation states that the loss of lift is not only caused by the airspeed but also by the loss of angle of attack which, in turn, reduces the lift coefficient.

A representative curve of a lift coefficient for swept-wing aircraft during a flap-down takeoff configuration is shown in Figure 3.3.4-2. Values in Table 3.3.4-1, computed from the figure, reveal that the loss of lift due to a tailwind is constant, irrespective of the angle of attack at which an aircraft flies. On the other hand, the loss of lift increases appreciably with decreasing angle of attack. Equation 10 suggests that the lowering of the pitch angle, selected for gaining airspeed is a tailwind/downflow wind shear, could result in a loss of lift and subsequent heavy sink.

Table 3.3.4-1 Fractional (%) loss of lift force due to a one knot increase of the tailwind or one knot increase of the downflow. For simplification, A = G = 150 kt was assumed.

Angle of attack (degrees)	0	5	10	15	20
Loss of lift by tailwind (% per kt)	1.3	1.3	1.3	1.3	1.3
Loss of lift by downflow (% per kt)	13.2	4.5	2.5	1.3	0.5

3.3.5 Types of Microbursts and Parent Clouds

Not all microbursts are alike; some are accompanied by heavy rain, while others form beneath small virga. The first major classification of microbursts is based on the precipitation received on the ground during a specific storm. Likewise, the temperature change can be used in distinguishing warm microbursts from cold microbursts. They can also be classified according to their appearance, movement, etc.

The parent clouds which induce microbursts are not always thunderstorms. Quite often, isolated rainshowers spawn relatively strong microbursts which endanger aircraft operations at low altitudes.

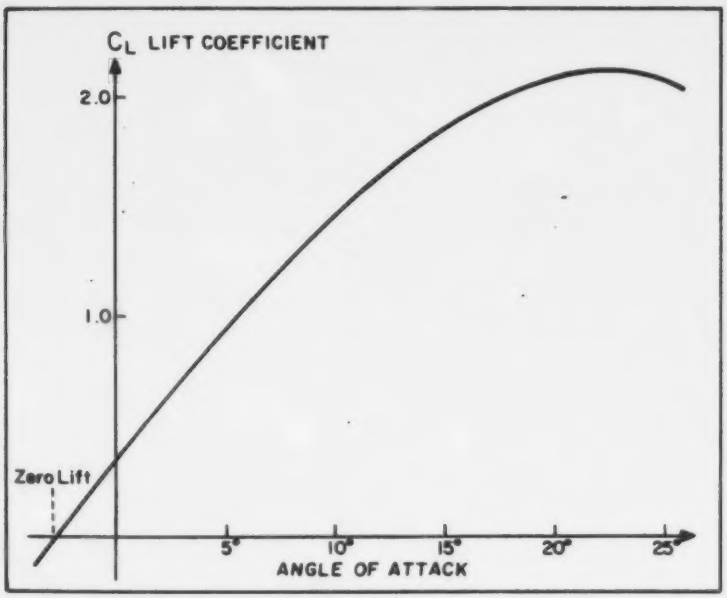

FIGURE 3.3.4-2 LIFT COEFFICIENT OF SWEPT-WING AIRCRAFT WITH A 15° FLAP SETTING AND GEAR-UP CONFIGURATION. THE ANGLE OF ATTACK IS FUSELAGE-RELATIVE. THE WIND-RELATIVE ANGLE OF ATTACK IS APPROXIMATELY 2° LARGER THAN THE FUSELAGE-RELATIVE ANGLE OF ATTACK.

3.3.5.1 Wet and Dry Microbursts

As indicated earlier, 36% of the NIMROD microbursts and 83% of the JAWS microbursts were not accompanied by rain on the ground. These statistics show evidence that the raindrops in microbursts in dry regions often evaporate completely before reaching the ground. Once it gains sufficient downward momentum, a downflow without rain could reach the ground to induce a microburst.

In the wet regions of the United States, such as Louisiana, Florida, etc., practically all microbursts are accompanied by heavy rain.

In general, the high cloud base in the dry region provides the falling raindrops with sufficient time and distance for their dissipation before reaching the ground. Furthermore, the low relative humidity in the subcloud layers accelerates evaporation processes, Figure 3.3.5-1.

3.3.5.2 Stationary and Travelling Microbursts

If a stationary microburst spreads inside an undisturbed environment, a perfect starburst outflow with an annular ring of high winds will be observed. In reality, however, the travelling motion of a microburst distorts the airflow from circular to elliptical shape. The front-side wind intensifies while the back-side wind weakens, resulting in a cresent-shaped area of high winds, Figure 3.3.5-2.

A fast-moving microburst is characterized by the surface winds with straight or mostly parallel streamlines. These types of winds are often called "straight-line winds".

3.3.5.3 Radial and Twisting Microbursts

Radial streamlines are seen if microburst winds are irrotational. However, when a microburst descends inside a strong mesoscale cyclone (mesocyclone), its airflow at the surface is characterized by a cyclonically curved (twisting) streamlines. This type of microburst has been confirmed during aerial surveys of tornadoes spawned by supercell thunderstorms Figure 3.3.5-3.

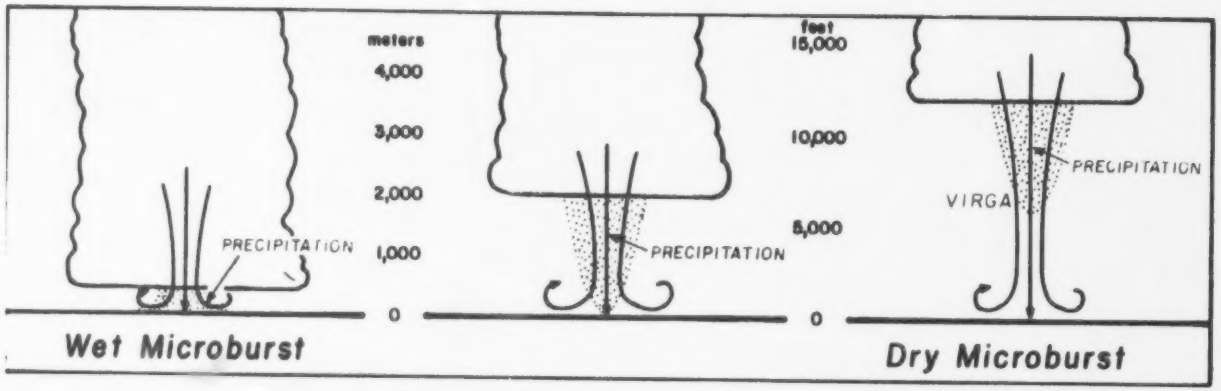

FIGURE 3.3.5-1 SCHEMATIC VIEWS OF WET AND DRY MICROBURSTS. WET MICROBURSTS ARE EXPECTED TO OCCUR IN THE WET REGIONS OF THE WORLD, WHILE DRY MICROBURSTS ARE COMMONLY SEEN IN THE DRY REGIONS WITH HIGH BASES OF CONVECTIVE CLOUDS.

(FUJITA, 1985)

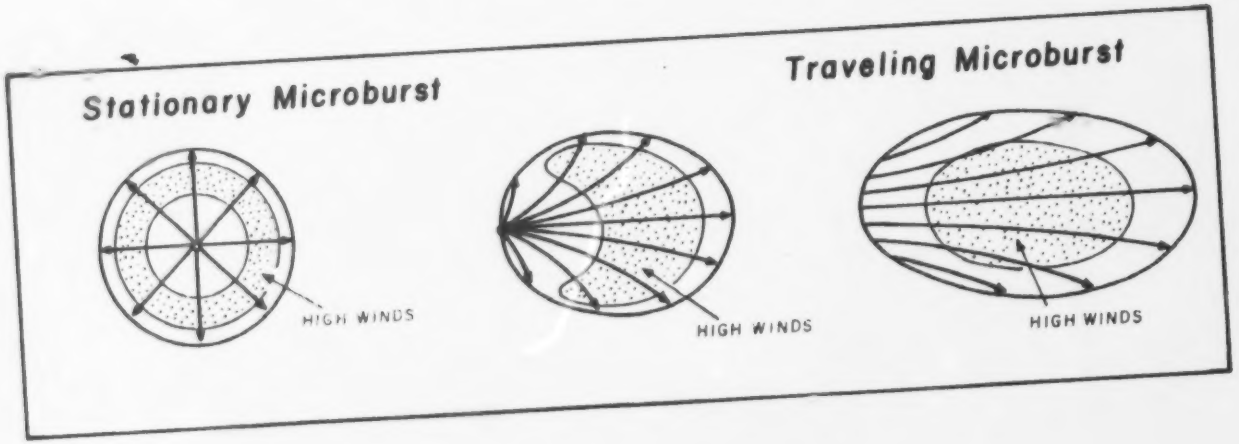

FIGURE 3.3.5-2 THE VARIATION OF AIRFLOW INSIDE MICROBURSTS WITH DIFFERENT TRAVELING SPEEDS. A STATIONARY MICROBURST SHOWS A STARBURST AIRFLOW WITH AN ANNULAR RING OF HIGH WINDS.

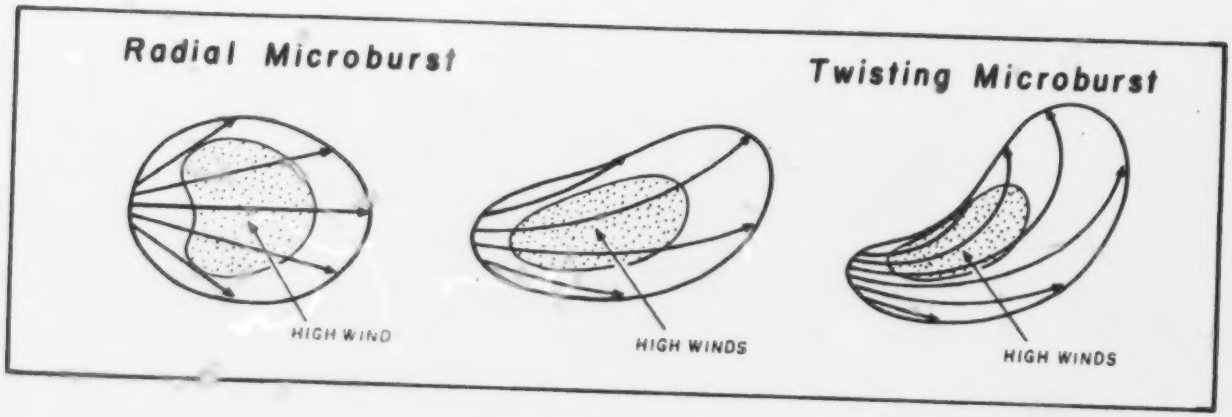

FIGURE 3.3.5-3 A RADIAL MICROBURST CHARACTERIZED BY THE STRAIGHT-LINE OUTFLOW AND A TWISTING MICROBURST WITH CURVED STREAMLINES. TWISTING MICROBURSTS OFTEN OCCUR IN MESOCYCLONES.

3.3.5.4 Midair and Surface Microbursts

No microbursts form on or near the ground. Instead, they descend from the bases of convective clouds Figure 3.3.5-4. A microburst with its characteristic winds located above anemometer heights is called a "midair microburst". A midair microburst may remain aloft until it dissipates, or it may keep descending to the ground.

A microburst after its touchdown is called a "surface microburst". When a surface microburst spreads out onto a large area, the downflow keeps supplying the mass until it sinks to the ground. After that, a microburst flattens and its expansion terminates.

3.3.5.5 Outflow and Rotor Microburst

A microburst accompanied by a strong downflow and outflow is called an "outflow microburst". This is a common type of microburst documented during the NIMROD and JAWS field experiments. Observational evidence shows that a slow-travelling outflow microburst is often, but not always, encircled by a vortex ring, Figure 3.3.5-5.

3.3.5.6 Microbursts with Misocyclones

The misoscale cyclone in which the downflow of a microburst is embedded is called a "misocyclone". It is very likely that a misocyclone aloft acts as a collector of hydrometers which funnel into a concentrated downflow, Figure 3.3.5-6.

3.3.6 Classification of Parent Clouds

3.3.6.1 Type "A", Anvil Cloud and Type "S", Supercell

During the JAWS experiment, the formation of microbursts were observed beneath virga; virga descending from Anvil clouds in a post-mature stage, figure 3.3.6-1. However, it is very unlikely that anvil clouds in wet areas induce microbursts on the ground.

Supercell thunderstorms are likely to produce strong tornadoes. Post-storm aerial surveys often reveal the existence of microburst winds in the vicinity of tornadoes, suggesting that these two types of storms are somehow related. However, their dynamic relationship is not known.

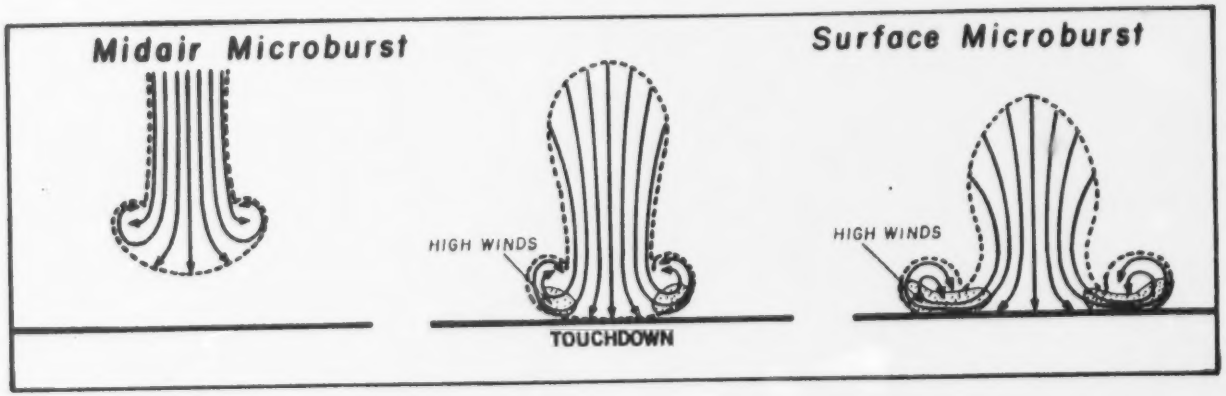

FIGURE 3.3.5-4 THREE STAGES OF A DESCENDING MICROBURST. A MID-AIR MICROBURST MAY OR MAY NOT DESCEND TO THE SURFACE. IF IT DOES, THE OUTBURST WINDS DEVELOP IMMEDIATELY AFTER ITS TOUCHDOWN.

(FUJITA, 1985)

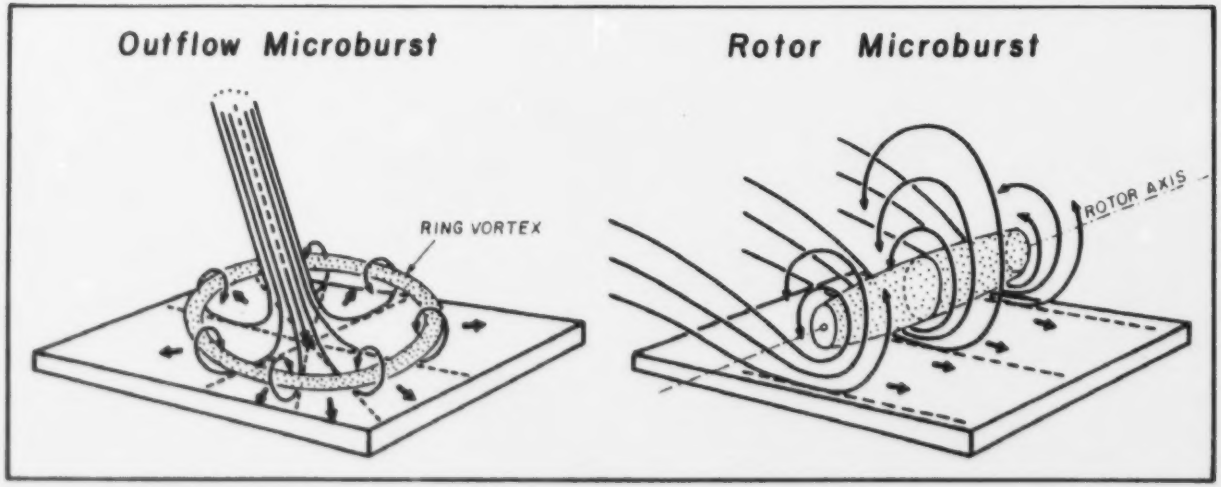

FIGURE 3.3.5-5 OUTFLOW MICROBURSTS ARE THE MOST COMMONLY OBSERVED TYPE OF MICROBURSTS. SOME ROTOR MICROBURSTS DEVELOP INSIDE MACRO-BURSTS BEHIND THEIR GUST FRONTS.

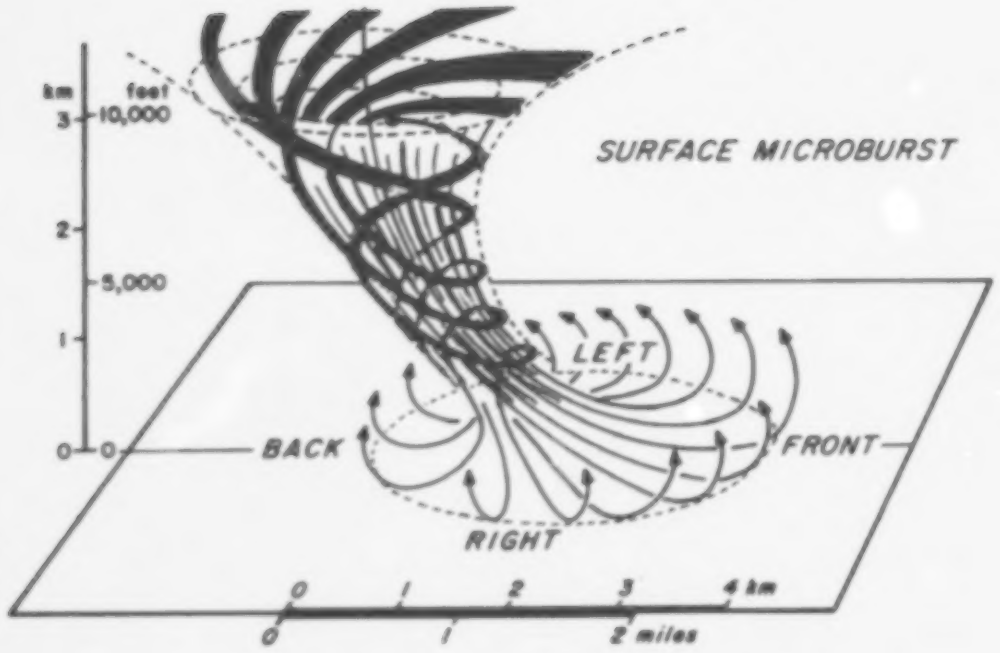

FIGURE 3.3.5-6 A SCHEMATIC VIEW OF A SURFACE MICROBURST ACCOMPANIED BY A MISOCYCLONE ALOFT. MOST MISOCYCLONES, LESS THAN 4 KM IN DIAMETER, ROTATE CYCLONICALLY WHILE EXCEPTIONAL ONES ROTATE ANTICYCLONICALLY.

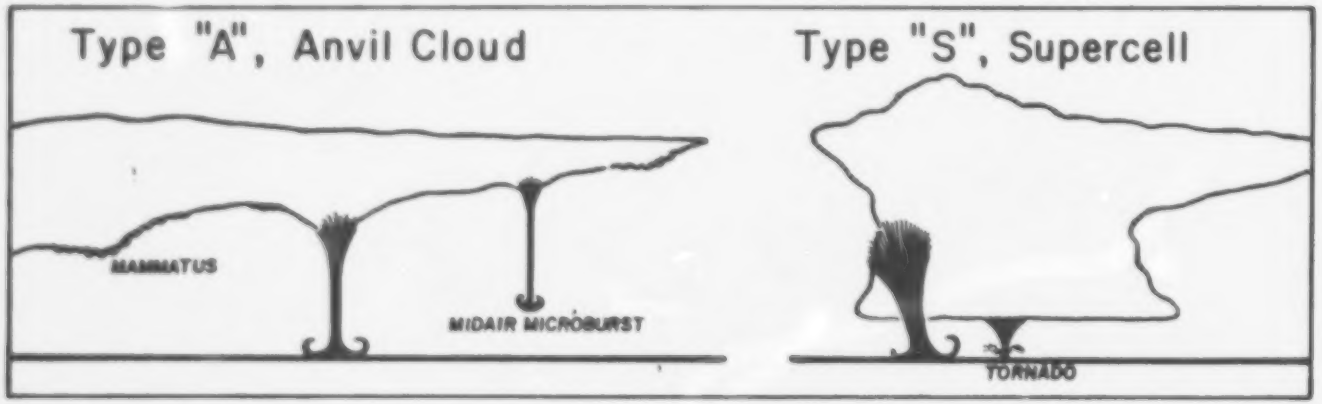

FIGURE 3.3.6-1 SCHEMATIC DIAGRAMS SHOWING THE FORMATION OF MICROBURSTS BENEATH AN ANVIL CLOUD IN DRY AREAS. SUPERCELL THUNDERSTORMS ARE INDUCERS OF TORNADOES AND MICROBURSTS.

3.3.6.2 Type "B", Bow Echo

A bow echo is an inducer of strong , see Figure 3.3.6-2. Usually, high winds push out from the position of an arrow attached to a bow. During the mature stage of a bow echo, both tornadoes and microbursts could occur simultaneously. During the dissipation stage of outburst winds, hydrometers are blown outward very rapidly, drying out the echoes in the source region.

3.3.6.2 Type "I", Isolated Shower

Isolated showers, with or without thunder, induce microbursts Figure 3.3.6-3.

3.3.6.3 Type "C", Cumulus Cloud

Type "C" parent clouds are large cumulus clouds, sometimes having an appearance of altocumulus castellanus, which produce rain or snow that may or may not reach the surface. Based on the observational evidence obtained in JAWS, these clouds are subdivided into mushroom, sinkhole, and giant anteater clouds Figure 3.3.6-4.

3.3.7 Location of Microburst-related Accident Cases

The locations of microburst-related accidents/incidents is presented in Figure 3.3.7-1. The high concentration of accidents/incidents in the United States does not necessarily mean that microbursts occur frequently in this part of the world, but is the result of frequent landings and takeoffs, as well as the method of the accident investigation based on established knowledge of microburst wind shear. It's worth recalling, as was stated at the beginning of this report, of the 19,332 accidents that occurred in the US between 1964 to 1982, only 27 were attributed to wind shear at airports. One concludes it is their low frequency of occurrence that makes them difficult to detect. On the other hand, in terms of number of fatalities caused by microbursts in the US microbursts make their presence known in a rather dramatic fashion.

Infrequent and spotty accident cases are seen in the tropics, on islands, along the coast, and inside the continent. One accident was reported at Bathurst, Australia in the southern hemisphere. Not until knowledge of microburst-related wind shear becomes known widely to international aviation communities, will microburst-induced wind shear be recognized as an important cause of world-wide accidents/incidents during the takeoff and landing operation.

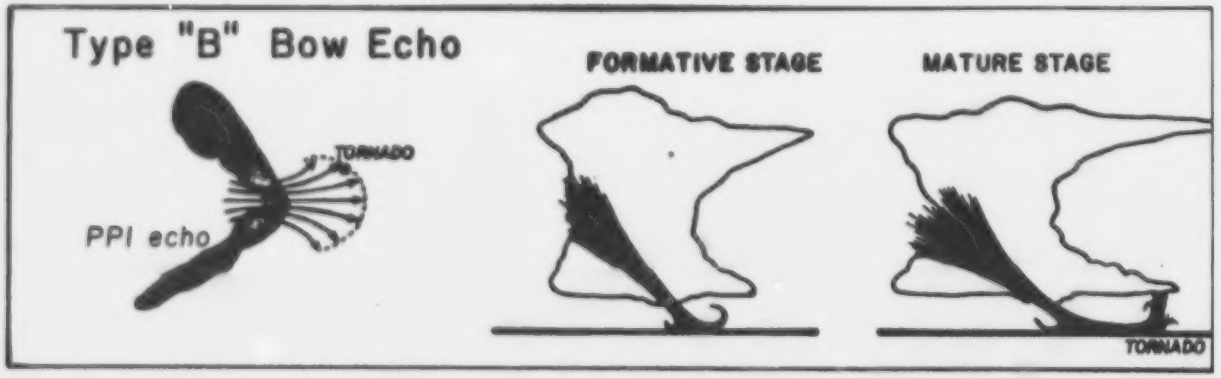

FIGURE 3.3.6-2 SCHEMATIC DIAGRAM SHOWING THE SHAPE OF THE BOW ECHO AND MICROBURSTS IN FORMATIVE AND MATURE STAGES.

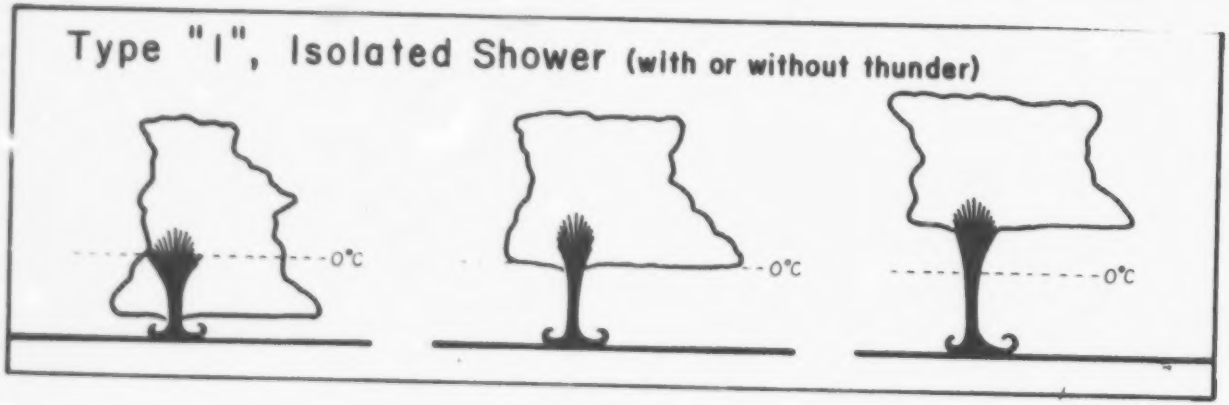

FIGURE 3.3.6-3 FREEZING LEVELS OF TYPE "I" SHOWERS, WHICH VARY FROM LOCATION TO LOCATION AND FROM SEASON TO SEASON. A CLOUD BASE WITH 0°C OR COLDER TEMPERATURE IS CALLED "COLD CLOUD BASE" AND OTHERS ARE CALLED "WARM CLOUD BASE".

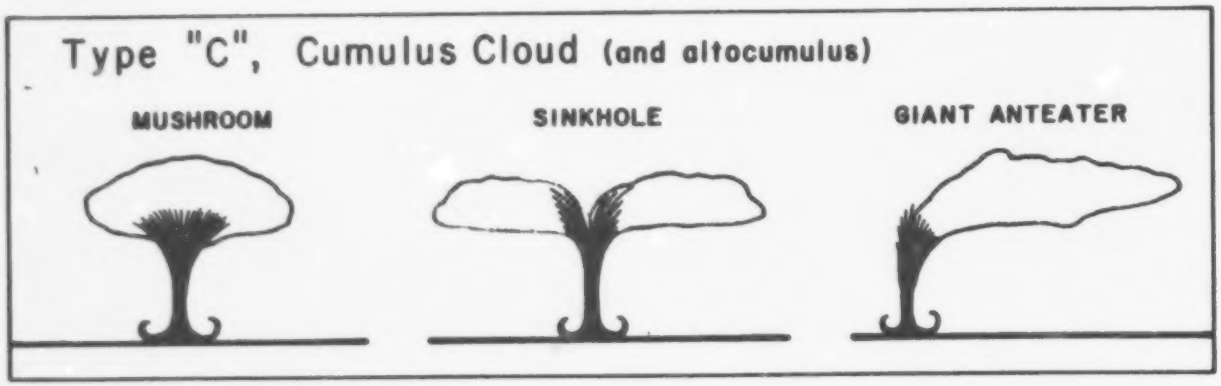

FIGURE 3.3.6-4 THREE SUBCLASSIFICATIONS OF TYPE "C" PARENT CLOUDS. THEY ARE THE MUSHROOM CLOUD, SINKHOLE CLOUD, AND GIANT ANTEATER CLOUD. MORE CLOUDS ARE EXPECTED TO BE ADDED IN FUTURE YEARS.

(FUJITA, 1985)

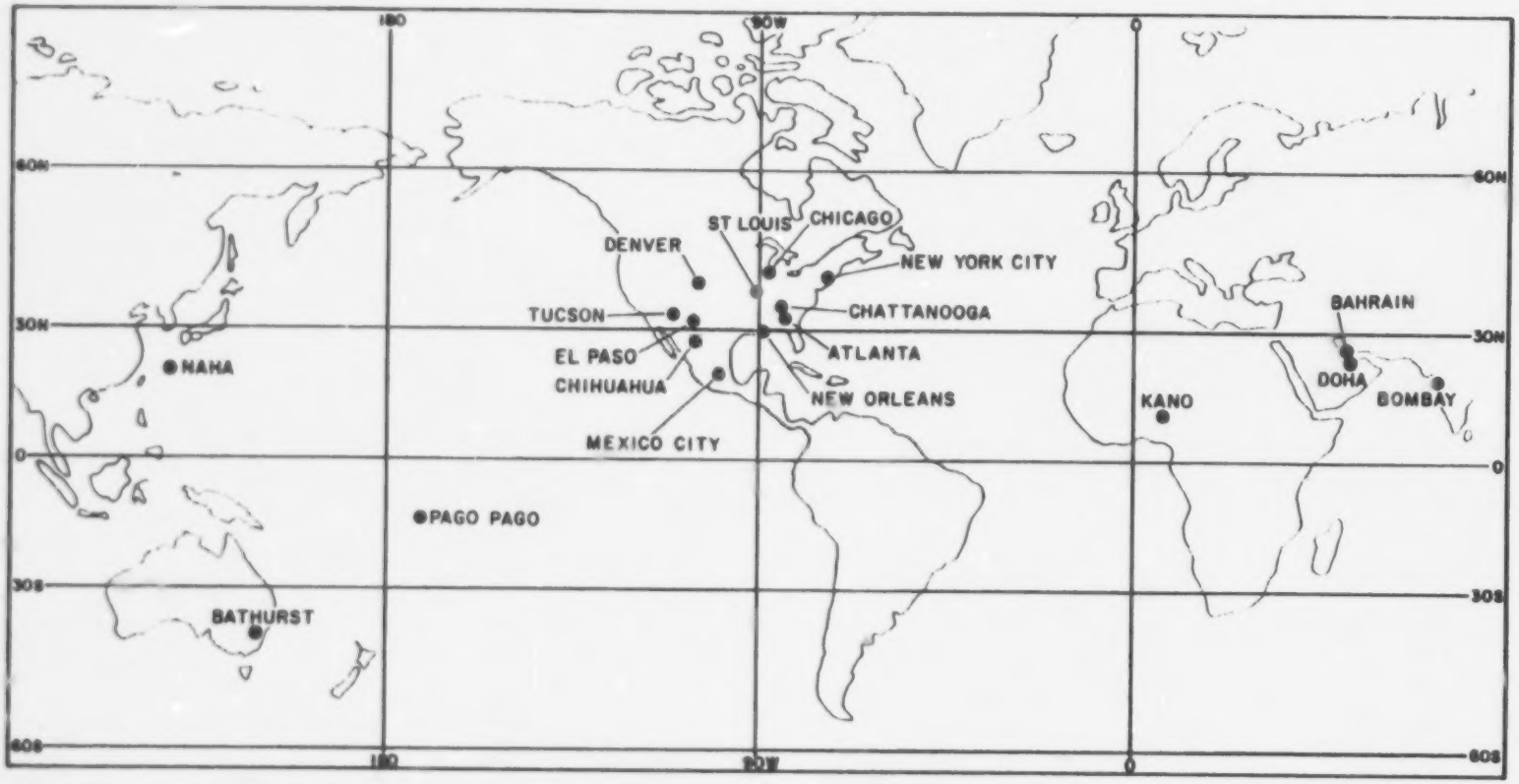

FIGURE 3.3.7-1 LOCATIONS OF MICROBURST-RELATED AIRCRAFT ACCIDENTS/INCIDENTS AROUND THE WORLD. BASED ON BOTH CONFIRMED AND UNCONFIRMED REPORTS AVAILABLE TO THE AUTHOR AS OF DECEMBER 1984.

(FUJITA, 1985)

3.4 Detailed Characteristics of Microbursts

(From: the general literature)

3.4.1 Microburst Visual Characteristics

Pilots traditionally have avoided thunderstorms (McCarthy, 1984). The aviation community has long known the seriousness of this hazard, and every pilot has been thoroughly trained to avoid the familiar dark and ominous clouds of thunderstorms, hailstorms, and tornadoes.

But regions of the sky where microbursts may lie hidden are something else to reckon with. They typically look benign. The potentially lethal low-altitude wind shear of a microburst may be packaged in a harmless-looking

rain shaft, or perhaps in the rain-free air below cloud base with no visible clues to warn of its presence. Sometimes there are tell-tale signs of the presence of a microburst that pilots can be trained to recognize. One of these is the sight of localized blowing dust near the ground. But, too often, microbursts can also occur in the heavy rain of a thunderstorm where they are obscured from view.

The best advice for pilots is not to pass through or under thunderstorms at any time. This is the surest way to avoid any microbursts imbedded in heavy rain. Based on the findings of the JAWS Project, this advice should be followed even when storm clouds look apparently harmless.

3.4.2 The JAWS Project

During the 1982 Joint Weather Studies Project JAWS 168 microbursts, 20 macrobursts, and 99 gust fronts where identified using surface sensors in the vicinity of Denver's Stapleton Airport (Bedard et al., 1986). Key results have been reported in four main areas: (a) statistical properties, (b) implications for wind shear detection, (c) implications for wind shear predictions, and (d) implications for wind shear modelling.

Data collected from the JAWS field program, conducted between 15 May and 13 August 1982, at Stapleton International Airport, provided a detailed picture of the microburst never before available to the meteorological community. Analysis of Doppler radar data collected on over 70 microbursts has enabled JAWS scientists to begin unraveling the mystery of wind shear.

3.4.2 The JAWS Project (cont'd)

The basic source of surface measurements was a Portable Automated Mesonet (PAM) system described by Brock and Govind (1977). Wind speed, wind direction, temperature, pressure, dew point and rain rate were provided at 1-minute intervals. These data were supplemented by wind velocity data provided at 11 seconds intervals from the airport Low-Level Wind Shear Alert System (LLWAS). The operation of LLWAS during the JAWS project is described by Bedard et al. (1985). Figure 3.4.2-1 shows the configuration of the PAM and LLWAS systems.

The other major data base was provided by three Doppler radars (CP-2 (10 cm), CP-3 (5 cm) and CP-4 (5 cm)), see the Appendix for electromagnetic theory relating to radars. These radars (Wilson et al., 1984) were located in a small triangle (with sides of 14, 18 and 28 km) with the southernmost radar located at the centre of Stapleton Airport. These research radars have 1 degree, half-power beam widths; CP-2 has a minimum detectable signal of -18 dBZ at 25 km (-116 dBm). These radars have excellent warm season, boundary-layer, optically clear air detection capabilities. CP-2 routinely observes reliable velocities throughout the boundary layer to a range of at least 100 km; the corresponding range for CP-3 and CP-4 is 50 km. However, both main beam and sidelobe ground clutter contamination can limit low-altitude wind observations.

3.4.2.1 Summary of Results (JAWS Program)

The statistics show a tendency for sporadic bursts of microburst activity during the summer months, rather than a broad peak with a relatively constant level of activity.

There is a well-defined diurnal variation in microburst activity (most occurring between 1200 and 2000 MDT), indicating the time interval during which heavy, summertime air traffic should be reduced in this region of the U.S.A whenever a microburst hazard is predicted.

The average wind vector change for impacting microbursts was 20 m/s while that for gust fronts was 13.7 m/s. Microbursts present a greater wind shear hazard than gust fronts, on the basis of total wind vector change.

The propagation speed for most microbursts was less than 4 m/s, many being essentially stationary. In contrast, most gust fronts moved with speeds from 4 - 12 m/s. Microbursts are a spatially stationary phenomenon relative to gust fronts.

Most microburst durations were between 4 and 30 min, most being less than 10 minutes. Gust fronts were much longer lived (30 to 80 minutes). Microbursts are a transient phenomenon relative to gust fronts.

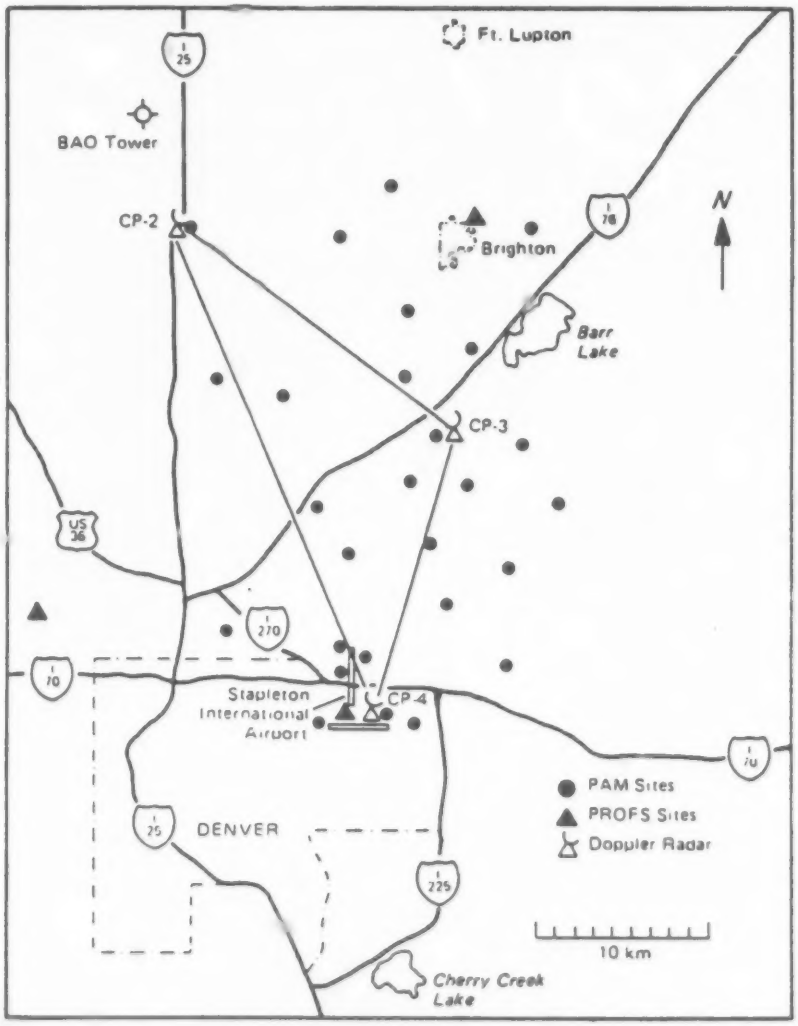

Map of JAWS Project research network, showing the location of three pulsed microwave Doppler radars (NVAR's CP-2, -3 and -4), and the 27 PAM stations (shown as dots)

From: Bedard and LeFebvre, 1986.

FIGURE 3.4.2-1 MAP OF JAWS PROJECT RESEARCH NETWORK

3.4.2.1 Summary of Results (JAWS Program) (cont'd)

Of the 168 microbursts in the Stapleton region, 54 were accompanied by measurable amounts of surface rain. This explains why there are often no visual clues of the presence of a descending microburst, most of the precipitation having evaporated during descent from the cloud base.

The average pressure change for microbursts that impacted the ground station was 0.66 mb. The average pressure change for microbursts not passing over a station was 0.24 mb. The difference suggests that the pressure field is a parameter that is sensitive to the distance from the measurement point. Widely varying values of temperature and pressure were measured for both microbursts and gust fronts, indicating the complexity of the problem of detecting these systems in the atmospheric boundary layer.

The microburst stagnation zone (the region directly beneath the descending downflow) is the most dangerous region in that it produces much larger local wind speed and wind vector changes than a more distant downflow region would produce. These results suggest the need for detecting microbursts directly beneath approach and take-off corridors and in the vicinity of runways.

These findings, that the strongest impacting microbursts are accompanied by the largest pressure changes (usually an increase), indicate the value of the use of pressure sensors as complements to wind sensors beneath approach and take-off corridors. Combined wind and pressure sensors offer advantages for the detection of microbursts.

No warning is provided of a descending microburst until the near-surface horizontal diverging flows are already occurring. The addition of pressure sensors may provide early warnings of microbursts descending above the sensor. Several minutes of additional warning are predicted from numerical and analytical calculations, and documented from tower measurements.

It was found that "wet" microbursts (those accompanied by surface rain) with the highest rain rates occur with the largest wind vector changes. This is in agreement with theoretical predictions and suggests that high-resolution radar measurements could estimate the severity of wind shear to be expected from descending rain shafts.

It was found that microbursts were more probable at higher, 500 to 700 mb, lapse rates, and that the 1800 GMT sounding correlated more highly with microburst occurrence than the 1200 GMT sounding did. More than 80% of microbursts were detected in 1800 GMT soundings with lapse rates greater than 8 degrees per km.

3.4.2.1 Summary of Results (JAWS Program) (cont'd)

The JAWS study shows that microbursts tend to occur in the vicinity of gust fronts, convergence lines, mesocyclones, and anticyclones. Outflow boundaries should be considered regions where the possibility of severe wind shear from microbursts is especially high.

Purdom (1982) has established that satellites provide an existing capability for tracking outflow boundaries.

Bedard et al. (1986) suggest that gust fronts are preferred regions for microburst occurrence. They recommend using Doppler radar to search the vicinities of gust fronts for indications of the existence of dynamic forcing processes (e.g., higher reflectivity returns indicating initiation of convection).

The gravity current relation, the fact that the pressure nose magnitude and the microburst wind speed change are related through Bernoulli's law (see later in Figure 3.4.3-6), and the relationship between rain rate and microburst wind vector change, all provide means of testing the applicability of microburst models.

Bedard et al. (1986) also recommend the combined use of wind and pressure sensors. Bedard (1984) calculated that an additional warning time of more than 2 minutes may be obtained for descending microbursts. The magnitude of the pressure nose is an indicator of the strength of the microburst. Because the most hazardous situation is for aircraft flying through the centre of microbursts (Frost et al., 1984), they suggest that approach zones are key regions for locating surface sensors. Because of the small scales and fine structure of microbursts, there is a need for sensor spacings of less 1 km. There is a need to develop techniques for discriminating against false alarms. It is felt that it may be possible to develop algorithms that specifically identify aircraft wake vortices, microbursts, gust fronts, and other small-scale disturbances.

3.4.3 The Microburst Examined

3.4.3.1 Wind Velocity

Figure 3.4.3-1 gives the results of an analysis of some data which were recorded on July 14, 1982 by the multiple Doppler radars that formed part of the JAWS instrumentation research network (McCarthy, 1984). They show the air flow pattern associated with a microburst. In particular, these diagrams illustrate two important features of a microburst, i.e. (1) the diverging air flow seen at the Earth's surface and (2) the intense downdraft seen in the microburst centre. Figure 3.4.3-2 shows the frequency of microbursts detected by Doppler radar over a 91 day period as a function of the time of day at which they were detected. Notice that the microburst events tended to peak during the early afternoon and again in the early evening and were generally associated with the convective weatherpeaks.

The intensity of Doppler radar-detected microbursts can be seen in Figure 3.4.3-3, which shows the microburst frequency as a function of the maximum differential wind velocity near the Earth's surface. In this illustration, the maximum headwind velocity difference is shown. This change in velocity ranged from 10 - 50 m/s (approximately 20 - 100 knots). One microburst observed by Doppler radar had a differential of 48 m/s (100 knots). In Figure 3.4.3-4, data from both the Low-Level Wind Shear Alert System (LLWAS) and the NCAR Portable Automated Mesonet (PAM) surface weather station system have been combined to show the maximum wind velocity for a particularly severe microburst event at Stapleton. In this case, the velocity differential over the north-south runways is approximately 85 knots. The shear was one of the most severe seen in JAWS and is believed to be unflyable either on an approach-to-landing or immediately upon takeoff. The microburst differential that brought down Pan Am Flight 759 was only 24 m/s, or approximately the median value of radar-observed JAWS microbursts.

When 50 microbursts were examined thoroughly with Doppler radar, it was found that 50 percent reached their maximum intensity within 5 minutes after first detection while 95 percent did so within 10 minutes from the time the diverging outflow first appeared at the surface. Sometimes the microburst dissipated within 5 to 10 minutes, with the maximum velocity differential increasing from 12 to 24 m/s in this period. Furthermore it was found that microbursts are not circularly symmetric in their horizontal diverging outflow as implied back in Figure 3.1-1, but are decidedly asymmetric. They are also clearly small-scale events, being only 1.8 km in diameter when first detected and growing to only 3.1 km on the average in 6.4 minutes, Figure 3.4.3-5.

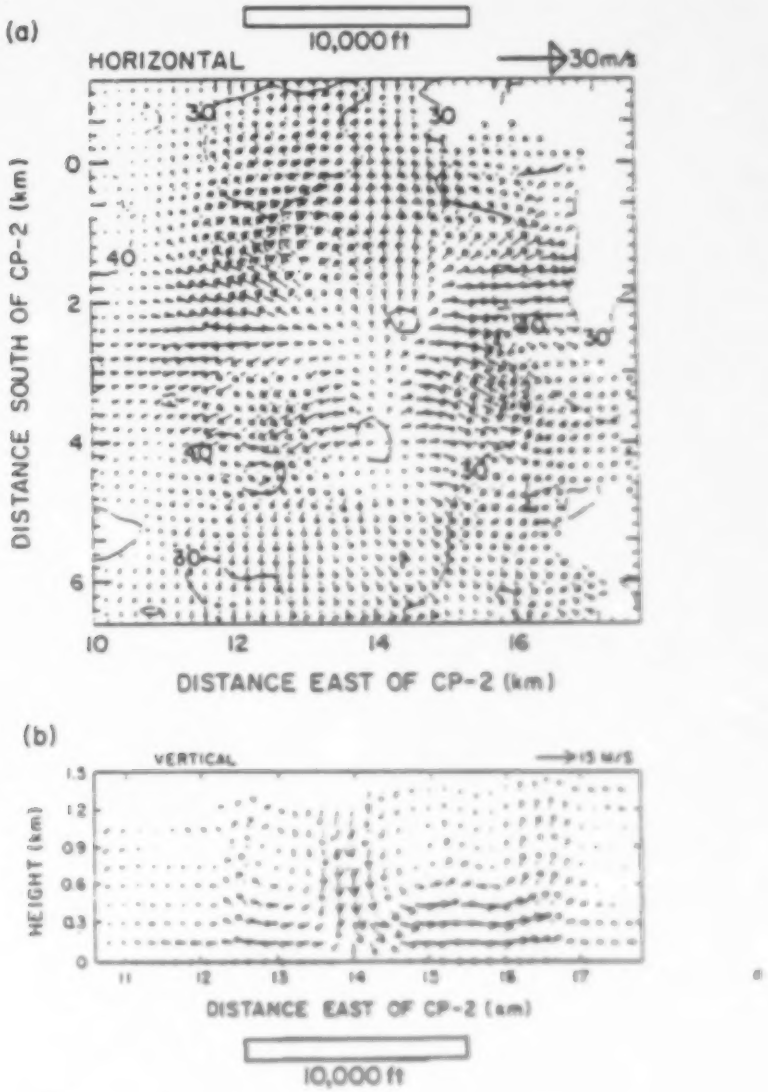

Dual Doppler radar analysis of a severe microburst, as seen over the JAWS network on 14 July 1982. Shown are (a) the horizontal wind field near the earth's surface (notice the strong diverging outflow typical of a microburst), and (b) a vertical cross section through (a) which shows the downdraft, outflow, and a commonly observed horizontal vortex circulation. Note also how remarkably similar this cross section airflow is to the "schematic" of Figures 3.1-1/3.1-2. For reference, typical 10,000 ft. jet runways are shown on the figure. This illustrates the small scale of the microburst.

From: McCarthy, 1984.

FIGURE 3.4.3-1 VELOCITY FIELDS BASED ON A DUAL DOPPLER ANALYSIS

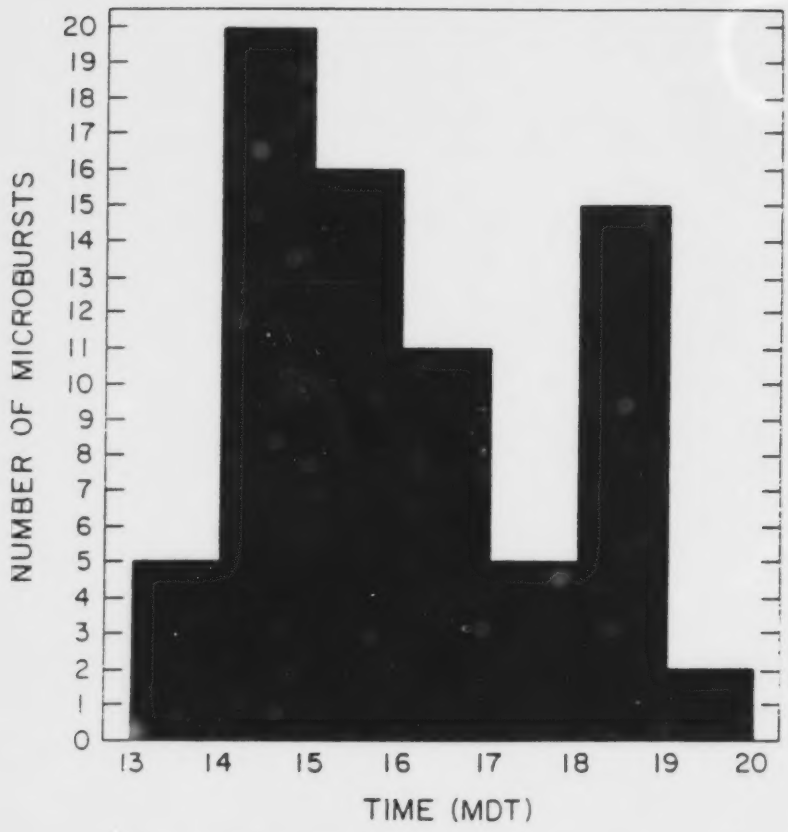

Number of JAWS microbursts identified by Doppler radar over a 91-day period as a function of the time of day. These microbursts are clearly related to convective phenomena, with significant peaks near 1400 and 1800 hours.

From: McCarthy, 1984.

FIGURE 3.4.3-2 NUMBER OF JAWS MICROBURST AS A FUNCTION OF TIME OF DAY

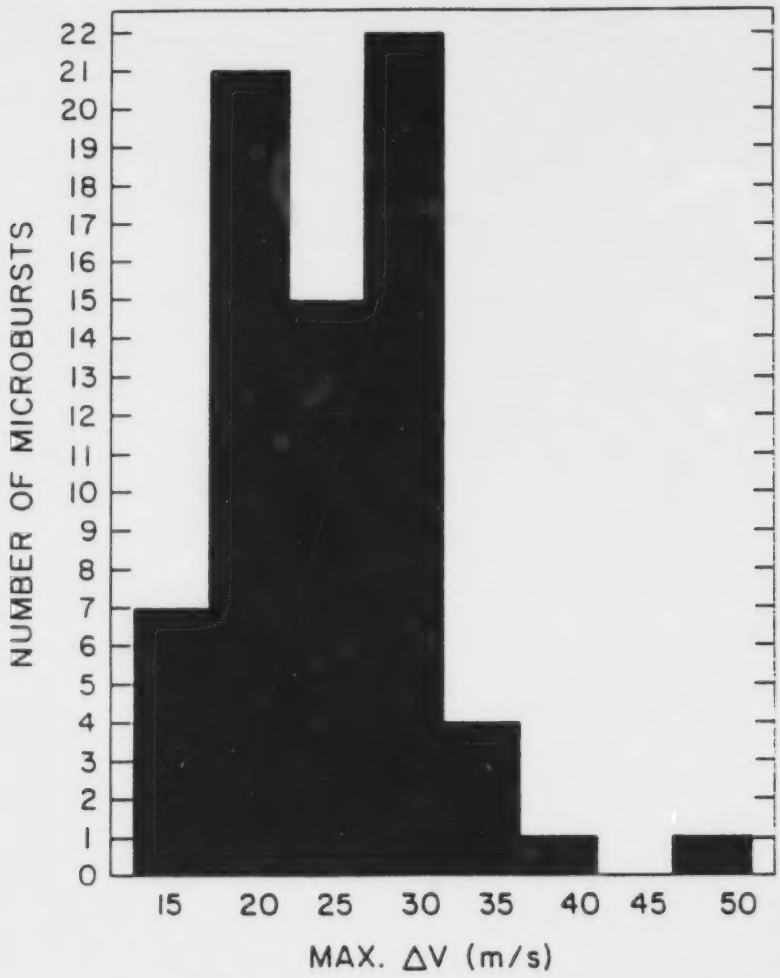

Number of JAWS microbursts as a function of the maximum differential velocity measured near the earth's surface by Doppler radar. The figure shows the approximate maximum headwind-to-tailwind shear that an aircraft would encounter.

From: McCarthy, 1984.

FIGURE 3.4.3-3 NUMBER OF JAWS MICROBURST AS A FUNCTION OF MAXIMUM DIFFERENTIAL VELOCITY

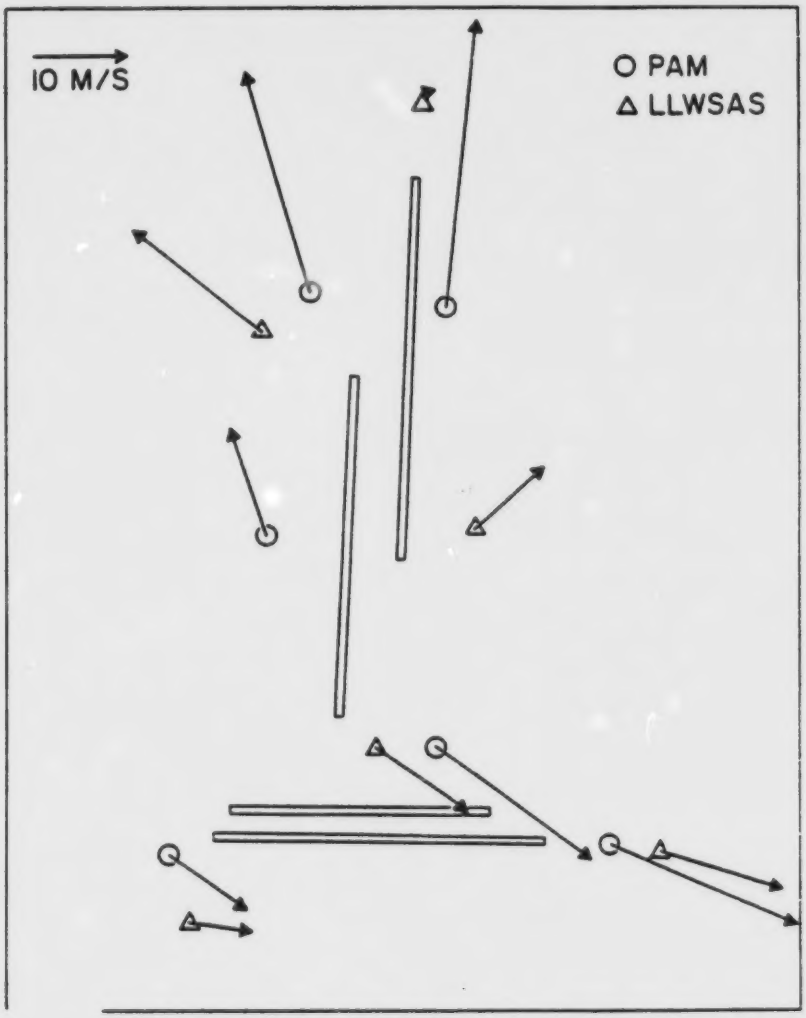

Merging of LLWSAS and NCAR PAM wind velocity data for 1359 Mountain Daylight Time, 15 July 1982, over Stapleton. In this situation, a 43 m/s (85 knot) headwind/tailwind differential existed along the pair of N-S runways. This is considered to be a lethal low-altitude wind shear which, fortunately, no aircraft encountered.

From: McCarthy, 1984.

FIGURE 3.4.3-4 WIND VELOCITY DATA OVER STAPLETON AIRPORT, 1982.

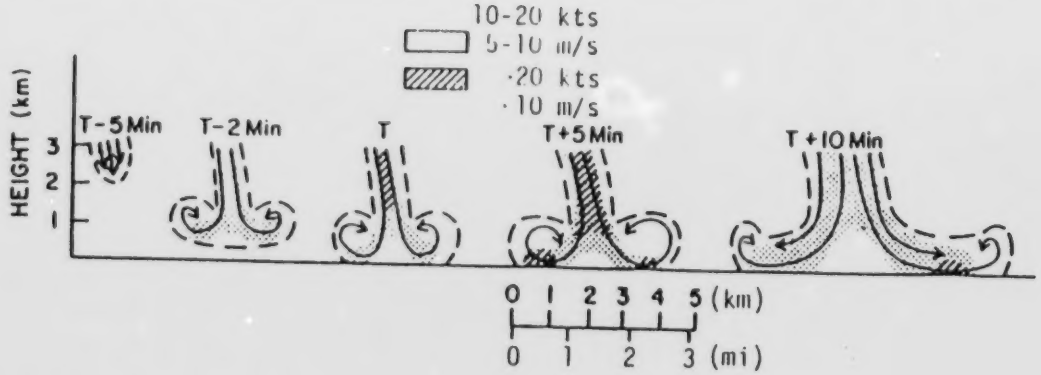

Vertical cross section of the evolution of the microburst wind field, based on a summary of examining 50 microbursts with Doppler radar. T is the time of initial divergence reaching the surface. Notice that it takes about 5 minutes after T for the microburst to reach maximum intensity. In addition, the divergence is observed above the surface several minutes before impact with the surface. Note the small scale of the phenomena, typically less than the length of a jet runway.

From: Frost, W., Ho-Pen Chang, K.L. Elmore, and J. McCarthy, "Microburst wind shear models from Joint Airport Weather Studies (JAWS)", DOT/FAA/PM-85-18 Final Report, June 1985.

FIGURE 3.4.3-5 EVOLUTION OF A MICROBURST, VERTICAL CROSS SECTION

3.4.3.2 Radar Reflectivity

Conventional aviation wisdom uses radar echo intensity (radar reflectivity) as an indication of storm severity. The more intense the return is, the more likely the "thunderstorm" will be severe. Of course, a conventional weather radar cannot measure windspeed. Figure 3.4.3-6 shows the correlation between microburst echo intensity (reflectivity) as seen on conventional radar and maximum velocity differential. Clearly, there is no correlation, with strong microburst wind shears having reflectivities ranging from nearly zero to above 70 dBZ. Hence, it is clear that a conventional airborne or ground-based radar cannot be used to detect severe microburst wind shears.

3.4.3.3 Rain Rate, Temperature and Pressure

In Figure 3.4.3-7 is shown a plot of maximum vector change at a single station as a function of the events rain rate maximum. This plot includes data for both microbursts and macrobursts, restricted to events with temperature decreases and pressure increases accompanied by some rain. Dry microbursts are not included (Bedard et al., 1986). These restrictions probably identify cases that are well represented at the surface, whose measured vector changes are not influenced by the presence of ground-based inversions. It is evident from Figure 3.4.3-7 that for "wet" microbursts, the strength of the surface wind vector change tends to be proportional to rain rate. Many dry microbursts produce large surface wind vector changes. Keeping this in mind, the results of Figure 3.4.3-7 suggest that rain rate is one of several parameters controlling the transfer of mass from the cloud base to the surface.

Figure 3.4.3-8 is a plot (including all microbursts with no restrictions) of the maximum pressure change measured in the PAM array (for the stations influenced by the microburst) as a function of the mean temperature change associated with the microburst. This plot shows significant scatter and a trend for the larger pressure increases to be associated with the decrease in temperature, as might be expected from the influence of the hydrostatic forces.

The value of restricting data is also illustrated in Figure 3.4.3-9. The open symbols in the figure represent the maximum wind vector change measured at one station as a function of the mean temperature change associated with the microburst. This plot, for all microbursts with no restrictions, shows considerable scatter with no evidence of a relationship. On the other hand, the solid symbols identify those microburst events with some rain, positive pressure changes, and temperature drops. This portion of the data set indicates a weak trend for the largest wind vector changes to occur with the largest temperature drops. The restrictions probably limited the data set to events that were well represented at the surface, again implying the other processes complicate the analysis of surface data for microbursts.

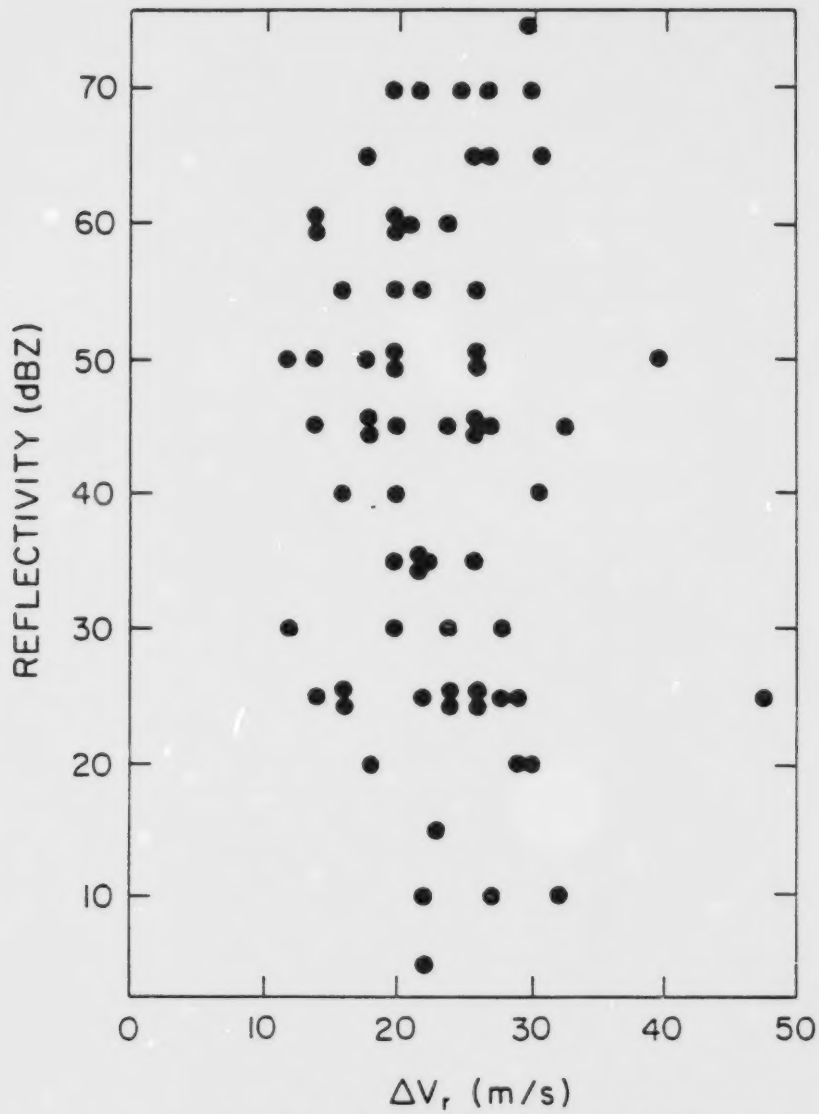

Plot of maximum radar reflectivity (echo intensity) as a function of maximum velocity differential. Serious low-altitude microburst wind shear can occur in a wide range of convective intensity, from non-thunderstorms (reflectivities generally less than 30 dBZ) to intense thunderstorms (reflectivities greater than 50 dBZ). In addition, severe shear can occur when the reflectivities are quite low, requiring very sensitive detection capabilities.

From: Bedard and LeFebvre, 1986.

FIGURE 3.4.3-6 RADAR REFLECTIVITY AGAINST MAXIMUM VELOCITY DIFFERENTIAL

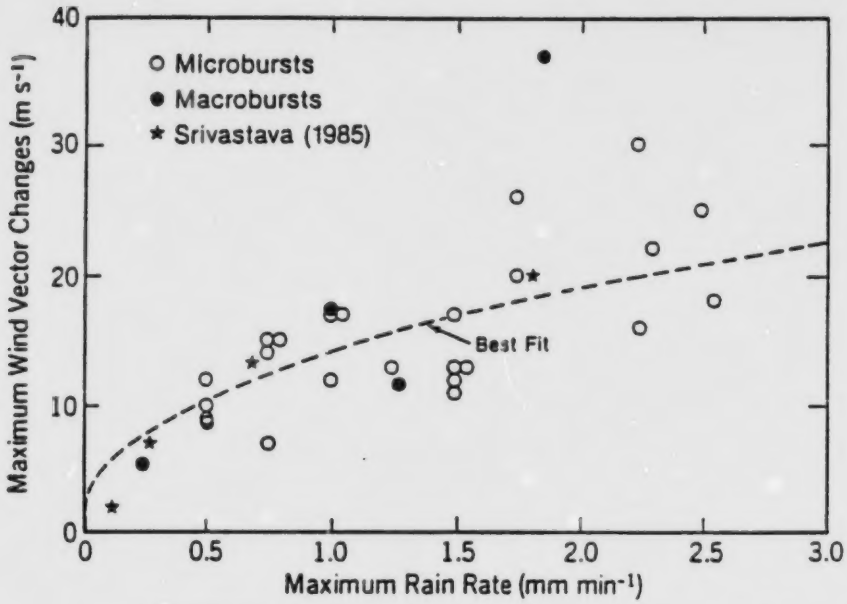

Maximum vector change for microbursts and macrobursts at a single station as a function of the rain rate maximum associated with each event. These data are for all microbursts accompanied by rain, temperature decreases, and pressure increases. The dashed line is a best fit to the microburst data, with a correlation coefficient of .51 for the 24 data points, is evidence of a significant relationship. The starred points are from the theoretical calculations of Srivastava (1985).

From: Bedard and LeFebvre, 1986.

FIGURE 3.4.3-7 WIND VECTOR CHANGE AGAINST RAIN RATE

From: Bedard and LeFebvre, 1986.

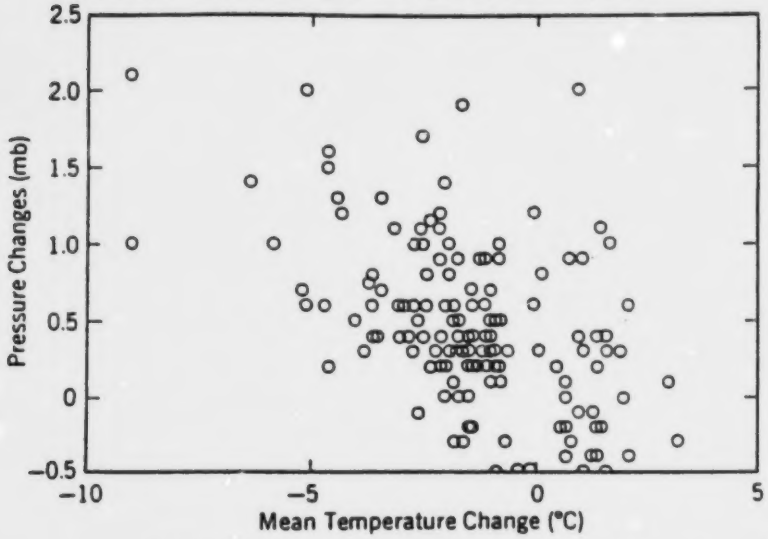

Maximum pressure change measured in the PAM array as a function of the mean temperature change associated with the microburst. This plot includes all microbursts with no restrictions. It illustrates the wide variety of combinations of pressure and temperature changes that accompany microbursts.

FIGURE 3.4.3-8 PRESSURE CHANGE AS A FUNCTION OF TEMPERATURE

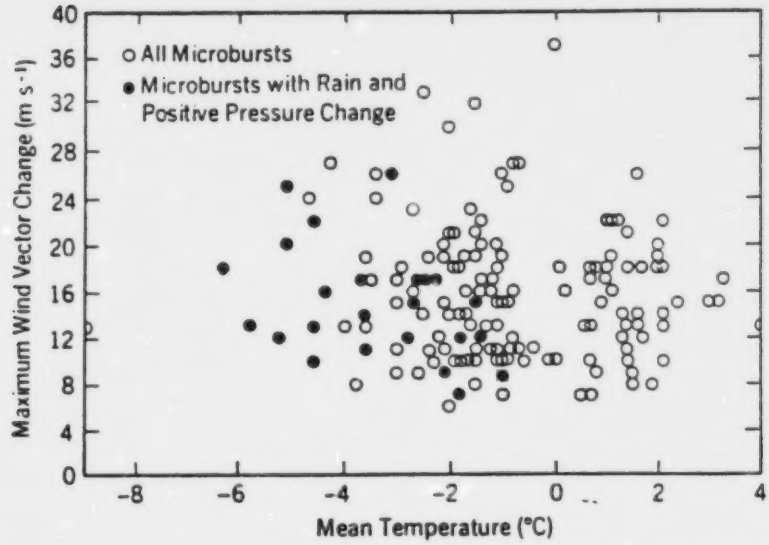

Maximum wind vector change at one PAM station as a function of the mean temperature change associated with the microburst, for all microbursts with no restrictions, over the range of temperature changes from -9°C to +4°C. Microbursts with some rain, positive pressure changes, and temperature drops appear as solid circles. Plots (a) and (b) underline the complexity of the surface parameter changes that accompany microbursts.

FIGURE 3.4.3-9 WIND VECTOR CHANGE PLOTTED AGAINST TEMPERATURE

3.4.3.3 Rain Rate, Temperature and Pressure (cont'd)

Figure 3.4.3-10 is a plot of maximum wind speed change as a function of pressure changes (greater than 0) for all microbursts. There is considerable scatter on this plot and no evidence of a relationship.

Figure 3.4.3-11 is a plot of maximum speed change as a function of pressure change for all impacting microbursts showing positive pressure changes. A curve has been added representing the relation between pressure and wind magnitude change according to Bernoulli's law, $P = 1/2\ U^2$. Some past surface measurements of impacting microbursts are shown on this plot. In contrast to Figure 3.4.3-10, Figure 3.4.3-11 shows that a clear relationship between wind speed and pressure change exists when the data set is restricted to impacting microbursts.

No evidence of a relationship was found between dew point change and the strength of impacting microbursts. Also, based on the analysis that was conducted there seems to be no correlation between the magnitudes of temperature drops and the associated speed change.

Figure 3.4.3-12a depicts a conceptual midair microburst directly over a surface station. In this example the downward inertial forces of the microburst are not sufficient to overcome the negative buoyancy forces of the ground-based inversion. A small pressure decrease resulting from the removal of a portion of the stable air may be the only surface perturbation. Conversely a stronger microburst could penetrate to the surface (Figure 3.4.3-12c), initially producing a pressure decrease as the dense, stable air is removed. A pressure nose will follow as the stagnation pressure from the descending air builds up. A temperature decrease will typically accompany this situation. If the microburst is translating, a complex series of wind, temperature, and pressure changes can result. These will differ depending upon the initial relative positions of the impacting microburst and the measurement station.

3.4.3.4 Microburst Formation

Five mechanisms (McCarthy & Wilson, 1984) have been proposed that may cause or contribute to the microburst downdraft: cooling of air by the evaporation of falling rain; cooling from melting precipitation; frictional drag from falling precipitation; dynamically induced pressure gradients; and downdraft transport of horizontal momentum. In addition, it has been proposed that rotation of the downdraft will restrict its dimensions so that a diverging outflow will be confined over a smaller area. Of these forcing mechanisms, precipitation melting, precipitation drag, and evaporation cooling are thought to be the most common. Evaporative cooling may occur as precipitation falls into the dry subcloud air or by entraining dry air above cloud base.

From: Bedard and LeFebvre, 1986.

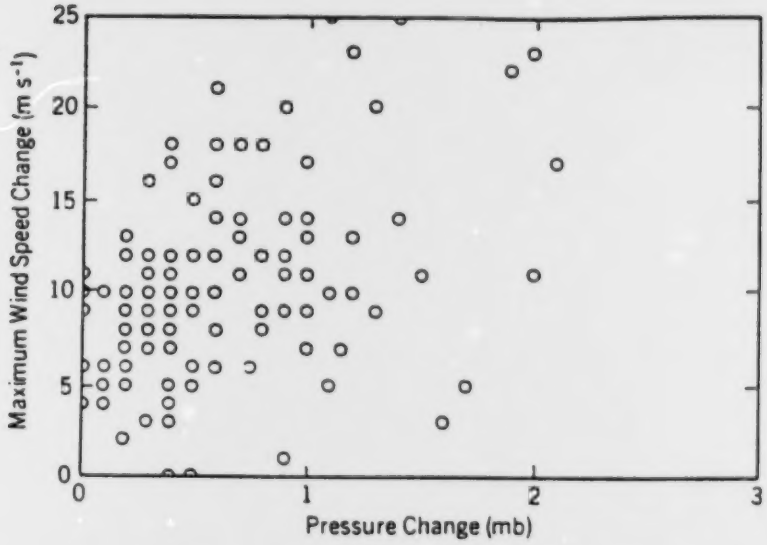

Maximum wind speed change measured at one PAM station as a function of pressure increses (>0) associated with microbursts. This scatter plot includes all microbursts and shows little evidence of any relationship.

From: Bedard and LeFebvre, 1986

FIGURE 3.4.3-10 MAXIMUM WIND SPEED CHANGE PLOTTED AGAINST PRESSURE CHANGE

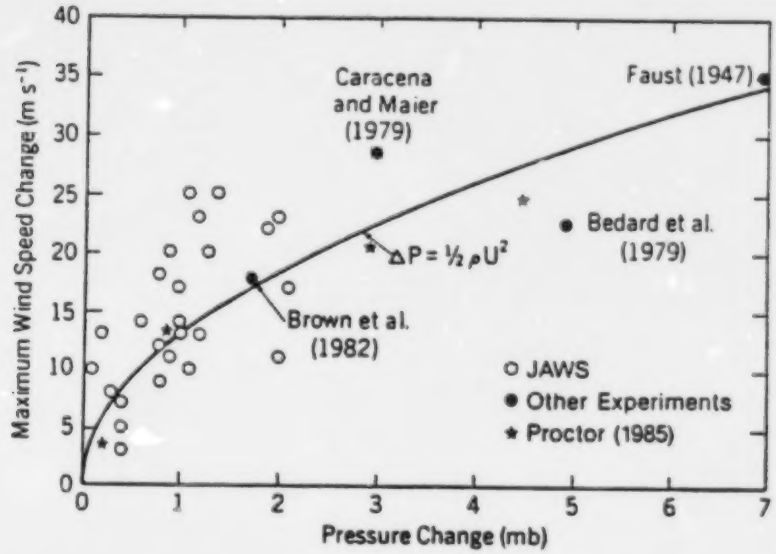

Maximum wind speed change as a function of pressure change for all impacting microbursts showing pressure increases. The few existing past measurements of impacting microbursts appear as solid circles. The solid line is Bernoulli's law, showing a correlation coefficient of .58 for the 27 data points. In contrast with Figure 3.4.3-10 this is evidence that for impacting microbursts the pressure change is related to the wind speed change.

FIGURE 3.4.3-11 MAXIMUM WIND SPEED CHANGE AS A FUNCTION OF PRESSURE

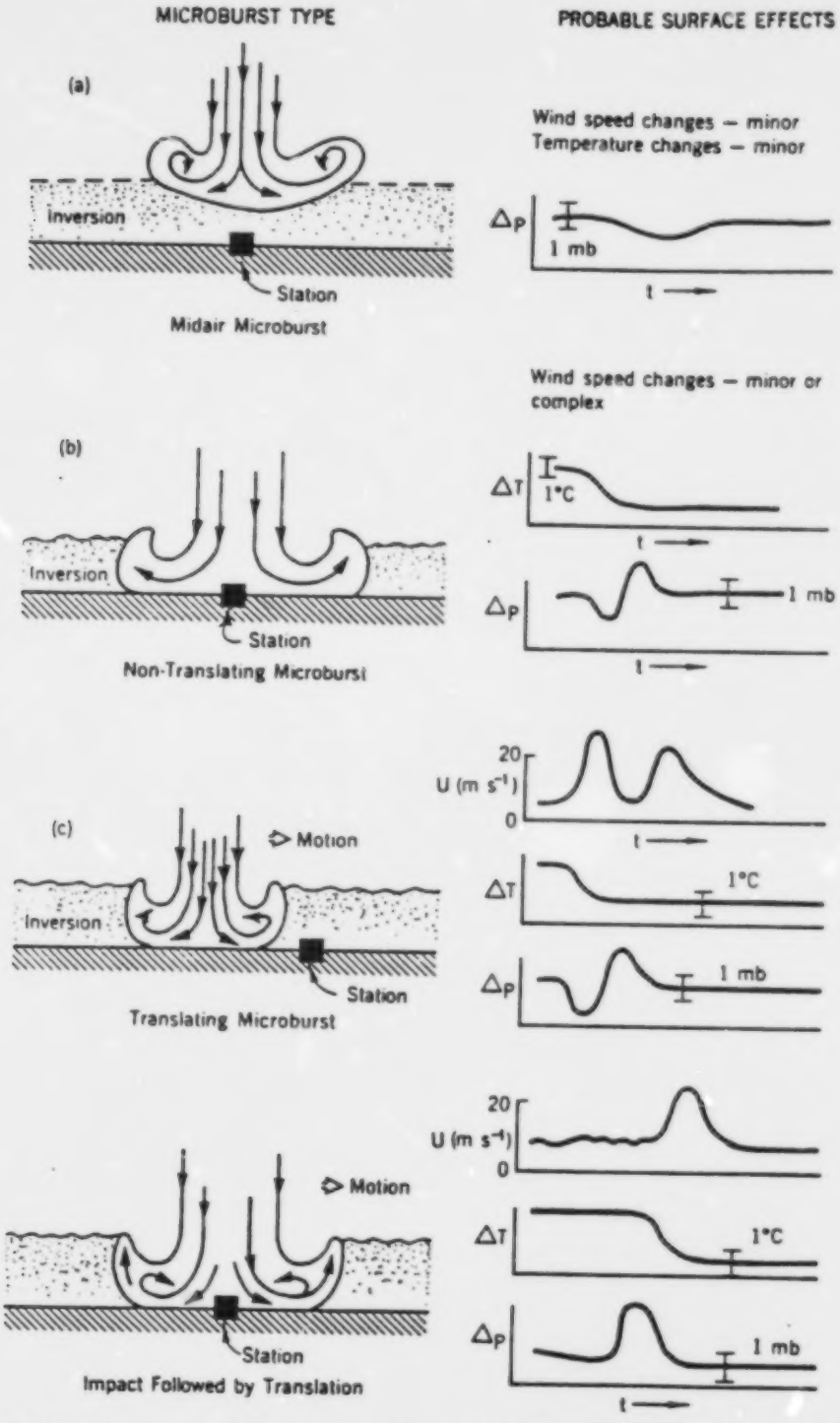

FIGURE 3.4.3-12 PROCESSES POSSIBLY CAUSING THE VARIETY OF PRESSURE DISTURBANCES FOR IMPACTING MICROBURSTS (COMMON FOR MORNING HOURS IN SUMMER)

3.4.3.4.1 Moderate Reflectivity Storms (40 - 55 dBZ)

Figure 3.4.3-13 is a conceptual model of a moderate type storm (Roberts & Wilson, 1986). Typically, the storm is reaching its maximum height at T-10 min. At this time dry air, as indicated on the sounding, may be penetrating into the storm above 4 km. Some convergence is usually present within the storm. Six minutes prior to microburst occurrence, Figure 3.4.3-13a, the precipitation core has typically begun its descent. By time T (Figure 3.4.3-13b), radial convergence has increased, azimuthal shear may be evident, and possibly a reflectivity notch is becoming more apparent from 3 to 6 km AGL. The maximum reflectivity core has descended from 6 km (Figure 3.4.3-13a) and is collocated with the first signs of diverging outflow at the surface. Finally, 5 min later (Figure 3.4.3-13c), the convergence is observed at 3 km and rotation may be more obvious. This storm typically dissipates as the microburst attains its maximum strength.

3.5 Canadian Wind Shear Assessment

As a result of this literature search it has become obvious that very little is known about either the likelihood of the occurrence or the characteristics of microbursts in Canada. This lack of information may stem from the fact that no fatalities can be attributed to microburst-related wind shear conditions at Canadian airports. Therefore, public safety has not been a driving force, as it has been in the United States, for directing research towards learning more about microbursts so that the likelihood of a wind shear related accidents can be reduced. In fact, from information made available by the Canadian Aviation Safety Board (Canada-Aids), it has been revealed that in the period from 1976-1983 only one accident involving the landing or takeoff of commercial- sized aircraft at Canadian airports could be related to wind shear. This accident involved a B737-200 at Sault Ste. Marie, Ontario, on January 2, 1982 at 2138 EST. Weather conditions were: sky obscured, visibility 3/4 miles in blowing snow, winds 26 knots. No injuries occurred and the Captain reported a "hot landing". Clearly, this wind shear occurrence could not be attributed to thunderstorm activity, when the date, time and winter-time weather conditions are considered. In the information provided by the Aviation Safety Board there are 29 other cases listed, involving light aircraft and helicopters, in which wind shear is listed as the likely cause for the accident.

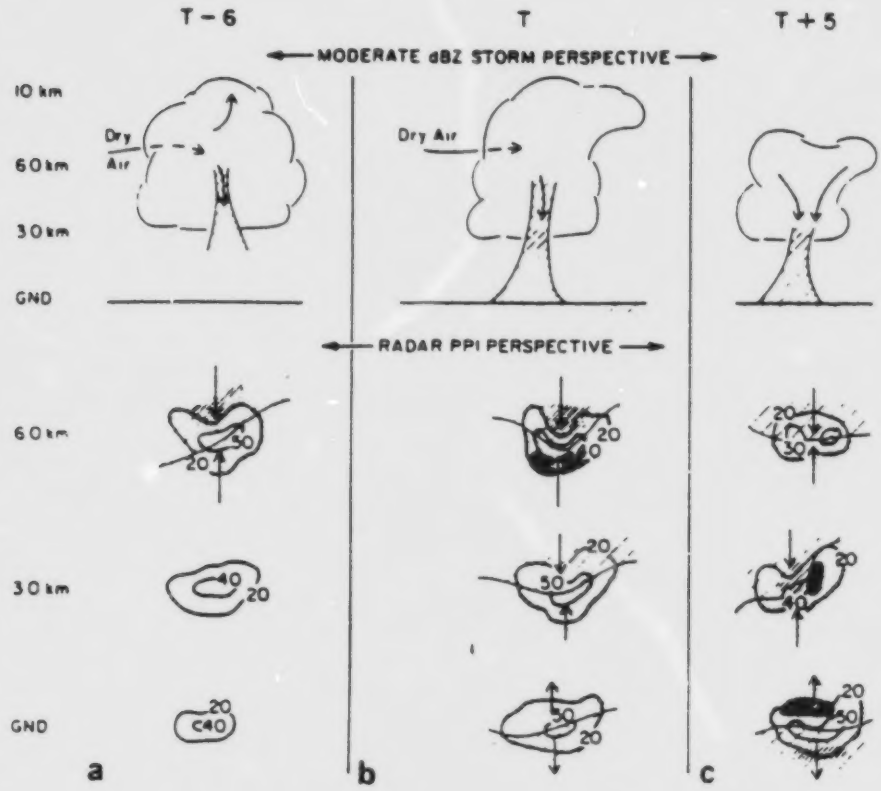

A schematic representation of the evolution of a moderate reflectivity, microburst-producing storm. The storm evolution is shown at the top of the figure. The hatched area indicates the area of precipitation. The evolution of the radar signatures at 3 altitudes are shown in the lower half of the figure. (T) indicates the time of microburst occurrence. Contours are reflectivity (in dBZ_e). Lightly shaded and hatched regions represent opposing radial velocities (see arrows) of 6 m/s. Darker shaded and hatched regions denote velocities of 12 m/s. (a) T-6 min; (b) T min; (c) T+5 min.

From: Roberts and Wilson, 1986.

FIGURE 3.4.3-13 SCHEMATIC OF EVOLUTIONARY MICROBURST REFLECTIVITY

3.5 Canadian Wind Shear Assessment (cont'd)

Programs such as the U.S. NIMROD and JAWS are multi-million dollar operations in terms of capital, operational, data collection and analytical costs. The information these studies have provided about microbursts and wind shear for specific storms and individual locations is tremendous. The major shortcoming lies in the fact that the results are not easily extrapolated to other U.S. locations, or for that matter, to any Canadian airport. In principle, one would expect that two locations, like New York and Toronto, which have similar climatic conditions, would have similar probabilities of occurrence of microbursts. No studies have, as yet, been carried out which show that the probability of microburst occurrences can be reliably predicted from one area to another. The fact that microbursts are difficult to detect by the naked eye and conventional radars, explains why no practical data base has been assembled in Canada. Basically, fundamental research is required, see Section 3.6 Future Needs, in Canada so that a better understanding of microbursts is developed, as well as the risk that they may pose at Canadian airports. An effort should be made to continue to monitor the U.S. experience with respect to their Doppler radar networks. One thing that is known for certain is that microbursts will not honor the Canadian-United States border (Fujita, 1987). What is known is that Canadian and other lives are at risk - the unknown is how big is the risk.

This survey into the literature has revealed that thunderstorms are one of the meteorological phenomena that spawn microbursts. It should be noted, though, that this is not an all encompassing criteria for determining the likelihood of the occurrence of microburst because they are observed to occur without thunderstorm activity. Also it has been found that microbursts are related in some way to tornadoes. The dynamics of this relationship is unknown at the present time. Since statistics exist in Canada with regards to the occurrence of thunderstorms and tornadoes, one might attempt to estimate the probability of occurrence of microbursts based on these statistics. This evidence is probably circumstantial at best, but it is the best that we have. One obviously has to use the best information that is available, regardless of how sketchy it might be, for estimating the likelihood of the occurrence of microbursts in Canada. The danger in making this estimate based on the incidence of thunderstorms and tornadoes is that the level of risk will be underestimated.

Figures 3.5-1 and 3.5-2 present maps of the U.S. and Canada depicting the mean number of thunderstorms. Of interest in the figures is the relative concentration of thunderstorms in the Gulf States, and the fact that the isolines have lower values over Canada. Except for Windsor, no station in Canada reports more than 30 thunderstorm-days per year.

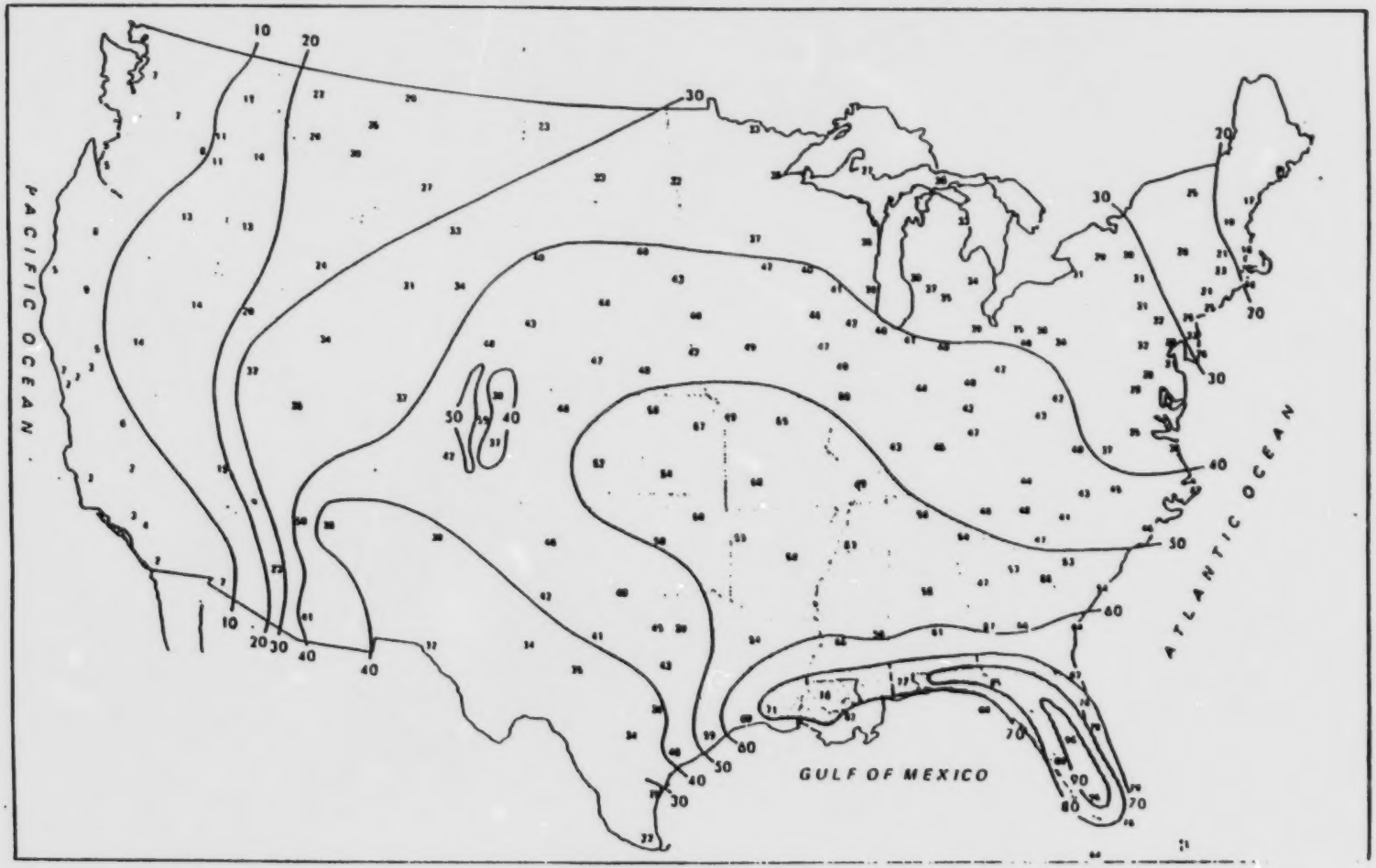

FIGURE 3.5-1 Mean Number of Days per Year with Thunderstorms; 1951-1975. (Source: Court and Griffiths, 1982).

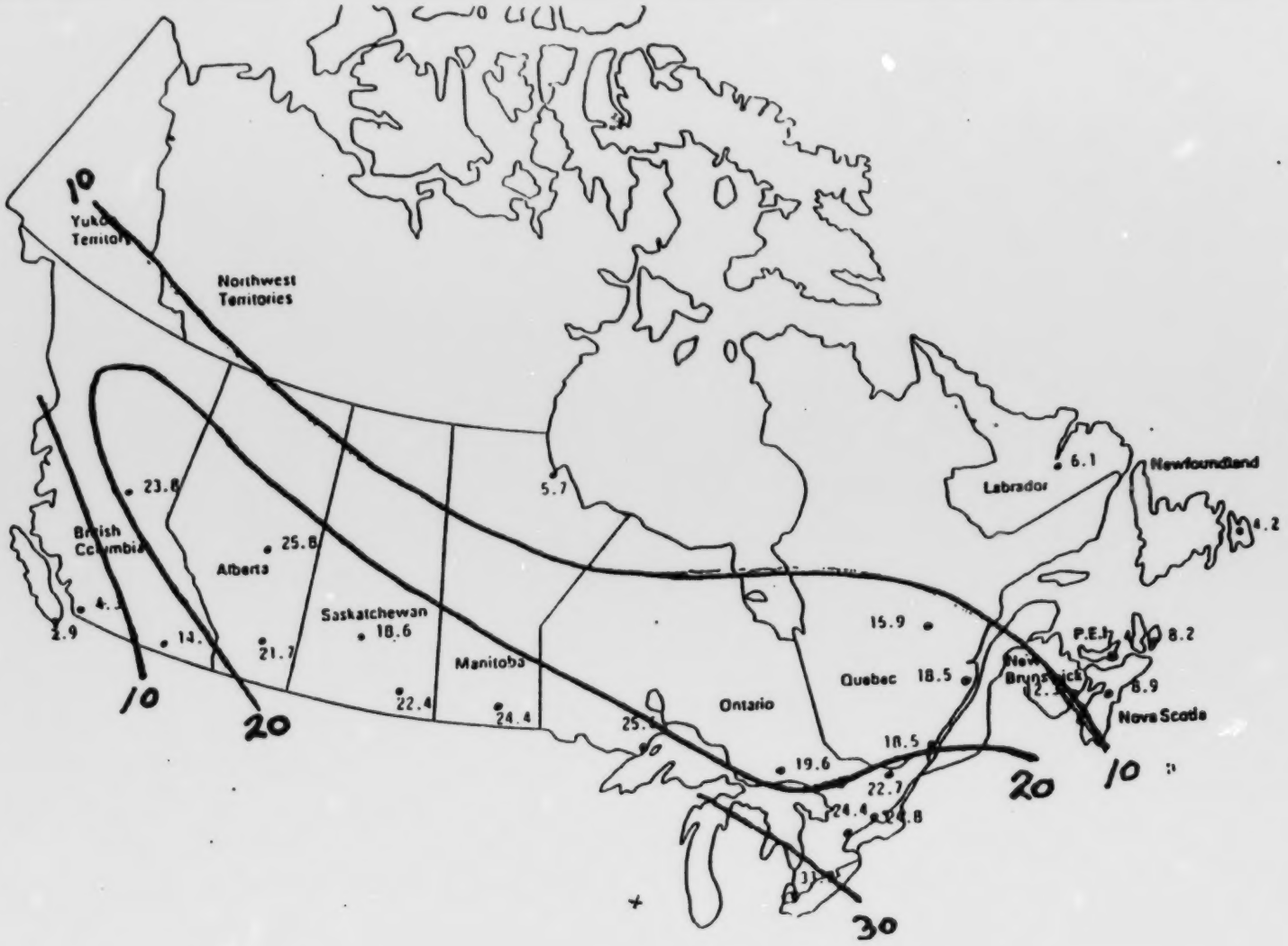

FIGURE 3.5-2 MEAN NUMBER OF DAYS PER YEAR WITH THUNDERSTORMS; 1941-1970

3.5 Canadian Wind Shear Assessment (cont'd)

Since thunderstorms infer the presence of downburst activity and related wind shear; contrasting the thunderstorm-days in Canada and the U.S. one may conclude that, in general, wind shear occurs with less frequency in Canada than in the U.S. As well, by looking at these sort of results one can make the following conclusions:

a. there should be a minimum frequency of occurrence of microbursts at Pacific or Atlantic airports, while airports such as Edmonton, Thunder Bay, Toronto or St. Hubert would be five times as likely to experience a microburst.

b. Since the annual occurrence of thunderstorms at Kennedy airport is 26 per year, which is comparable to most Canadian inland airports, one might conclude that the risk of microburst occurrence at Canadian inland airports is as great as at Kennedy. (Fujita has chronicled the accident of Eastern 66 at Kennedy, caused by a microburst, in which there was a loss of 112 lives.)

c. Since the vertical development in thunderstorms is a function of tropopause height, and since summertime tropopause heights are greater over the U.S. than in Canada, it can be concluded that the induced microbursts would be stronger in the U.S. than in Canada.

d. During the summer months of June, July and August, it is likely that those inland Canadian airports with a frequency of thunderstorm occurrence of 5-6 per day, would experience 20-30 identifiable microbursts each month.

The frequency of tornadoes in Canada is another statistic one might consider when attempting to estimate the likelihood of the occurrence of microbursts at Canadian airports. In Figures 3.5-3 and 3.5-4 are shown the seasonal and diurnal distributions of tornadoes in Western Canada for the period between 1890-1958. From these data one sees that if in fact there is a relationship between tornadoes and microbursts then the worst months for microbursts in Canada would be June, July and August. This is the same conclusion that was reached by looking at the incidence of thunderstorms in Canada. The other interesting fact is that in a period of 60 odd years there were 242 tornadoes in Western Canada. One concludes that these were major tornadoes because by and large the statistics were compiled from newspaper clippings as well as interviews of people who had personally experienced the tornadoes. This is on average the occurrence of 4 tornadoes per year. One asks the question; if major events such as tornadoes occur with this rate of incidence how much more often do microbursts occur, which on a scale of meteorological events fall far short of tornadoes.

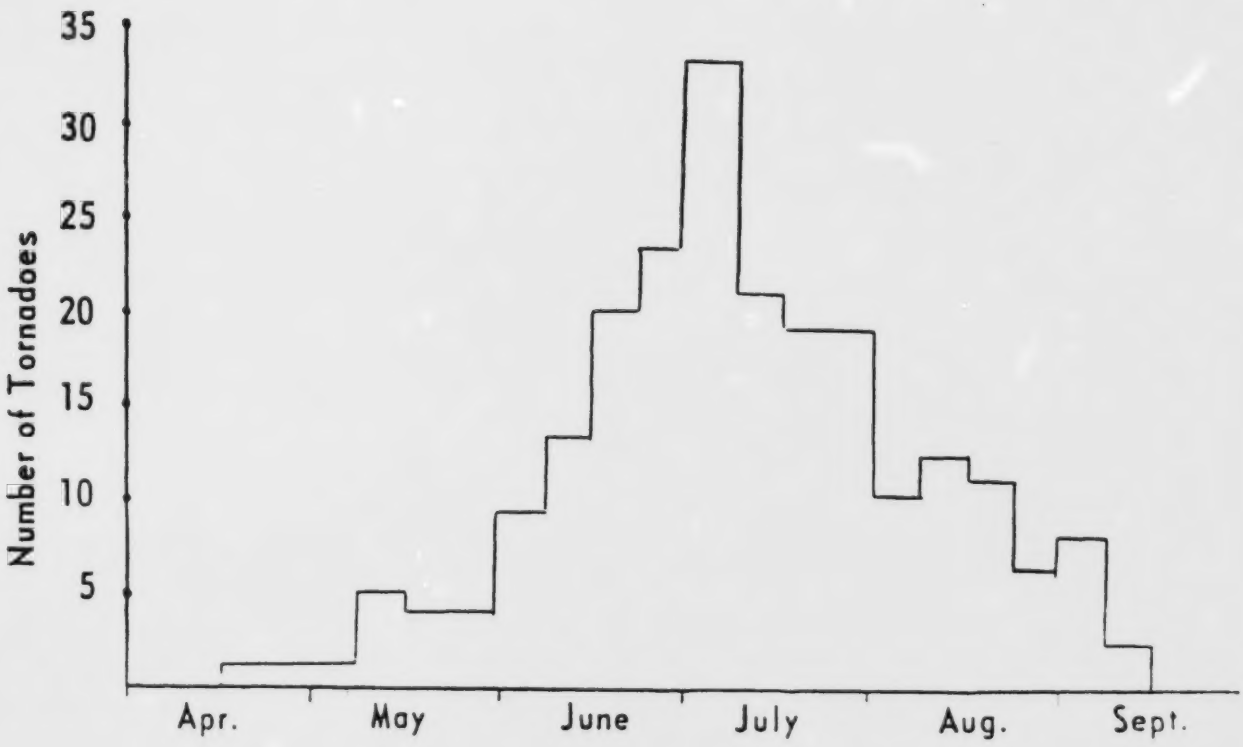

FIGURE 3.5-3 SEASONAL DISTRIBUTION OF TORNADOES IN WESTERN CANADA

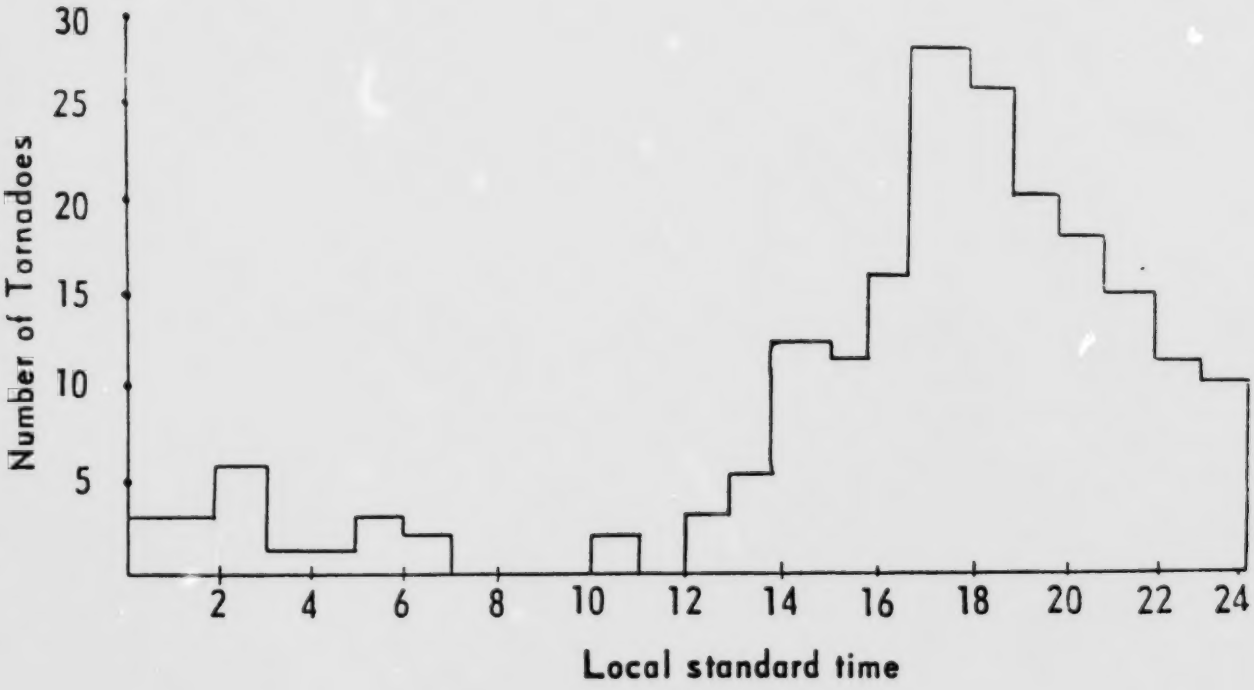

FIGURE 3.5-4 DIURNAL DISTRIBUTION OF TORNADOES IN WESTERN CANADA

3.6 Future Needs

a. There is a great need to improve our knowledge of the fine structure of microbursts so that detection and prediction methods can be optimized. Optimization of remote sensor detection algorithms can depend critically on understanding microburst fine structure. Parallel efforts involving full-scale atmospheric measurements, physical scale modelling, and numerical and analytical modelling are necessary.

b. There is a need to design experiments to study the processes involved in the initiation of microbursts by gust fronts and other mechanisms. This search for dynamic forcing weather mechanisms should include a variety of remote and in situ sensors.

c. Another need is for independent verification of the measurements carried out at Stapleton. Will the correlation between gust fronts and microbursts hold for other regions of the globe?

d. There is a need to monitor the U.S activity in this area of measurement and in particular to learn more about their measurement methodology. Effective monitoring is best carried out by an active Canadian participation in the American programs. This would provide an incentive to the Americans to allow Canada access to future U.S. measurement programs and data.

e. In particular, there is a need for Doppler radar data and meteorological measurements in Canada. What is the likelihood of the occurrence of microbursts in the different regions of Canada? How large of a hazard do they pose to Canadian aviation? Do they exhibit similar characteristics to those that were detected and studied at Stapleton?

4.0 MICROBURST MODEL

This section presents the characteristics of a microburst phenomena. This microburst characterization is based on JAWS data found in the open literature. In particular, the following sources have proved useful.

"The Microburst as a Hazard to Aviation: Structure, Mechanisms, Climatology and Nowcasting" by John McCarthy and James W. Wilson of NCAR.

"Evaluation of Doppler Radar for Airport Wind shear Detection" by James Wilson and Rita Roberts of NCAR.

"Simulated Flight through JAWS wind shear: In-depth Analysis Results" by Frost et al.

This and other wind shear literature can be found in the Reference Section. Figure 3.3.3-5 presents, in schematic form, the life cycle of a translating, impacting microburst as monitored by a Doppler radar, Frost et al, 1985. The figure shows, at a glance, how wind velocity, time, physical extent and position relate during the life cycle time of a microburst occurrence. The symbol T denotes the time of initial divergence reaching the surface. The small scale of the phenomenon is noteworthy. A detailed snapshot of a microburst occurring on July 14, 1982 as viewed by radar is presented in figure 3.3.3-1. The figure is in two parts, part (a) and Part (b); Part (a) is the horizontal wind field at a height of 50-100m above ground level (AGL) and Part (b) is the vertical wind field. The classical profiles of headwind, downdraft and tailwind are clearly visible.

The characterization of microbursts is given below and is based on JAWS data.

4.1 Physical Extent

4.1.1 Horizontal Dimensions

Downflow Diameter	:1 km
Outflow Diameter	:3 km typically up to 6 km

4.1.1 Horizontal Dimensions (cont'd)

Translation Distance
- Total for life cycle : 20 km (max)
- Severe wind shear : 5 km

4.1.2 Vertical Dimensions

Height of microburst : 3 km

4.2 Event Duration

Life cycle of microburst : 4-30 minutes for most events
Average duration : 10 minutes
Duration of severe wind shear : 2-4 minutes

Time to reach maximum event intensity

50% of all detected events : ≤ 5 minutes
95% of all detected events : ≤ 10 minutes

4.3 Windspeed

Windspeeds are dependent on position in microburst, and most microbursts exhibit asymmetric behavior.

4.3.1 Horizontal Windspeeds

Windspeed : 10-48 m/s
Average windspeed differential : 20 m/s
Median windspeed differential : 22 m/s
Maximum windspeed differential : 48 m/s

N.B. Differential refers to the difference in speed between the headwind and tailwind

4.3.2 Vertical Windspeeds

Downdraft decreases with decreasing altitude. Representative values are given below.

Windspeed at 200 m : 6 m/s
Windspeed at 400 m : 9 m/s
Windspeed at 600 - 1200m : 12 m/s

These vertical windspeed figures are based on a microburst measured by a dual Doppler radar on 14 July 1982 at 14.52 MDT during the JAWS project.

4.4 Frequency of Occurrence

The occurrence of microbursts has been investigated in both the JAWS and NIMROD projects and is only applicable to specific airport locations i.e. Denver and Chicago respectively. Data concerning Canadian airports is ,in comparison , limited and only one wind shear related incident concerning commercial-size aircraft has been identified.

4.5 Pressure

The average pressure for microbursts that impacted the ground station in the JAWS program was 0.66 mb.

The average pressure change for microbursts not passing over a station was 0.24 mb. There is evidence of a relationship between pressure and maximum wind speed change.

4.6 Temperature

When wet and dry microbursts are considered there is no evidence found of a relationship between microbursts and temperature.

4.7 Rain Rate

For wet microbursts the strength of the surface wind vector change tends to be proportional to rain rate.

4.8 Propagation Speeds

The propagation speed for most microbursts observed in the JAWS project was less than 4 m/s, many being essentially stationary.

4.9 Lapse Rates

It was found in the JAWS project that microbursts were more probable at higher 500 to 700 mb lapse rates, and that the 1800 GMT sounding correlated more highly with microbursts occurrence than the 1200 GMT sounding did. More than 80% of microbursts were detected in 1800 GMT soundings with lapse rates greater than 8 degrees per km.

4.10 Diurnal Variations

There is a well-defined diurnal variation in microburst activity in the JAWS project, most occurring between 1200 and 2000 MDT.

There appears to be no indication that the diurnal distribution of microbursts in Canada should be different to that identified in the JAWS project.

4.11 Seasonal Variations

Statistics from the JAWS project show a tendency for sporadic bursts of microwave activity during the summer months, rather than a broad peak with a relatively constant level of activity.

If there exists a relationship between tornadoes and microbursts then data on Western Canada suggests June, July and August are the worst months for microbursts.

5.0 WIND SHEAR DETECTION TECHNOLOGY

Basically there exists five descriptive elements of the atmosphere: gaseous constituents, density, pressure, temperature and motion. Generic instrument types commonly used to measure these elements include thermometers, barometers, anemometers, vanes, rain gauges and "eyes". Many of the conventional measuring techniques and systems, including spaceborne, are applicable to large-scale processes and, are not necessarily applicable to small scale events such as microbursts. Specific or new instruments and systems are required to provide the reliable detection of microbursts and for current purposes can be divided into three broad categories viz. groundbased, airborne and spaceborne. Spaceborne instruments although appealing from coverage aspects, cannot, as yet, provide the very high resolution (~ 1 km) necessary to detect microbursts. For this reason they will not be considered further.

5.1 Airborne Instruments

The instruments discussed here are limited to those that are fitted or could be fitted to aircraft with the dedicated role of detecting wind shear conditions. To date, three systems have been identified in the open literature

- Honeywell Sperry Wind shear Computer
- Airbus Industrie Speed Reference System
- Safe Flight Wind shear Computer

In all the systems, the acceleration of the plane relative to the ground is compared with the acceleration of the plane relative to the air around it. A difference between the two measurements means the plane is in a wind shear, and a difference larger than a certain preset value means the plane may be in a headwind caused by a microburst; in this case, the flight crew is alerted.

If the plane is in a microburst, a second alarm is triggered by the downdraft and tail wind.

In particular, Sperry has developed the wind shear detection and alert system as an enhancement to its Performance Management System, PMS. The system is designed to provide two levels of detection: caution and warning. For a caution condition, the system provides flashing amber wind shear lights on the glareshield. Caution is activated when updrafts or increasing headwinds are detected, and is operational only in approach mode. A warning condition produces red lights, reinforced with an aural warning. This mode is activated when the system detects a down-draft, increasing tailwind or negative rate of change of total acceleration vector due to wind shear.

5.1 Airborne Instruments (cont'd)

The Sperry system has logged over a thousand flights on Boeing 737s operated by Piedmont Airlines. The systems have alerted six times but only one of these warnings was followed by the second alarm.

The Safe Flight wind shear warning system is self maintaining and is designed to sense and integrate horizontal and vertical (or downdraft) wind shear components. It uses existing on-board sensors and its own computer to resolve the two orthogonal components of a wind shear, horizontal wind shear and downdraft drift angle.

The system derives horizontal wind shear by subtracting longitudinal acceleration from airspeed rate. Airspeed rate is derived by passing airspeed analog data from the airspeed indicator of the aircraft's airdata computer through a high-pass filter. Longitudinal acceleration is sensed by the integral accelerometer. Vertical computation of downdraft drift angle is derived from the comparison of sensed normal acceleration with calculated glidepath maneuvering load. Flight path angle is determined by subtracting the pitch attitude signal from an angle of attack signal. Data are processed in a 6-lb computer housed in a 1/4-ATR box. The Safe Flight system has been widely used on company jets; Boeing plans to install systems on Safe Flight's patents on all new 737-300, 757, 767 and 747-400 aircraft.

Detection systems such as those described above are useful for alerting pilots to their imminent passage through a microburst and only gives the crew a few seconds to react correctly to avoid a calamity. Clearly, it would be preferable for the pilot to receive information on how to avoid flying into a microburst. Avoidance can be achieved by early detection of a hazardous microburst situation. Timely data can be passed from either a groundbased wind shear system, see Section 5.2 and/or from an onboard forward looking sensor. Three types of forward looking sensors are applicable: microwave radar, lidar and radiometer.

Conventional, non-coherent radar systems are not well suited to wind shear detection, whether they are groundbased or airborne. These radars cannot resolve wind motion from fixed or faster moving objects; thus the "tell-tale" sign of wind shear i.e. wind speed diversity cannot be resolved from other, generally larger, returns. However, the suitability of Doppler radar, which can measure wind speed directly, to wind shear detection has been demonstrated successfully in the JAWS program.

An airborne forward looking Doppler radar can operate well, in clear and adverse weather conditions; they can be used on take-off and landing and appear to be a prime candidate for future avionic fits to aircraft.

5.1 Airborne Instruments (cont'd)

Lidar (light detection and ranging), the light emitting equivalent to Doppler radar, functions in much the same way as Doppler radar. It not only offers better angular resolution than radar but simultaneously can offer very high sensitivity to small changes in airspeed. Compared to a microwave system the lidar would require smaller transmitting/receiving apertures. One such system is under consideration in France by Crouzet. The potential system is an outgrowth of their existing Doppler laser anemometer air-data measurement systems.

Design techniques for Crouzet's instrument are based on the detection of the natural aerosol present in the atmosphere. Recent tests carried out by Crouzet have shown that these aerosols exist in the air at altitudes in excess of 3000m. Radial motion of these particles relative to the instrument beam are detected and the particle speeds estimated.

Crouzet claims that using their system a wind shear alarm will be initiated 5-10 seconds prior to the aircraft entering a dangerous situation.

Tests of a prototype airborne radiometer, observing in the 13-16 μm portion of the spectrum, were carried out during the Denver JAWS project in the summer of 1982. The infrared sensor was fitted aboard the NASA Ames B57B jet aircraft during several landing approaches and departures. This system is intended to augment, not replace, other wind shear detection sensors.

The physical basis of the radiometer is the relationship between temperature difference and gust fronts. Specifically, the relationship between the temperature gradient from undisturbed air across a shear-producing gust front or downburst outflow and the windspeed and direction of the gust front outflow wind.

The higher temperature gradients produce higher wind shear or peak gusts. The system employs multiple channels, one channel to sense static air temperature very close to the aircraft and a second channel for long range sensing. As a cool outflow gust front is approached, the long range channel begins to sense a cooler temperature well before the aircraft reaches the gust front, and the near channel senses the warmer static temperature at the aircraft until the cool downdraft or gust front is penetrated. At this point, both channels sense the same temperature for a period of time. A low altitude wind shear alert is produced when the temperature difference between the two channels reaches -0.5C/s.

The instrument performance in rain is undefined and apparently is being studied. In clear conditions warning times of 1/2-1 minute are indicated, time enough for a "go-around" decision to be made.

5.2 Groundbased Instruments

There are a number of groundbased instruments that potentially could act as sensors for microburst activity. Typical examples include:

- Surface Measurement Devices
  - cup anemometer
  - laser anemometer
  - propellor vanes
  - transverse wind sensor
  - laser weather identifier
- Boundary Layer Measurement Devices
  - radar (conventional and Doppler)
  - lidar
  - sodar

A discussion now follows on these devices.

5.2.1 Cup Anemometry

In the late 1970s most major airports in the U.S. installed Low Level Wind shear Alert Systems (LLWAS). Each system is built around a network of six anemometers. Five are stationed around the perimeter of the airport, and one is at the centre. The anemometers monitor the speed and direction of the winds every 10 seconds near the ground and relay the information to a minicomputer, which compares the inputs with a 2-minute running mean. If the wind velocity indicated by the central anemometer differs by more than 15 knots (NCAR supplied figure) from the velocity reading of any of the five other anemometers, an alarm is sounded in the control tower and is indicated visually on several monitors in the room as well. A higher threshold figure of, say, 20 knots will reduce false alarms but will also lower the system's sensitivity to wind shear detection. The choice of threshold is an important matter and its value is strongly dependent on the local topography of the site.

The LLWAS system has several limitations for microburst detection and include:

- system cannot measure winds above the sensors
- spatial resolution is poor but can be improved. Temporal resolution is poor since it is limited by the long averaging carried out at the centre site

5.2.1 Cup Anemometry (cont'd)

- surface wind effects outside the system perimeter cannot be detected
- vertical wind motions are not detected
- sensors do not measure wind along flight paths

LLWAS is not ideally suited to detect microburst and cannot provide reliable detection and good false alarm control. However, a substantial performance improvement to LLWAS is possible by increasing density of sensors and their individual responsiveness and the addition of pressure sensors.

5.2.2 Sodar

As lidar is the light equivalent to radar, sodar is the sound equivalent to radar. Doppler sodar measures wind speed and direction, vertical wind speed and turbulence on thermal stratification.

Sodar has adopted some of the techniques employed by radars, techniques such as frequency coding and clutter rejection by virtue of frequency shift. Currently systems can offer accuracies of one knot for speed measurements and 3 degrees for wind direction. Detection ranges are approximately 1 km for low noise sites. For Sodar systems sited close to airport runways consideration must be given to frangibility and zoning requirements(T.P.1247).

A new system, Megasodar, see figure 5.2.2-1 for operating principle, is under consideration in France. The system is baselined to operate out to ranges of 3 km. It would need to operate at a low frequency of 800 Hz. This is a good compromise between low atmospheric absorption (0.3 dB/100 m), antenna size and increasing ambient noise with low frequency. In addition, a longer pulse allied with compression is expected to yield a 29 dB gain which is approximately an order of magnitude better than present systems. The antenna would be phase steered and nominally pointed up the glide path. With phase steering it will be possible to make 3-dimensional measurements along and adjacent to the glide path giving vertical and transverse wind speeds.

It is claimed that an acoustic sensor like Megasodar would be cheap, compared to its Doppler radar counterpart, and is well suited to measure wind shear events during severe meteorological conditions. Further it can provide information along the glide path unlike the LLWAS discussed earlier.

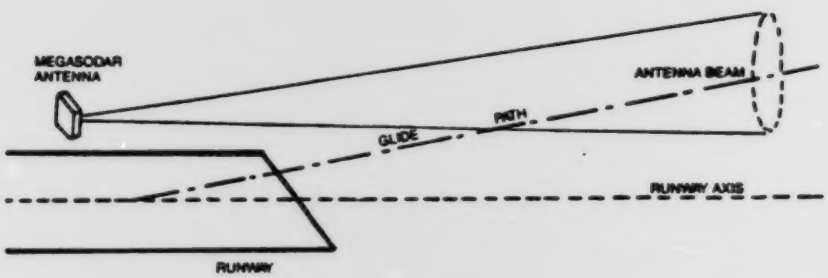

FIGURE 5.2.2-1 DIAGRAM OF THE OPERATING PRINCIPLE OF THE NEW MEGASODAR

5.2.3 Radar

Radar is noted for its ability to remotely sense large volumes of space. It can divide this space into cells -resolution cells - each cell being bounded by the antenna beam and time divisions known as range - gates. The amount of energy, echo strength, present in a resolution cell is dependent on target physical size and type.

Heavy precipitation, such as that associated with thunderstorms, presents a strong radar echo and is routinely detected by conventional radars. Unfortunately, wind shear can exist when there is no rainstorm activity present. Specifically, there is no guarantee that "if a strong echo exists then a wind shear hazard is present" and alternatively "if no echo is received then there is no wind shear hazard".

Clearly, conventional radar cannot offer a reliable means for detecting hazardous low wind shear under all conditions.

Coherent radar, when properly designed,can detect wind shear activity by virtue of its ability to measure target Doppler. In the case of wind shear and, in particular, microbursts, Doppler radar can measure the speed of the wind relative to its antenna's electrical boresight, see Figure 5.2.3-1. Only when the wind is travelling parallel to the antenna's boresight does the radar measure the actual wind velocity. For other geometries the radar can only measure the resolved component of the wind; in general the Doppler shift is given by $f_d = 2v/\lambda \cos\theta$. From this simple formulation it can be seen that if the wind is travelling orthogonal to the beam then zero Doppler is measured - a weakness of any Doppler measuring device. Also, due to the finite extent of the radar beam, errors in estimating shear will be present. The problem is that the radar will provide an average value within its beamwidth and will not be able to give an estimate in the variation of shear with height (if present) within the beam.

Single Doppler radars, as discussed so far, can be used effectively against certain phenomena which exhibit symmetric behavior. Phenomena such as small scale cyclones and some microburst can be remotely sensed by a single Doppler radar and their wind vector patterns inferred from the radial velocity only. Wind shears associated with gusts and other frontal systems can be measured accurately using the gradients of radial velocity in the vicinity of the front along with contiguous radial velocity measurements on both sides of the front.

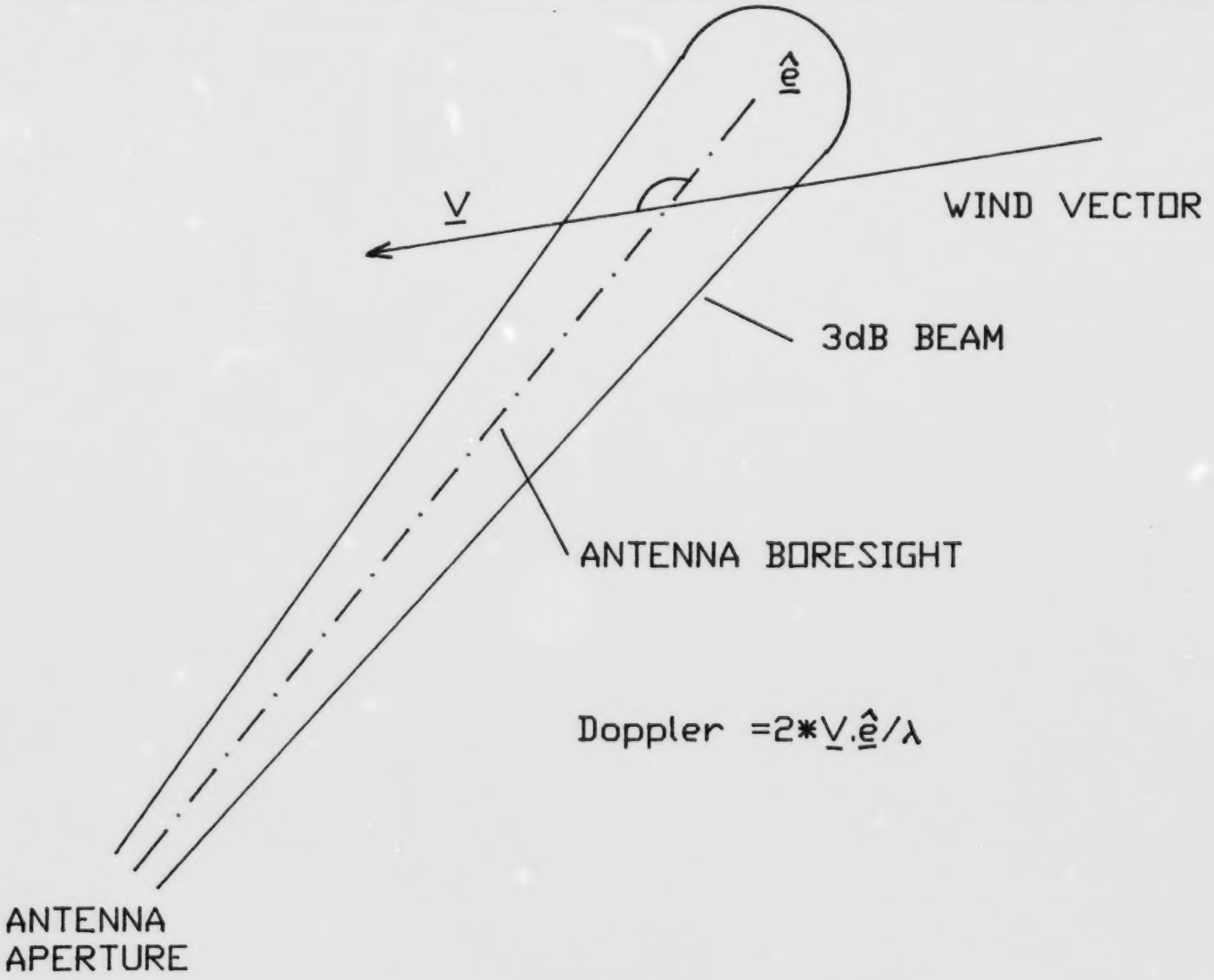

FIGURE 5.2.3-1 DOPPLER MEASUREMENT

5.2.3 Radar (cont'd)

Thus a single Doppler radar located away from an airport can effectively detect and quantify many hazardous phenomena over the airport. Unfortunately, most microbursts are asymmetric and measurements are no longer independent of viewing angle, thus denying 3-dimensional wind data to be generated; resulting, perhaps, in microbursts going undetected. The situation can be remedied by employing radars at the airport looking along the runways. The disadvantage here is that space above the airport is not being monitored; monitoring of this space could be achieved by a dedicated vertical pointing, long wavelength Doppler radar, see Section 5.2.5.

An alternative to using a single, on-or off - airport, Doppler radar is to employ several Doppler radars each synchronized to observe a common intersection volume. The advantage gained is that, since the same scattering volume is examined from different aspects, spatially independent measurements are available from which a complete 3-dimensional wind field can be reconstructed. In many respects this appears a very attractive option, but the use of multiple radars does, of course, significantly increase the cost of a microburst detection system.

In addition to cost there is also a significant processing overhead with multiple systems. Radars operated in the JAWS program were successful in detecting wind shear conditions. However, microbursts alarms were initiated by meteorologists experienced in the recognition of microburst conditions. Clearly, the use of meteorologists is not a long term solution to the microburst detection and recognition problem, but it does emphasize the point that detecting wind shear conditions is just part of the problem. Significant problems reside with automatic recognition of hazardous wind shear conditions and much effort is going on presently, particularly in the U.S., and will no doubt continue for some time to come.

One possible alternative is to employ multistatic radar, see Figure 5.2.3-2. The Figure presents one possible configuration where the elements of the system form the vertices of a triangle, one of which is a transmitter and the other two are receivers only.

This system may have reduced cost and performance benefits compared to a dual Doppler radar but it is not possible, at this point of the study, to comment further.

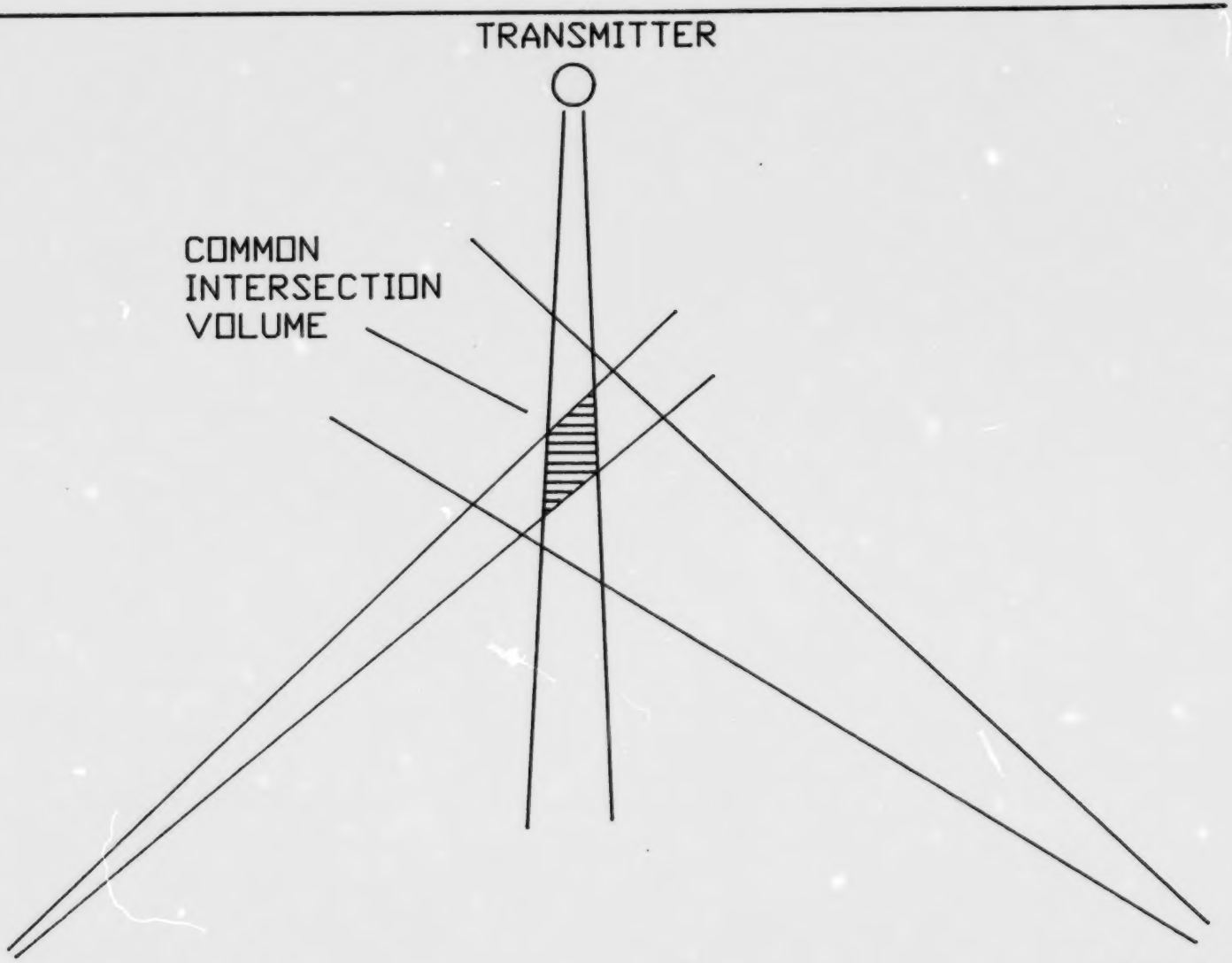

FIGURE 5.2.3-2 MULTISTATIC EXAMPLE

5.2.4 Lidars

Laser anemometers and Lidars detect the motion of aerosols in the atmosphere. Aerosol is a general term used to describe large particles (larger than air molecules) such as dust, moisture, fog, rain and pollution - droplets. Lidars can obtain wind speed and direction by detecting these aerosols as they move with the air mass. It is not difficult to appreciate why Lidars have been proffered as microburst detection systems. Indeed, laser anemometers are currently being used to detect wing tip vortices at airports in order to optimize take-off times.

Lidars have been discussed in Section 5.1 with respect to airborne systems. Much of the comments there hold true for a groundbased system. Also the remarks on Doppler radar are relevant since Doppler radar and Doppler lidar are systems which use the same techniques but with different implementations. Generally, it is worth noting that Lidars are suited to small volume surveillance and high precision measurement whereas radar lends itself to larger volumes, all weather and long range performance. The accuracy of a Laser device, and a radar, is dependent on the ratio of received signal power to noise power. If there exists precipitation between the Lidar and the resolution cell of interest then signal/noise ratios will be reduced. This, in turn, can effect measurement accuracy if signal level is reduced to a level close to threshold.

If the precipitation is part of the process under examination, i.e. wet microburst, then accuracy could be improved. Perhaps consideration should be given to using higher frequency (mm) radars, such as 30 GHz, as a compromise between radar and lidar.

5.2.5 Other Laser Devices

The mean value of transverse wind speed can be determined by measuring the speed of motion of an optical diffraction pattern across a receiving plane. As an optical wave propagates through the atmosphere slight inhomogeneities produce a non-uniform, fluctuating distribution of light across a receiving aperture.

Transverse wind sensors have proved very reliable and can operate for long periods of time with very little maintenance. Their good performance has been demonstrated convincingly but it is limited as is all light based systems, in range performance, particularly in precipitation and fog conditions.

5.2.5 Other Laser Devices (cont'd)

The light source can be a laser, although light with less coherence than a laser is preferable when used in conjunction with large receiving apertures and transmitters. The use of a less coherent light source offers advantages in the measurement accuracy of very turbulent conditions.

Currently, due to poor range performance in precipitation this instrument does not appear suitable for providing early warning of wind shear.

Another instrument based on optical scintillations is the laser weather identifier. Typically it operates over short paths at remote locations to identify the local surface weather conditions. In particular, precipitation parameters such as rainfall rate and drop size distributions can be determined over very short distances.

At present it does not seem a useful technique for the detection of all microburst phenomena and will not be considered further at this stage.

5.2.6 Profiler

The Profiler, a vertical profiling system utilizes a radar and a radiometer for remote sensing of the atmosphere. Additional, in-situ measurements for temperature and humidity are carried out and used in the retrieval of temperature and humidity profiles from the radiometer. The radar is used for providing profiles of windspeed versus altitude. One radar investigated operates at 915 MHz (UHF) and it can operate at heights down to 100 m. It can be used to monitor wind profiles in the atmospheric boundary layer.

No mention, as yet, has been found for the use of the Profiler as a microburst detection system. Clearly, in terms of the comparatively long horizontal detection ranges required, it is unsuitable; and although a useful device, it does not warrant further consideration at this time.

6.0 SUMMARY & CONCLUSIONS

This report has presented the work carried out on User Requirements and Technical Specifications. In particular, information on requirements as defined by Transport Canada and additional requirements suggested by Spar were presented. A review of meteorology conditions specific to wind shear has been completed which concluded with a list for future needs. A characterization of microburst events was outlined and based on data from projects such as JAWS. A discussion on the state of wind shear detection technology was presented and split between on-board and groundbased sensors.

The main conclusions drawn from the work carried out to date are as follows:

Key Requirements

- Cost

  The cost for an installed wind shear/microburst detection system should not exceed an order of magnitude $1,000,000 Canadian per airport.

- Range of Coverage

  The wind shear/microburst detection system should be capable of detecting and reporting wind shear/microburst events out to fifteen (15) kilometers from the centre of the airport and to an altitude of one (1) kilometer.

- Detection Parameters

  The wind shear/microburst detection system should be able to detect wind shear/microburst and provide, as a minimum the location of any wind shear/microburst detected.

- User Interface

  The wind shear/microburst detection system should provide sufficient warning, of wind shear/microburst, such that,

  pilots are able to effectively utilize this information to operate their aircraft in a safe manner.

  Air Traffic Controllers are able to effectively utilize this information in the provision of advisories and the management of their control area.

6.0 SUMMARY & CONCLUSIONS

Key Requirements (cont'd)

- Detection Status

  The detection system must provide "positive" or "negative" status

  Positive means: A hazardous wind shear/microburst condition is present within the area of coverage.

  Negative means: A hazardous wind shear/microburst is NOT present within the area of coverage.

- Probability of Detection vs False Alarm Rate

  The design of the wind shear/microburst detection system should give the best possible balance between a high probability of detection and false alarm rate.

- It is desirable that the wind shear/microburst system be able to provide its information to a possible future wind shear/microburst forecasting system.

- Technical and Environmental Constraints

  Any installation must conform to the requirements and standards detailed in "General Specification for Procurement of Electronic Equipment", DFS 1000 (TP3131 supplied by Transport Canada).

  Further, any operating equipment must not interfere with other airport/aircraft equipment. Table 2.2.7-1, supplied by Aviation Group of Transport Canada: Facility Engineering and Systems Development Branch, presents the equipments and their respective frequency bands of operation. Also, any installed airport equipment must conform to zoning requirements as detailed in the Transport Canada publication T.P. 1247 "land Use in the Vicinity of Airports".

Following the key initial requirements identified by TC the following Spar comments are presented:

- A revisit time of 1-2 minutes (maximum) to the same spatial position seems reasonable.

- Minimization of false alarms by good control of interference sources such as ground clutter, system noise, noise background, etc.

6.0 SUMMARY & CONCLUSIONS

Key Requirements (cont'd)

- Detection system must be reliable, easy to maintain and user friendly.

The main conclusions for future needs identified in the meteorology review are:

- There is a great need to improve our knowledge of the fine structure of microbursts so that detection and prediction methods can be optimized. Optimization of remote sensor detection algorithms can depend critically on understanding microburst fine structure. Parallel efforts involving full-scale atmospheric measurements, physical scale modelling, and numerical and analytical modelling are indicated.

- There is a need to design experiments to study the processes involved in the initiation of microbursts by gust fronts and other mechanisms. This search for dynamic forcing mechanisms should include a variety of remote and in situ sensors.

- Another need is for independent verification of the measurements carried out at Stapleton. Will the correlation between gust fronts and microbursts occur for other regions of the globe?

- There is a need to monitor the U.S. activity in this area and in particular to learn more about their methodology. Effective monitoring is best carried out by an active Canadian participation in the American programs.

- In particular, there is a need for Doppler radar and meteorological measurements in Canada. What is the likelihood of the occurrence of microbursts in the different regions of Canada? How large of a hazard do they pose to Canadian aviation? Do they exhibit similar characteristics to those that were detected and studied at Stapleton?

The survey into the literature has revealed that thunderstorms are one of the meteorological phenomena that spawn microbursts. It should be noted, though, that this is not an all encompassing criteria for determining the likelihood of the occurrence of microburst because they are observed to occur without thunderstorm activity. Also, it has been found that microbursts are related in some way to tornadoes. The dynamics of this relationship is unknown at the present time. Since statistics exist in Canada with regards to the occurrence of thunderstorms and tornadoes, one might attempt to estimate the probability of occurrence of microbursts based on these statistics.

6.0 SUMMARY & CONCLUSIONS

Key Requirements (cont'd)

This evidence is probably circumstantial at best, but it is the best that is available. The danger in making this estimate based on the incidence of thunderstorms and tornadoes is that the level of risk will be underestimated.

Since thunderstorms infer the presence of downburst activity and related wind shear; contrasting the thunderstorm-days in Canada and the U.S. one may conclude that, in general, wind shear occurs with less frequency in Canada than in the U.S. As well, by looking at these results one can make the following conclusions:

- there should be a minimum frequency of occurrence of microbursts at Pacific or Atlantic airports, while airports such as Edmonton, Thunder Bay, Toronto or St. Hubert would be five times as likely to experience a microburst.

- Since the annual occurrence of thunderstorms at Kennedy airport is 26 per year, which is comparable to most Canadian inland airports, one might conclude that the risk of microburst occurrence at Canadian inland airports is as great as at Kennedy. (Fujita has chronicled the accident of Eastern 66 at Kennedy, caused by a microburst, in which there was a loss of 112 lives.)

- Since the vertical development in thunderstorms is a function of tropopause height, and since summertime tropopause heights are greater over the U.S. than in Canada, it can be concluded that the induced microbursts would be stronger in the U.S. than in Canada.

- During the summer months of June, July and August, it is likely that those inland Canadian airports with a frequency of thunderstorm occurrence of 5-6 per day, would experience 20-30 identifiable microbursts each month.

The frequency of occurrence of tornadoes in Canada is another statistic one might consider when attempting to estimate the likelihood of the occurrence of microbursts at Canadian airports. From seasonal and diurnal distributions of tornadoes in Western Canada for the period between 1890 - 1958 one sees that if in fact there is a relationship between tornadoes and microbursts then the worst months for microbursts in Canada would be June, July and August. This is the same conclusion that was reached by looking at the incidence of thunderstorms in Canada. The other interesting fact is that in a period of 60 odd years there were 242 tornadoes in Western Canada. One concludes that these were major tornadoes because generally the statistics were compiled

6.0 SUMMARY & CONCLUSIONS

Key Requirements (cont'd)

from newspaper clippings as well as interviews of people who had personally experienced the tornadoes. This gives,on average, the occurrence of 4 tornadoes per year. One asks the question; if major events such as tornadoes occur with this rate of incidence how much more often do microbursts occur, which on a scale of meteorological events fall far short of tornadoes.

The main characteristics of a microburst can be split into: Physical extent; duration windspeeds and directions; frequency of occurrence; pressure, temperature and rainfall rate. These characteristics are defined in the main body of the text, however, the general characteristics are given below:

Diameter	:	1km (Downflow), 3km (Outflow)
Translation distance	:	20km (total); 5km (severe)
Height	:	3km
Life cycle	:	10 minutes (average); 2-4 minutes (severe)
Time to reach maximum intensity	:	≤ 5 minutes (50% of all detected events) ≤ 10 minutes (95%) of all detected events)
Horizontal windspeed differential	:	22 m/s (average); 48 m/s (maximum)
Vertical windspeed	:	6-12 m/s typically (dependent on altitude)
Frequency of occurrence	:	Believed to be rare in Canada
Pressure	:	0.66 mb (impacting)
Temperature	:	Not a strong indicator
Rain rate	:	Proportional to surface wind ("wet")
Propagation Rates	:	< 4m/s; many stationary
Lapse Rates		> 8 degrees/km (80% cases)
Diurnal Variations		1200-2000 MDT
Seasonal Variations		Summer months

The examination into detection technology revealed a few suppliers (Sperry Honeywell, Safe Flight and Airbus Industrie) of on-board wind shear detection systems. Operation of the systems developed to date is based on the difference between the acceleration of the aircraft relative to the ground compared with the acceleration of the aircraft relative to the air around it. The flight crew are alerted if the difference is greater than a preset threshold.

6.0 SUMMARY & CONCLUSIONS

Key Requirements (cont'd)

The above systems do offer a degree of safety to the aircraft but typically provide only very short alert times. Improved warning times would be available from forward looking sensors such as radars, lidars and radiometers. At present these sensors are not commercially available.

Instruments such as radars and lasers are also candidates for groundbased sensors in addition to sodar and conventional anemometers etc. At present radars appear to offer the most attractive overall technical solution to the detection of microbursts. However, there appears to be a conflict between their expected operational effectiveness and possible procurement cost limitations.

This conflict is particularly apparent when considering the application of the next generation U.S. weather radars, NEXRAD. It should be noted, however, that these radars are not designed solely for the detection of microbursts; if a radar, which could be multistatic, was designed specifically for microburst detection then the cost could almost certainly be reduced.

Recent work on sodar has proved interesting and relevant to the study. This is perhaps, a technology worthy of further study.

The use of and effectiveness of in-situ equipment such as cup anemometers, barographs etc. should not be underestimated. Although they are restricted to measuring the atmosphere directly surrounding them, they remain excellent indicators of wind shear conditions.

BIBLIOGRAPHY

This part of the report comprises the computer search carried and much of the literature found by manual means.

COMPUTER SEARCH

NOVEMBER 3, 1987

LITERATURE SEARCH KEYWORDS: AVIATION, AIRPORT(S), WIND SHEAR, MICROBURSTS

DATABASES SEARCHED

File 6:NTIS - 64-87/ISS22 (COPR. 1987 NTIS)
File 8:COMPENDEX - 70-87/OCT (COPR ENGINEERING INFO INC 1987)
File 165:EI ENGINEERING MEETINGS 84-87/SEP (Copr Engineering Info INC-87)
File 292:GEOBASE 80 - APR 87 Copr. Geo Abstracts Ltd. 1987

TOTAL: 219 REFERENCES RETRIEVED FROM 4 DATABASES

10 REFERENCES TYPED FROM NTIS DATABASE (FILE 6)

Bowles, R. L., "Wind Shear and Turbulence Simulation", In Its Wind Shear/Turbulence Inputs to Flight Simulation and Systems Certification, p67-95, July 1987.

Eilts, M. D., Doviak, R. J., "Oklahoma Downbursts and Their Asymmetry", Program Engineering and Maintenance Service. Report No.: DOT/FAA/PM-87/7, 50p, Nov 86.

Elmore, K. L., "JAWS (Joint Airport Weather Studies) Multiple Doppler Derived Winds", Langley Research Center Wind Shear/Turbulence Inputs to Flight Simulation and Systems Certification, p29-42, July 1987.

Levitt, L., Essenwanger, O. M., "Vertical Windshear Below 5.5 Kilometers in the Vicinity of Berlin, Germany", Shared Bibliographic Input. Report No.: AMSMI/TR-RD-RE-86-9; SBI-AD-E951 031, 80p, Aug 86.

McCarthy, J., "Introduction to the JAWS (Joint Airport Weather Studies) Program", Langley Research Center Wind Shear/Turbulence Inputs to Flight Simulation and Systems Certification, p13-27, July 1987.

McCarthy, J., "Status of the JAWS (Joint Airport Weather Studies) Program", Langley Research Center Wind Shear/Turbulence Inputs to Flight Simulation and Systems Certification, p43-47, July 1987.

Rinehart, R. E., DiStefano, J. T., Wolfson, M. M., "Preliminary Memphis FAA (Federal Aviation Administration)/Lincoln Laboratory Operational Weather Studies Results", Program Engineering and Maintenance Service. Report No.: ATC-141; DOT/FAA/PM-86-40, 192p, 22 Apr 87.

Schlickenmaier, H., "Case History of FAA/SRI (Federal Aviation Administration/Stanford Research Institute) Wind Shear Models", Langley Research Center Wind Shear/Turbulence Inputs to Flight Simulation and Systems Certification, p3-10, July 1987.

Shipman, K. W., "Simulator Systems Integration", Langley Research Center, Wind Shear/Turbulence Inputs to Flight Simulation and Systems Certification, p205-207, Jul 87.

Stengel, R. F., "Unresolved Issues in Wind Shear Encounters", Langley Research Center Wind Shear/Turbulence Inputs to Flight Simulation and Systems Certification, p197-204, July 1987.

****

5 REFERENCES TYPED FROM GEOBASE

Bell, G. J., Tsui, K. S., "A Low-Level Wind Shear Detection System", Weather v 36(2), pp 42-46, 4 figs, table, 5 refs, 1981.

Enders, J. H., Melvin, W. W., Frost, W., Camp, D. W., "Summary Proceedings of a Wind Shear Workshop", (US NASA, Marshall Space Flight Center, Huntsville, AL; NASA-CP-2270), 20 pp, October 1982.

McCarthy, J., Serafin, R., "The Microburst: Hazard to Aircraft", Nat Center for Atmos Res (NCAR), Weatherwise v 37(3), pp 120-127, 3 figs, 11 photos, 1984.

McCarthy, J., Wilson, J. W., " The Microburst as a Hazard to Aviation: Structure, Mechanisms, Climatology, and Nowcasting", Proceedings Nowcasting II Symposium, Norrkoping, pp 21-30, 1984.

Wilson, J. W., Roberts, R. D., Kessinger, C., McCarthy, J., "Microburst Wind Structure and Evaluation of Doppler Radar for Airport Wind Shear Detection", Journal of Climate & Applied Meteorology, v 23(6) pp 898-915, 1984.

****

38 REFERENCES TYPED FROM ENGINEERING INDEX MEETINGS

Anonymous, "37th Annual Meeting - Flight Safety Foundation. International Air Safety Seminar Proceedings: Human Factors in Managing Aviation Safety", International Air Safety Seminar Proceedings 37th Annual, 269p, 1984.

Anonymous, "Wind Shear", SAE Special Publications SP-681, 69p, 1986.

Bach, R. E. Jr., Wingrove, R. C., "Analysis of Airline Flight Records for Winds and Performance with Application to the Delta 191 Accident", AIAA Paper, p 361-373, 1986.

Barsony-Nagy, A., Hanin, M., "Lift and Drag of Airfoils in NonUniform Supersonic Stream", Collection of Papers of the 26th Israel Annual Conference on Aviation and Astronautics, p 195-204, 1984.

Beach, Berton E., "Experience with Wind Shear Simulator Training", International Air Safety Seminar Proceedings 37th Annual, p 169-173, 1984.

Biley, John B., "Windshear Detection/Alert and Guidance Cockpit Displays: A Pilot's Perspective", IEEE Service Centre (Cat. No. 86CH2359-8), p 302-306, 1986.

Brasunas, John C., Merritt, Mark W., "Short-Term Prediction of High Reflectivity Contours for Aviation Safety", American Meteorological Society, p 118-122, 1983.

Bray, Richard S., "Aircraft Performance and Control in Downburst Wind Shear", SAE Special Publications SP-681, p 13-38, 1986.

Caracena, F., McCarthy, J., Flueck, J. A., "Forecasting the Likelyhood of Microbursts along the Front Range of Colorado", Conference on Severe Local Storms 13th, p 261-264, 1983.

Frost, Walter, Chang, Ho-Pen, Elmore, Kimberly L., McCarthy John, "Simulated Flight Through JAWS Wind Shear: Indepth Analysis Results", AIAA Paper, AIAA-84-0276, 13p, 1984.

Fujita, T Theodore, Wakimoto, Roger M., "Microbursts in JAWS Depicted by Doppler Radars, PAM, and Aerial Photographs", Conference on Radar Meterology of the American Meteorological Society 21st., p 638-645, 1983.

Goff, R. Craig, "Communicating Critical Weather Information to Pilots", AIAA Paper, AIAA-82-0016, 11 p, 1982.

Haggard, William H., "Weather After the Event", American Meteorological Society, p 139-142, 1983.

Hay, George C., "Overview of the Integrated Federal Aviation Administration (FAA) Wind Shear Program Plan", SAE Special Publications SP-681, p 61-64, 1986.

Higgins, Charles R., Baker, Edward L., "Insight Gained from Analysis of Windshear Related Accidents and Incidents", SAE Special Publications SP-681, p 39-47, 1986.

Hjelmfelt, M. R., "Radar and Surface Data Analysis of a Microburst in JAWS", Conference on Radar Meterology of the American Meteorological Society 22nd., p 64-69, 1984.

Ivan, Michael, "Ring-Vortex Downburst Model for Real-Time Flight Simulation of Severe Wind Shears", AIAA Paper, p 57-61, 1985.

Johnson, D. E., "Federal Aviation Administration Weather Radar Research and Development Program", IEE Conference Publication n 216, p 375-379, 1982.

Kessinger, Cathy, Hjelmfelt, Mark, Wilson, James, "Low-Level Microburst Wind Structure Using Doppler Radar and PAM Data", Conference on Radar Meteorology of the American Meteorological Society 21st., p 609-615, 1983.

Kuhn, Peter M., Kurkowski, Richard L., Caracena, Fernando, "Airborne Operation of an Infrared Low-Level Wind Shear Prediction System", AIAA Paper, AIAA-82-0153, 6 p 1982.

Laynor, William G., "Summary of Windshear Accidents and Views about Prevention", SAE Special Publications SP-681, p 1-12, 1986.

Lee, J. T., "1983 Lightning, Turbulence, Wind Shear, and Doppler Radar Studies at the National Severe Storms Laboratory", AIAA Paper, AIAA-84-0113, 6p, 1984.

McCarthy, John, "Joint Airport Weather Studies Project: Current Analysis Highlights in the Aviation Safety Context", AIAA Paper, AIAA-84-0111, 10p, 1984.

McCarthy, John, Elmore, Kim, "Jaws Analysis Highlights in the Aviation Context", Corporate Aviation Safety Seminar 29th Annual Meeting, p 146-175, 1984.

McCarthy, John, Roberts, Rita, Schreiber, Wendy, "JAWS Data Collection, Analysis Highlights, and Microburst Statistics", Conference on Radar Meteorology of the American Meteorological Society 21st., p 596-601, 1983.

McCarthy, John, Wilson, James W., "Applications of Doppler Radar to Aviation Operations - JAWS Experiences", AIAA Paper, AIAA-83-0205, 4p, 1983.

McCarthy, John, Wilson, Jim W., "Low Level Wind Shear Detection and Warning - A Systems Update", AIAA Paper, AIAA-83-0444, 6p, 1983.

McCarthy, John, Wilson, James W., "Microburst as a Hazard to Aviation: Structure, Mechanisms, Climatology, and Nowcasting", European Space Agency, (Special Publication) ESA SP 208, p 21-30, 1984.

McCarthy, John, Wilson, James W., Fujita, T. Theodore, "Joint Airport Weather Studies Project", AIAA Paper, AIAA-82-0017, 8 p, 1982.

McCarthy, John, Wilson, James W., Hjelmfelt, Mark R., "Operational Wind Shear Detection and Warning: The 'Claws' Experience at Denver and Future Objectives", SAE Special Publications SP-681, p 65-69, 1986.

Melvin, William W., "New Look at Piloting Procedures in Microbursts", SAE Special Publications SP-681, p 49-59, 1986.

Mueller, Cynthia K., Hildebrand, Peter H., "Structure of a Microburst: As Observed by Ground-Based and Airborne Doppler Radar", Conference on Radar Meteorology of the American Meteorological Society 21st., p 602-608, 1983.

Offi, D. L., Lewis, W., "Wind Shear Detection with a Modified Airport Surveillance Radar", Conference on Radar Meteorology of the American Meteorological Society 20th., p 424-429, 1981.

Psiaki, Mark L., Stengel, Robert F., "Optimal Flight Paths Through Microburst Wind Profiles", AIAA Paper, p 494-503, 1985.

Roach, W. T., "Mesoscale Studies of some Weather Hazards to Aviation", European Space Agency, (Special Publication) ESA SP 165., p 43-47, 1981.

Rodi, Alfred R., Elmore, Kimberly L., Mahoney, William P., "Aircraft and Doppler Air Motion Comparisons in a JAWS Microburst", Conference on Radar Meteorology of the American Meteorological Society 21st., p 624-629, 1983.

Simmons, Peter D., "Characteristics and Detection of Low Level Wind Shear in the Critical Phases of Flight", International Air Safety Seminar Proceedings 34th, Flight Safety Foundation, p 131-145, 1981.

Wilson, James, Roberts, Rita, "Evaluation of Doppler Radar for Airport Wind Shear Detection", Conference on Radar Meteorology of the American Meteorological Society 21st., p 616-623, 1983.

****

34 REFERENCES TYPED FROM COMPENDEX

Anonymous, "37TH Annual Meeting - Flight Safety Foundation, International Air Safety Seminar Proceedings: Human Factor in Managing Aviation Safety", Flight Safety Foundation Inc., Arlington, Va., 269p, 1984.

Anonymous, "Wind Shear (Papers Presented at the SAE Aerospace Technology Conference and Exposition", SAE Spec Publ SP-681, 69p, 1986.

Beaulieu, Gaston, "Effects of Wind Shear on Aircraft Flight Path and Methods for Remote Sensing and Reporting of Wind Shear at Airports", Technical Note, (University of Toronto, Institute for Aerospace Studies) n 216, p 1-32, 1978.

Bedard, Alfred J. Jr., "Sources and Detection of Atmospheric Wind Shear", AIAA, AIAA 81-0391, 10p, 1981.

Beran, D. W., Mandics, P. A., Bedard, A. J., Strauch, R. G., "Wind Shear and Gust Front Warning System", Conference on Aerospace and Aeronautic Meteorology and Symposium on Remote Sensing from Satellite, 7th, Prepr., p167-174, 1976.

Brashears, M. R., Hallock, J. N., "Measurement of Wind Shear and Wake Vortices by Laser Doppler Velocimetry", Conference on Aerospace and Aeronautic Meteorology and Symposium on Remote Sensing from Satellite, 7th, Prepr., p 175-181, 1976.

Chadwick, Russell B., Moran, Kenneth P., Campbell, William Carroll, "Design of a Wind Shear Detection Radar for Airports", IEEE Transactions on Geoscience Electronics, v GE-17, n 4, p137-142, 1979.

Dietenberger, Mark A., Haines, Patrick A., Luers, James K., "Reconstruction of PAN AM New Orleans Accident", Journal of Aircraft, v 22, n 8, p 719-728, August 1985.

Enders, John H., Melvin, William W., Frost, Walter, Camp, Dennis W., "Summary Proceedings of a Wind Shear Workshop", NASA Conf Publ 2270, 17p, 1983.

Fichtl, George H., Camp, Dennis W., Frost, Walter, "Sources of Low-Level Wind Shear around Airports", Journal of Aircraft, v 14, n 1, p 5-14, 1977.

Fredrickson, J. T., "Wind Shear an Update", Shell Aviation News, n 439, p 24-36, 1977.

Frost, Walter, Chang, Ho-Pen, Elmore, Kim L., McCarthy, John, "Simulated Flight Through JAWS Wind Shear", Journal of Aircraft, v 21, n 10, p 797-802, Oct 1984.

Frost, Walter, Chang, Ho-Pen, McCarthy, John, Elmore, Kimberly L., "Aircraft Performance in a JAWS Microburst", Journal of Aircraft, v 22, n 7, p 561-567, 1985.

Fujita, T. Theodore, "Downbursts and Microbursts - an Aviation Hazard", Conference Radar Meteorol Am Meteorol Soc. 19th, Prepr., p 94-101, 1980.

Fujita, T. Theodore, "Microbursts as an Aviation Wind Shear Hazard", AIAA, AIAA 81-0386, 9 p, 1981.

Ivan, Michael, "Ring-Vortex Downburst Model for Flight Simulations", Journal of Aircraft, v 23, n 3, p 232-236, Mar 1986.

Kalafus, Rudolph M., Hallock, James N., "Requirements for an Airport Ground-Based Wind Shear Detection System", Conference on Aerospace and Aeronautic Meteorol and Symposium on Remote Sensing from Satellite, 7th, Prepr., p 182-187, 1976.

Keller, John L., "Physical and Empirical Basis for a Specific Clear-Air Turbulence Risk Index", "University of Dayton Research Inst, 39p, Apr 1986.

Killinger, Dennis K., Menyuk, Norman, "Laser Remote Sensing of the Atmosphere", Science, v 235, n 4784, p 37-45, Jan 1987.

Koenig, Reinhard, Krauspe, Peter, "Influence of Wind Shear and Vertical Winds on Takeoffs and Go-Arounds", Airport Forum, v 11, n 5, p 43, 45-46, Oct 1981.

Kuhn, Peter M., Kurkowski, Richard L., "Airborne Infrared Low-Altitude Wind Shear Detection Test", Journal of Aircraft, v 21, n 10, p 792-796, Oct 1984.

Luers, J. K., Haines, P., "Effect of Heavy Rain on Wind Shear Attributed Accidents", AIAA, AIAA 81-0390, 8 p, 1981.

McCarthy, John, Blick, Edward F., Elmore, Kim L., "Airport Wind Shear Detection and Warning System Using Doppler Radar - A Feasibility Study", NASA Contractor Reports, n 3379, 97p, 1981.

McCarthy, John, Frost, Walter, Terkel, Barry, Doviak, Richard J., Camp, Dennis W., Blick, Edward F., Elmore, Kim L., "Airport Wind Shear Detection and Warning System Using Doppler Radar", Conference Radar Meteorol Am Meteorol Soc 19th, Prepr., p 135-142, 1980.

Miele, A., Wang, T., Melvin, W. W., Bowles, R. L., "Maximum Survival Capability of an Aircraft in a Severe Windshear", Journal of Optimization Theory and Applications, v 53, n 2, p 181-217, May 1987.

Offi, D. L., Lewis, W., Lee, T., "Wind Shear Detection with an Airport Surveillance Radar", Conference Radar Meteorol Am Meteorol Soc. 19th, Prepr., p 130-134, 1980.

Psiaki, Mark L., Stengel, Robert F., "Analysis of Aircraft Control Strategies for Microburst Encounter", Journal of Guidance, Control, and Dynamics, v 8, n 5, p 553-559, Sep-Oct 1985.

Psiaki, Mark L., Stengel, Robert F., "Optimal Flight Paths Through Microburst Profiles", Journal of Aircraft, v 23, n 8, p 629-635, Aug 1986.

Schuring, J., "Wind Shear on the Approach - An Investigation on the Influence of a Tower Measured Wind Environment on the Symmetric Motions of a Simulated Aircraft in an Automatic Approach", Amsterdam, Neth., Natl Lucht Ruimtevaartlab Versl Verh TR 77078 U, 40p, 1977.

Strauch, R. G., Moninger, W. R., "Radar Measurement of Wind Shear and Wind Profiles for Air Safety", Conference on Radar Meteorol of the Am Meteorol Soc., 18th, Prepr., p 432-436, 1978.

Tinsley, H. Guice, Coons, Frank G., Wood, Larry W., "Possible Near-Term Solutions to the Wind Shear Hazard", SAE Preprints, n 780572 , 7p, 1978.

Wilson, James, Carbone, Richard, Serafin, Robert, "Detection and Display of Wind Shear and Turbulence", Conference Radar Meteorol Am Meteorol Soc. 19th Prepr., p 150-156, 1980.

Wilson, James W.. Roberts, Rita D., Kessinger, Cathy, McCarthy, John, "Microburst Wind Structure and Evaluation of Doppler Radar for Airport Wind Shear Detection", Journal of Climate and Applied Meteorology, v 23, n 6, p 898-915, Jun 1984.

Zrnic, D. S., Doviak, R. J., Lee, J. T., Eilts, M. D., "Oklahoma Weather Phenomena that may Affect Aviation", Journal of Aircraft, v 24, n 5, p 310-316, May 1987.

****

10 REFERENCES FROM NTIS DATABASE (FILE 6)

Caracena, F., Ortiz, R., Augustine, J. A., "Crash of Delta Flight 191 at Dallas-Fort Worth International Airport on 2 August 1985: Multiscale Analysis of Weather Conditions", National Oceanic and Atmospheric Administration, Report No.: NOAA-TR-ERL-430; ESG-2, 38p, 1986.

Donaldson, C. D., Sullivan, R. D., "Effect of Heavy Rain on an Airfoil at High Lift", National Aeronautics and Space Administration, Report No.: NAS 1.26:178248; ARAP-597; NASA-CR-178248 , 36p, 1987.

Eilts, M. D., "Low-Altitude Wind Shear Detection With Doppler Radar", Program Engineering and Maintenance Service. Report No.: DOT/FAA/PM-87/6, 47p, 1987.

Federal Aviation Administration, "Integrated FAA Wind Shear Program Plan", Report No.: DOT/FAA/DL-87/1; DOT/FAA/VS-87/1; DOT/FAA/AT-87/1 , 93p, 1987.

Killinger, D. K., Menyuk, N., "Laser Remote Sensing of the Atmosphere", Report No.: JA-5872; ESD-TR-86-173, Science, v 235, p37-47, 1987.

National Technical Information Service, "Doppler Radar: Aviation Safety, January 1972-April 1987 (Citations from the International Aerospace Abstracts Database) (Rept. for Jan 72-Apr 87)", National Aeronautics and Space Administration, 51p, 1987.

Psiaki, M. L., "Development of Control Strategies for Safe Microburst Penetration: A Progress Report", NASA Langley Research Center Joint University Program for Air Transportation Research, p 73-82, 1983.

Skoda, G., "Fractal Analysis of Radar Precipitation Data over Hilly Terrain", WMO Proceedings of the Conference on the Scientific Results of the Alpine Experiment (ALPEX), v2, p697-703, 1986.

Stengel, R. F., "Investigation of Air Transportation Technology at Princeton University, 1984", Langley Research Center Joint University Program for Air Transportation Research, p133-137, 1984.

Streeter, B. G., "Simulation Investigation of the Effect of the NASA (National Aeronautics and Space Administration) Ames 80-by 120-Foot Wind Tunnel Exhaust Flow on Light Aircraft Operating in the Moffett Field Traffic Pattern', National Aeronautics and Space Administration, Report No.: NAS 1.15:86819; A-85372; NASA-TM-86819, 33p 1986.

LITERATURE FOR METEOROLOGY REVIEW

Atlas, D., K.R. Hardy and J. Joss, "Radar Reflectivities of Storms Containing Spongy Hail", J. Geophys. Res., 69, 1955-61, 1961.

Batchelor, G.K., "The Scattering of Radio Waves in the Atmosphere by Turbulent Fluctuations in Refractive Index", Tech. Rept. No. 26, Ithaca, N.Y.: School of Electrical Engineering, Cornell Univ., 1955.

Battan, L.J., "Radar Observation of the Atmosphere", The U. of Chicago Press, 1973.

Ben, R.R., E.J. Dutton and B.D. Warner, "Weather Effects on Radar", Radar Handbook (Skolnik, ed.), McGraw-Hill Book Co., 1970.

Bedard, A.J., "Optimising the Use of Surface Sensors for Wind Shear Detection", J. Aircraft, 21, 971-977, 1984.

Bedard, A.J., J. McCarthy and T.J. Lefebvre, "Statistics From the Operation of the Low-Level Wind Shear Alert System (LLWAS) During the JAWS Project: An Interim Report From the JAWS Project at NCAR", Federal Aviation Administration Report DOT/FAA/PM-84?32, 1985.

Bedard, A.J. and T.J. Lefebvre, "Surface Measurements of Gust Fronts and Microbursts During the JAWS Project: Statistical Results and Implications for Wind Shear Detection, Prediction, and Modelling", Joint Airport Weather Studies Report No. 01-86, August 1986.

Brock, F.V. and P.K. Govind, "Portable Automated Mesonet in Operation", J. Appl. Meteorol., 16, 299-310, 1977.

Byers, H.R. and R.R. Braham, "The Thunderstorm", U.S. Government Printing Office, 1949.

Canada-Aids, "Wind Shear Accidents in Canada 1976-1983: Completed Reports Only", 25 Sept. 1985.

Elmore, K.L. and J. McCarthy, "A High Resolution Spatial and Temporal Multiple Doppler Analysis of a Microburst and its Application to Aircraft Flight Simulation", J. of Climate and Appl. Meteorol., Vol. 25, No. 10, October 1986.

Frost, W., H. Chang, K.L. Elmore and J. McCarthy, "Simulated Flight Through JAWS Wind Shear", J. Aircraft, 21, 797-802, 1984.

Fujita, T.T. and H.R. Byers, "Spearhead Echo and Downburst in the Crash of an Airliner", Mon. Wea. Rev., 105, 129-146, 1977.

Fujita, T.T., and R.M. Wakimoto, "Five Scales of Airflow Associated With a Series of Downbursts on 16 July 1980", Mon. Wea. Rev., 109, 1438-1456, 1981.

Fujita, T.T., "Andrews AFB Microburst", SMRP res. Pap. 205, University of Chicago, Depart. of Geophysical Sciences, Satellite and Mesometeorology Res. Proj., 1983.

Fujita, T.T., "The Downburst", Published by the University of Chicago, 1985.

Gossard, E.E. and R.G. Strauch, "Radar Observations of Clear Air and Clouds", Elsevier Science Publishers, 1983.

Hardy, K.R., D. Atlas and K.M. Glover, "Multiwavelength Backscatter From the Clear Atmosphere", J. Geophysical Res., 71, 1537-52, 1966.

ICAO Circular, "Wind Shear", ICAO Circular 186-AN/122, 1987.

Lawrence, R.S., C.G. Little, and H.J.A. Chivers, "A Survey of Ionospheric Effects Upon Earth-Space Radio Propagation", Proc. IEEE, 4-27, January 1964.

Lowe, A.B. and G.A. McKay, "The Tornadoes of Western Canada", Meteorological Branch, Department of Transport, 1962.

McCarthy, J., "Recommendations for Coping With Microburst Wind Shear: An Aviation Hazard", J. of Air Law and Commerce, Vol. 49, No. 2, 1984.

McCarthy, J. and R. Serafin, "The Microburst - Hazard to Aircraft", Weatherwise, June 1984.

McCarthy, J. and J.W. Wilson, "The Microburst as Hazard to Aviation: Structure, Mechanisms, Climatology, and Nowcasting", Proc. Nowcasting-11 Symp., Norrkoping, Sweden, 3-7 Sept. 1984.

Obukhov, A.M., "Strukture Temperaturnogo Polia v Turbelentnom Potoke (Structure of the Temperature Field in a Turbulent Current)", Izvest Akad. Nank SSSR, Ser. Geogr. i Geofiz., Moscow 13:58-69, 1949.

Ottersten, H., "Radar Angels and Their Relationships to Meteorological Factors", Forsvarets Forskningsanstalt (Res. Inst. of Nat. Defence, Stockholm) 4, No. 21-33, 1970.

Purdom, J., "Subjective Interpretation of Geostationary Satellite Data for Nowcasting", Chap. 3.1 in Nowcasting, K. Browning (Ed.), Academic Press., 149-165, 1982.

Roberts, R.D. and J.W. Wilson, "Nowcasting Microburst Events Using Single Doppler Radar Data", Proc. 23rd Conf. on Radar Meteor. and Conf. on Cloud Physics, Snowmass, Colo., Sept. 22-26, 1986.

Silverman, R.A., "Turbulent Mixing Theory Applied to Radio Scattering", J. Appl. Phys., 27, 690-705, 1956.

GLOSSARY OF TERMS

This section provides a short list of terminology used in this report. The terms included should not be interpreted as strict definitions, rather clarifications of terms in the context of this report.

AGL	Above Ground Level
CYCLONE	General cyclonic flow throughout the sensor site with a radius of at least 20 km
DIFFERENTIAL	The difference in speed between the headwind and the tailwind.
DISTANT MICROBURST	Distant microburst are microbursts with impact regions outside the sensor array area
DIVERGENCE	A term used to describe the splitting of the downburst winds.
DOWNBURST	A strong downdraft which induces an outburst of damaging winds on or near the ground.
FALSE ALARM	An unwanted detection produced by an unwanted target e.g., ground clutter, thermal noise
GUST FRONT	Translating convergence line with a radius of curvature greater than 15 km
IMPACTING MICROBURST	When a ground station is beneath the stagnation of a microburst (i.e. centered on the downflow source of diverging winds and hence at a zone of little or no horizontal wind speed increase) such an event has been called an impact
ISOLATED GUST	A wind speed surge, only at a solitary sensor site, not lasting more than 5 (1-min) samples
JAWS	Joint Airport Weather Studies
LASER	Light Amplification by Stimulated Emission of Radiation
LASER ANEMOMETER	A Laser that is designed specifically for measuring wind speed

LIDAR	LIght Detection And Ranging instrument
LLWAS	Low Level Wind Shear Alert System
MACROBURST	From Fugita and Wakimoto (1981) a macroburst is defined as downflow regions larger than 4 km
MEDIAN	The middle value of a rank ordered set of numbers
MEGASODAR	The name assigned to a new French Sodar system
MICROBURST	A downburst covering less than 4 km
NEAR MICROBURST	When a downflow stagnation region does not strike a station and the dimension of the initial divergence are estimated at less than 4 km
NCAR	National Center of Atmospheric Research
NIMROD	Northern Illinois Meteorological Research On Downbust
PAM	Portable Automated Mesonetwork observing system
PROBABILITY OF DETECTION	The probability of detecting a wanted target
PROBABILITY OF FALSE ALARM	The probability of detecting an unwanted target
RADAR	RAdio Detection And Ranging
RADIOMETER	A <u>passive</u> electromagnetic sensor which measures changes in received radiation.
SODAR	SOund Detection And Ranging
WIND SHEAR	Change of wind vector (speed and direction) from one point in space to another.

APPENDIX

PHYSICAL EFFECTS OF THE ATMOSPHERE ON ELECTROMAGNETIC WAVES

A.1 Physical Effects of the Atmosphere on Electromagnetic Waves

In general (Grossard & Strauch, 1983), the non-ionized atmosphere can influence radio waves in several ways: (a) reflection,)b) refraction, (c) absorption by atmospheric gases, (d) absorption by hydrometeors, (e) scattering by dielectric inhomogeneities and (f) scattering by hydrometeors.

The main cause of radar returns from the clear air has now been well established to be the inhomogeneities in refractive index that results from turbulence. The radar refractive index at commonly used radar wavelengths is nondispersive and depends on the atmospheric temperature, humidity and pressure. Radar returns from clouds, on the other hand, usually consist of reflections from hydrometeors.

A.1.1 Propagation of Electromagnetic Waves

Using Maxwell's equations (Battan, 1973), one can show that in a homogeneous medium the velocity of a wave is given by

$$v = \frac{1}{\sqrt{\varepsilon_1 \mu_1}} , \qquad (1)$$

where

ε_1 = permittivity

μ_1 = permeability.

A.1.1 Propagation of Electromagnetic Waves (Cont'd)

In free space the speed of the wave is equal to the speed of light and is given by

$$c = \frac{1}{\sqrt{\varepsilon_0 \mu_0}} \qquad (2)$$

where the zero subscript designates conditions in free space. For most purposes, the speed of propagation of an electromagnetic wave may be considered to be constant and equal to the speed of light in free space, 3×10^8 m/s. However, for some problems one has to recognize that the atmosphere is significantly different from free space and that the observed air-mass properties are sufficiently variable to produce small changes in the speed of propagation. These small changes are important because they may lead to refraction of the radar ray and produce marked changes in the direction of propagation.

In the study of optics, it is common to define a term n, the index of refraction, as

$$n = \frac{c}{v} . \qquad (3)$$

Substituting for v and c, one obtains

$$n^2 = \varepsilon \mu \qquad (4)$$

where the dielectric constant of a medium, $\varepsilon = \varepsilon_1 / \varepsilon_0$, magnetic permeability $\mu = \mu_1 / \mu_0$. Since μ is approximately equal to unity in most media usually considered, it can be said that, for most practical cases,

$$n^2 = \varepsilon . \qquad (5)$$

Since ε usually exceeds unity, the index of refraction does also, and the speed of propagation in most media is less than the speed of light in free space by a small but significant amount.

A.1.1 Propagation of Electromagnetic Waves (Cont'd)

It should be noted that in its most general form the refractive index is a complex function,

$$m = n - ik, \qquad (6)$$

where the real term, n, is the factor denoted in the equation c = nv. The term ik is equal to zero in a perfect dielectric and is associated with the absorption of the medium.

A.1.1.1 Meteorological Factors Determining the Index of Refraction

For dry air, the index of refraction, n, is given by

$$(n - 1)\, 10^6 = K_1 \frac{p}{T} \qquad (7)$$

where p is the pressure in millibars, T is temperature in degrees Kelvin, and K_1 is a constant which has a value of 77.6. By substitution from the equation of state, one obtains

$$(n - 1)\, 10^6 = K_1 R \rho = (\text{constant})\, \rho \qquad (8)$$

where R is the individual gas constant for air and ρ is the air density. For convenience, the term on the left side of the equation is often set equal to N, called the "radio refractivity", and units of $(n - 1)10^6$ are referred to as "N units".

In dry air the index of refraction has the same value over almost the entire range of electromagnetic spectrum, it is the same for light and radio waves. However, when water vapour is added to the air, the value of N for the mixture becomes frequency dependent. The index of refraction (and dielectric constant) of water vapour is greater for radio than for optical frequencies. For radio waves,

A.1.1.1 **Meteorological Factors Determining the Index of Refraction** (Cont'd)

$$N = (n-1)\,10^6 = K_3 \frac{e}{T^2} - K_2 \frac{e}{T} \qquad (9)$$

where e is the vapour pressure in millibars. For microwaves with wavelengths greater than 2 cm, K_1, K_2 and K_3 have values of approximately 77.6° K/mb, 5.6° K/mb, and 3.7×10^2 $(^oK)^2$/mb.

Since the index of refraction is an additive quantity, the index of moist air can be calculated from

$$N = 77.6 \frac{p}{T} - 5.6 \frac{e}{T} + 3.75 \times 10^5 \frac{e}{T^2} \qquad (10)$$

At all atmospheric temperatures the second term will be much smaller than the others. Hence for all practical purposes the equation can be written

$$N = \frac{77.6}{T}\left[p + 4810 \frac{e}{T}\right] \qquad (11)$$

A.1.1.1 Meteorological Factors Determining the Index of Refraction (Cont'd)

Near sea level a typical value of n is about 1.0003 and N = 300.

Accurate determinations of n depend on accurate measurements of the three meteorological parameters, i.e., p, T, and e. It has been shown that, for T = 15° C, p = 1013 mb, and e = 10.2 mb (a relative humidity of 60 percent), errors in N are given by

$$N \simeq -1.27\Delta T + 4.50\Delta e + 0.27\Delta p \qquad (12)$$

Radio refractive index can be measured directly by means of instruments called refractometers. Microwave refractometers are based on the fact that the resonant frequency of a microwave cavity depends on the dimensions of the cavity and refractive index of the enclosed medium. As air is passed through the cavity, the resonant frequency changes as the refractive index of the air changes. Changes in refractive index are given by an expression such as

$$\Delta f/f = -\Delta n = -10^{-6}\,\Delta N \,. \qquad (13)$$

Thus if the refractometer operates at X-band, a one-N unit change of refractivity produces a 9.4 kHz change in frequency.

A.1.1.2 Change in Phase-Path Length Introduced by the Troposphere

In order to determine (Lawrence et al., 1964) the effect of the troposphere upon the phase-path length of a radio path between two terminals, we remember that the effective phase-path length P is given by

$$P = \int_0^s n\, dl \qquad (14)$$

A.1.1.2 Change in Phase-Path Length Introduced by the Troposphere (Cont'd)

where the integral is taken along the ray path. The change Δl in the (phase) path length introduced by the presence of the troposphere is given by

$$\Delta l = \int_0^s (n-1)\,dl = -\int_0^s \Delta n\,dl \quad . \qquad (15)$$

The refractive effects of the troposphere may be considered as due to a gradient, in a direction transverse to the optical line of sight, of the radio path length from the radio source to the observer. Such a gradient could be introduced by a microburst, due to the changes in parameters p and T which accompany a microburst. If we can treat the microburst as a wedge, the tilting of the wave front produced by such a wedge is given by

$$\tau = \frac{d(\Delta l)}{dx} = -\frac{d\int \Delta n dl}{dx} \text{ radians} \quad , \qquad (16)$$

where x denotes displacement at right angles to the line of sight.

A.1.1.3 Radar Reflectivity and Scattering from Hydrometeors

The performance of some radars can be strongly affected by the presence of meteorological particles (Hydrometeors). In general (Bean et al., 1970), radars at the lowest frequencies are not bothered by meteorological or weather effects, but at the higher frequencies, weather echoes may be quite strong and mask the desired target signals just as any other unwanted clutter signal. Radar has been used extensively for the study of thunderstorms, squall lines, tornadoes, hurricanes, and in cloud physics research.

The simple radar equation is

$$P_r = \frac{P_t G^2 \lambda^2 \sigma}{(4\pi)^3 R^4} \qquad (17)$$

A.1.1.3 Radar Reflectivity and Scattering from Hydrometeors (Cont'd)

where, P_r = received power

P_t = transmitted power
G = antenna gain
λ = wavelength
σ = target cross section
R = target range.

In extending the radar equation to meteorological targets, it is assumed that rain, snow, hail, or other hydrometeors may be represented as a large number of independent scatters of cross section σ_i located within the radar resolution cell. Let $\sum\sigma_i$ denote the average total backscatter cross section of the particles per unit of volume. The radar cross section may be expressed as $\sigma = V_m \sum\sigma_i$ where V_m is the volume of the radar resolution cell. The volume occupied by a radar beam of vertical beamwidth ϕ_B, horizontal beamwidth θ_B, and a pulse duration τ is approximately $V_m \approx (\pi/4) R^2 \theta_B \phi_B h/2$, where $h = c\tau$ and c = velocity of propagation. If it is assumed that the scatterers are distributed over the volume of the beam, the received power from meteorological echoes averaged over many independent radar sweeps may be written

$$\bar{P}_r = \frac{P_t A_e h}{32 R^2} \sum_i \sigma_i \qquad (18)$$

where A_e = effective antenna aperture.

It can be shown that if the wavelength is long compared with the circumference of a scattering particle of diameter D (Rayleigh scattering region), the radar cross section is

$$\sigma_i = \frac{\pi^5 D^6}{\lambda^4} |K|^2 \qquad (19)$$

where $|K|^2$ depends upon the dielectric constant of the scatterer and varies slowly with wavelength. In particular, $K = (m-1)/(m+2)$, where m is the complex index of refraction and is equal to $m = n - ik$, n is the refractive index, and k is the absorption of the material involved. For water at a temperature of 10°C, $|K|^2$ is approximately 0.93 at 10 cm wavelength.

A.1.1.3 Radar Reflectivity and Scattering from Hydrometeors (Cont'd)

$$\bar{P}_r = \frac{\pi^5 P_t A_e h}{32 R^2 \lambda^4} \sum_i D_i^6 |K|^2 \qquad (20)$$

Since the particle diameter D appears as the sixth power, it follows that in any distribution of particles a small number of large drops will contribute the largest amount of returned power.

The two-way attenuation of the radar signal in traversing the range R and back is an exponential function of the distance, that is,

$$\text{Attenuation} = \exp(-2 \alpha R).$$

Thus, for describing two-way propagation, equation (20) can be more completely written as

$$\bar{P}_r = \frac{\pi^5 P_t A_e h}{32 R^2 \lambda^4} \exp(-2 \alpha R) \sum_i D_i^6 |K|^2 . \qquad (21)$$

or, in a simplified form, as

$$\bar{P}_r = \frac{C |K|^2 z}{R^2} , \qquad (22)$$

where C is a constant depending on the characteristics of the radar set. If the scatterers are known to be raindrops which are small with respect to λ, measurements of $\bar{P}_r$ and R allow calculations of Z, which in turn gives $\sum D_i^6$ per unit volume. In many instances, the conditions for Rayleigh backscattering may not be fulfilled or it might not be possible to state whether they are fulfilled. In such instances, it would be more appropriate to write

$$\bar{P}_r = \frac{C |K|^2 Z_e}{R^2} , \qquad (23)$$

A.1.1.3 Radar Reflectivity and Scattering from Hydrometeors (Cont'd)

where Z_e is the "effective radar reflectivity factor". It can be calculated if $\bar{\rho}_r$ and R are known. The quantity Z_e may be written in terms of reflectivity

$$\eta = \frac{\pi^5}{\lambda^4} |K|^2 Z_e , \qquad (24)$$

which leads to

$$Z_e = \frac{\lambda^4 \eta}{\pi^5 |K|^2} . \qquad (25)$$

In calculating Z_e, the quantity $|K|^2$ conventionally is taken to be 0.93.

If each of the scatterers has a diameter D and a backscattering cross section σ, it can be shown that

$$Z_e = \frac{6 \lambda^4 \sigma M}{\pi^6 |K|^2 \rho D^3} \qquad (26)$$

where M is the liquid-water content represented by particles with diameter D and density ρ. Atlas, Hardy, and Joss (1964) showed that $Z_e = 7.48 \times 10^3 \lambda^4 \sigma \mu / D^3$ for particles with density 0.9 g/cm. The units of Z_e are millimeters to the sixth power per cubic meter when λ and D are in centimeters, σ in square centimeters, and M in grams per cubic meter. This expression is useful for calculating the liquid-water contents required to give particular reflectivities at known wavelengths, particle diameter, and backscattering cross section.

A.1.1.4 Radar Reflectivity and Refractive Index Variations

The refractive index, n, in the atmosphere depends on the vapour pressure, temperature, and pressure. In the lower atmosphere, vapour pressure differences are most important in accounting for differences in n, but at higher altitudes where vapour pressures are low, changes in n are mostly a result of changes in temperature. In

A.1.1.4 Radar Reflectivity and Refractive Index Variations (Cont'd)

the discussion of the propagation of a radar beam through the atmosphere, it was assumed that it varied smoothly with height and was spherically stratified. For many purposes such an assumption is valid. On the other hand, if through a region of the atmosphere where the spatial gradient of n is high there is also a considerable amount of turbulence, the irregular, small-scale fluctuations of n can lead to appreciable scattering of the incident microwaves.

Tatorski (1961) showed that the reflectivity in the backscattered direction is given by

$$\eta = \frac{\pi^2}{2} k^4 F_n^*(k) \ , \qquad (27)$$

where the wave number $k = 4\pi/\lambda$ and F_n^* is called the space spectrum, or the "spatial power-spectral density", a three-dimensional representation of the refractive index field which is obtained by a Fourier transform of the three-dimensional refractive index covariance function (Ottersen, 1970).

The spectrum $F^*(k)$ extends over a wide range of scales, but only the Fourier mode with a wavelength of $\lambda/2$ contributes significantly to the backscattering. Over the inertial subrange limited by wave numbers k_o and k_m, one can write $F^*_n(k)$ in terms of $F_n(k)$, the so-called normalized one-dimensional spectrum of refractivity. Turbulence is assumed to be homogeneous and isotropic over this range of wave numbers. Wave number k_o is associated with macroscale eddies of scale L_o and is the scale beyond which turbulence is no longer isotropic. Eddies with wave numbers beyond k_m lose energy rapidly by viscosity. The turbulent eddies in the inertial subrange do not lose much energy as a result of viscosity. Instead, there is a transfer of energy from eddies of scale greater than L_o, through the inertial subrange of the smaller-scale-eddies.

Batchelor (1955) and Silverman (1956) showed that

$$F(k) = 2/3\, k_o^2\, k^{-5/3} \ . \qquad (28)$$

A.1.1.4 Radar Reflectivity and Refractive Index Variations (Cont'd)

From Obuklov (1949), Hardy, Atlas, and Glover (1966) obtained

$$F_n^*(k) = 0.033\, C_n^2\, k^{-5/3} \quad , \qquad (29)$$

which is valid in the inertial subrange. The quantity C_n^2 is a measure of the mean-square fluctuations of the refractive index as a function of distance ($\overline{\Delta n^2}$) and is given by

$$C_n^2 = 1.56\, (\overline{\Delta n^2})\, k_o^{2/3} = 5.26\, (\overline{\Delta n^2})\, L_o^{-2/3} \quad , \qquad (30)$$

where $k_o = 2\pi/L_o$.

By substitution, it is found that the reflectivity

$$\eta = 0.39\, C_n^2\, \lambda^{-1/3} \quad , \qquad (31)$$

and hence

$$\eta = 0.61\, (\overline{\Delta n^2})\, k_o^{2/3}\, \lambda^{-1/3} \quad . \qquad (32)$$

THIS PAGE INTENTIONALLY LEFT BLANK

PART B

DOPPLER RADAR TECHNOLOGY ASSESSMENT

THIS PAGE INTENTIONALLY LEFT BLANK

1.0 INTRODUCTION

This first section of this part of the report introduces the idea of radar as a wind shear detection sensor by outlining its use in meteorology and also places microbursts in historical perspective.

1.1 Uses of Radar in Meteorology

Radar represents one of the key remote sensors available for weather forecasting and related studies [1-3]. Three radar discriminants are of particular interest to a meteorologist. They are: amplitude, Doppler, and polarization. Variations in the amplitude of radar echoes from weather formations are used to supply estimates of rainfall intensity, and to provide indications of the movement and evolution of showers and thunderstorms. Doppler radar is used to reveal hazardous weather conditions such as tornadoes, microbursts, and gust fronts. Polarization radar is used to identify the form of precipitation particles within storms. It is noteworthy that, to a meteorologist, radar echoes from atmospheric targets contain "useful information" about the prevalent weather conditions. Yet, these very same echoes are viewed as "unwanted clutter" by a radar user interested in the detection and tracking of point targets such as aircraft. It is therefore the application of interest that determines what is "signal, and what is "interference" to the radar user.

The use of amplitude as a radar discriminant is the least demanding in terms of system complexity. Typically, a magnetron is used in the transmitter to provide the source of RF energy; in the receiver, envelope detection is used to extract weather-related information contained in the amplitude variations of radar echoes.

In Doppler radar [4,5,6], a klystron (that lends itself to phase control) is used to supply the RF energy, and coherence is thereby maintained between the receiver and transmitter. The receiver has an in-phase and a quadrature channel, the combination of which enables the extraction of Doppler information related to horizontal or vertical gradients of wind velocity.

1.1 Uses of Radar in Meteorology (cont'd)

In polarization radar, a dual-polarized antenna is used to transmit RF pulses with alternate horizontal and vertical polarizations (i.e., an orthogonal pair of linearly polarized waves). The receiver processes echoes in the respective principal plane of polarization (i.e., the same as that in the transmitter). Thus, the use of dual polarization provides information about the size of raindrops, and the microphysical nature of ice particles (both hail and snow). The idea of differential reflectivity measurement using polarization diversity (advanced originally by Seliga and Bringi [7] has recently generated considerable interest among radar meteorologists. This measurement has the potential of improving the accuracy of radar rain rate estimation.

In this survey report, we focus on the application of Doppler radar for the detection of small, short-lived downdrafts known as microbursts. The reason for giving microbursts such a special attention as an atmospheric target of interest is that they represent serious hazards to aircraft during landings and takeoffs. In spite of its small size, an intense microburst may induce damaging winds as high as 270 kilometres per hour, which makes it a deadly weather phenomenon. This is well illustrated by the spectacular photograph, figure (i), of a thunderhead shown on the next page, which was taken near Grand Forks, North Dakota.

Figure (i) This spectacular photograph of a thunderhead was taken near Grand Forks, North Dakota. Its size only hints at the stored energy waiting to be unleashed. (The photograph is reproduced with the permission of Boeing Airlines).

1.2 Some Historical Notes on Microbursts

It appears that downdraft as the cause of an air accident was first reported in a book published in 1958 [8]. Oliver Stewart, author of the book, describes an accident involving a four-engined Argonaut aircraft that belonged to the British Overseas Airways Corporation. The accident took place at Kano Airport, Nigeria, on the afternoon of 24 June, 1956; the aircraft was on a routine flight to Tripoli. At that time, storms were raging around the airport. Figure 1, reproduced from Stewart's book, presents a schematic interpretation of the unusual weather conditions that led to the Kano accident in 1956. In the final paragraph of the chapter describing this accident, Stewart states:

> "So in this finding, the result of the scrupulous examination of the evidence, we have a fresh statement of one of the oldest causes of air accidents and a fresh indication that the theory of flight must be modified in the practice and that even when an aircraft is in the air it may not be entirely of the air because - presumably because of inertia or wind gradient effects - sudden wind changes will produce alterations in its air speed as well as in its altitude. Violent turbulence is a generally known danger to aircraft and cumulo-nimbus clouds are avoided because of it; the line squall, with its roll-cloud formation, is also known and avoided. But the thunderstorm cell was not perhaps sufficiently widely recognized as a possible cause of powerful down draughts until the results of the investigation into this accident to "Hotel Echo" were made known."

Hotel Echo in this statement refers to the aircraft involved in the accident.

Another historical point of special interest relates to an Eastern Airlines Flight 66 accident that occurred on 24 June, 1975, at the John F. Kennedy Airport. While investigating this accident, Theodore Fujita [9] hypothesized that the aircraft attempted to penetrate a "downburst". This terminology was used by Fujita to refer to a strong downdraft that induces an outburst of damaging winds on or near the ground.

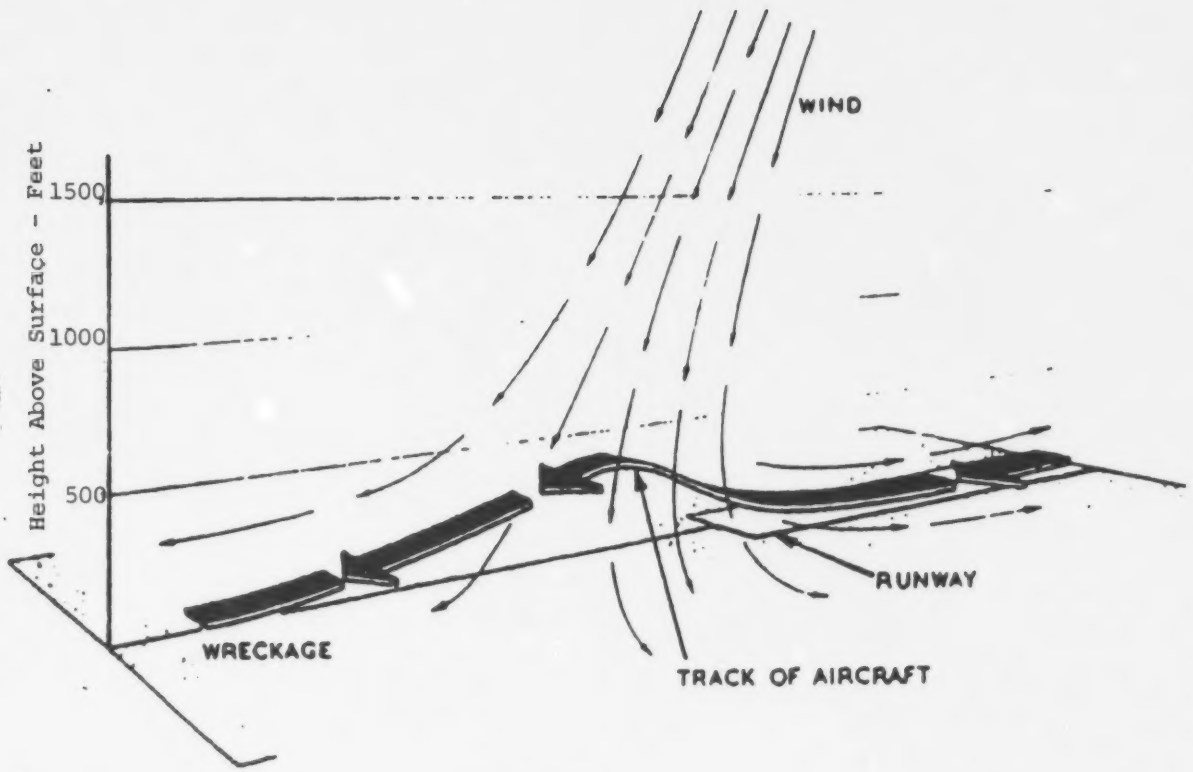

Figure 1 The unusual conditions which led to the Kano accident in 1956. The height indications are those of the accident investigation committee.

(Reproduced from Stewart [8])

1.2 Some Historical Notes on Microbursts (cont'd)

However, Fujita's concept of the downburst was regarded controversial by meteorologists at the time. To prove his point, Fujita used low-flying Cessna aircraft for taking close-up photographs of damage patterns left behind by windstorms in the mideastern United States.

In order to distinguish relatively small downbursts from their larger counterparts, Fujita subclassified a downburst into "macroburst" and "microburst", according to the horizontal extent of the damaging winds [9].

Further confirmation of Fujita's thesis was provided in 1982 by a second experiment called JAWS (Joint Airport Weather Studies), which was conducted jointly by the University of Chicago and the National Center for Atmospheric Research (NCAR) [10-11]. The principal investigators in the experiment were Fujita, McCarthy and Wilson. The objective of the JAWS Project was to design a suitable Doppler radar network for observing the three-dimensional wind field within a microburst.

Wind shears in the lowest few hundred meters of the atmosphere have been responsible for numerous aircraft accidents [12]. In particular, one month after the Pan American Flight 759, which crashed shortly after taking off from New Orleans International Airport on July 9, 1982, the Subcommittees on Investigations and Oversight and on Transportation, Aviation, and Materials of the U.S. House of Representatives' Committee on Science and Technology held joint hearings on weather problems affecting aviation [13]. Subsequently, a law was passed requiring the Federal Aviation Administration (FAA) to contract with the National Academy of Sciences (NAS) "to study the state of knowledge, alternative approaches and the consequences of wind shear alert and severe weather condition standards relating to takeoff and landing clearances for commercial and general aviation contract". To conduct the study, NAS created an ad hoc Committee for the study of Low-Altitude Wind Shear and its Hazard to Aviation. The Committee produced its report in 1983 [13]. In the context of wind shear detection and prediction, the Committee made several recommendations. There were two specific recommendations with far-reaching consequences:

1. The development of the next generation Doppler weather radar system (NEXRAD), intended to replace the present network of noncoherent weather radars.

2. The development of an Airport Terminal Weather Radar (TDWR) by the FAA to observe weather conditions at and around airport terminals.

It may thus be said that although the importance of Doppler radar has been recognized by meteorologists for a long time [4], the will on the part of the United States to perfect and deploy Doppler weather radar on a national scale emerged only after the ad hoc Committee on Low-Altitude Wind Shear and its Hazard to Aviation completed its study [13].

2.0 MICROBURSTS AND GUST FRONTS

This section clarifies the interpretation of these meteorological terms in the context of wind shear.

2.1 Microbursts

For our purposes, a microburst is defined as a **downdraft-induced, diverging, horizontal flow of air near the earth's surface, which has an initial horizontal dimension of less than 4 km and a surface differential velocity of 10 m/s or greater** [14]. When an aircraft flies through a microburst, the encounter can be lethal. Figure 2 depicts a vertical cross-section of a microburst, with the flight track of an aircraft penetrating it shortly after takeoff. This figure clearly illustrates the effect of wind changes, particularly near the earth's surface, on the aircraft's motion. According to Figure 2, an aircraft on takeoff first encounters an **increasing headwind**, next a **downdraft**, and finally an increasing tailwind. The result of such a sequence of rapidly changing events is a serious loss of energy for an aircraft that is about to take off or on its final landing approach.

Not all microbursts are alike.* In particular, the division of microbursts into two types has been recognized by various scientists [9,15]:

a) **Wet microburst**, which is a microburst accompanied by heavy rain between the onset and the end of the high winds, including intermediate calm periods, if any. This type of microbursts is usually associated with intense precipitation shafts from thunderstorms, as in Figure 3(a).

b) **Dry microburst**, which is a microburst accompanied by little or no rain between the onset and the end of the high winds, including intermediate calm periods, if any. This type of microburst is usually associated with a virga, as in Figure 3b). In a dry microburst, the rain (if any) evaporates before reaching the ground.

Typically, wet microbursts occur in the wet (humid) regions of the world, whereas dry microbursts are encountered in the dry regions with high bases of convective clouds.

* For a review of microbursts, their characteristics and types, see Litva [44].

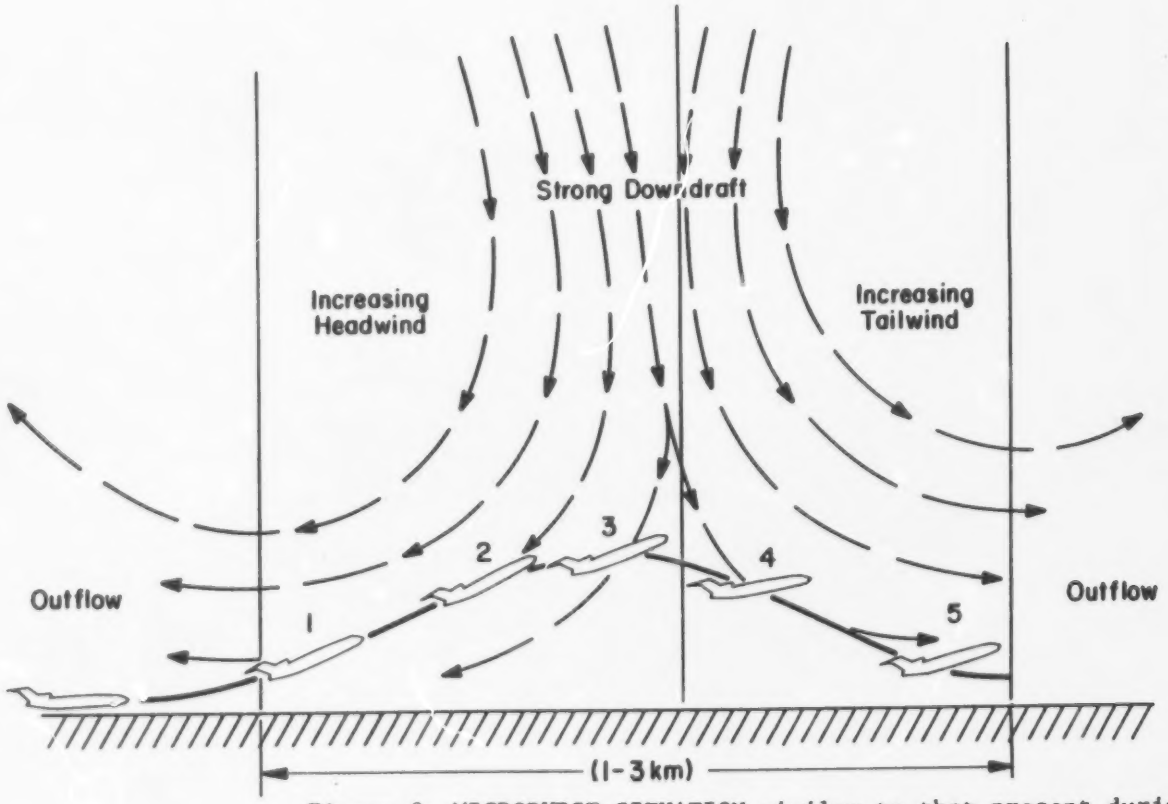

Figure 2 MICROBURST SITUATION similar to that present during the takeoff of Pan Am Flight 759 in New Orleans in July 1982. The airplane first encounters a headwind and experiences increasing performance (1); this is followed in short succession by a decreasing headwind component (2), a downdraft (3), and finally a strong tailwind (4), where 2 through 5 all result in decreasing performance of the airplane. Position (5) represents an extreme situation just prior to impact.

(Reproduced from McCarthy [14])

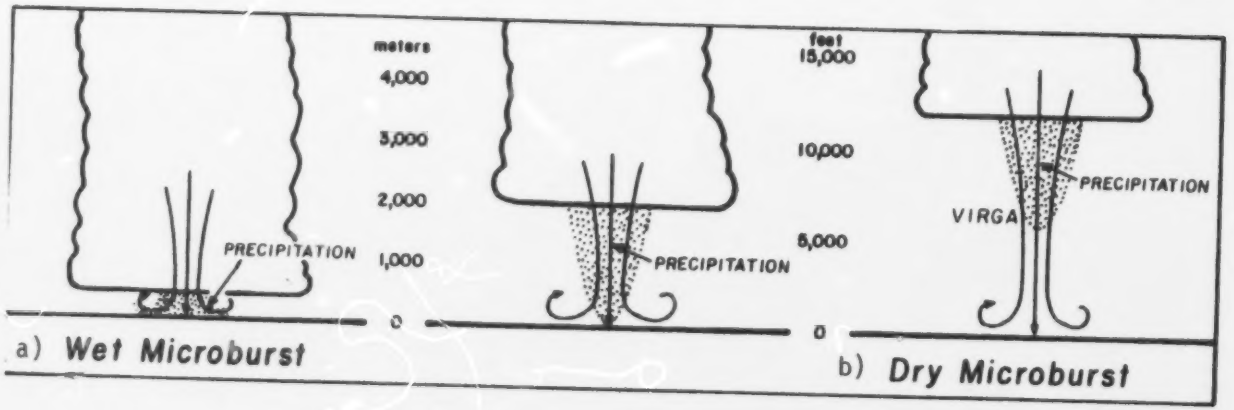

FIGURE 3: SCHEMATIC VIEWS OF WET AND DRY MICROBURSTS. WET MICROBURSTS ARE EXPECTED TO OCCUR IN THE WET REGIONS OF THE WORLD, WHILE DRY MICROBURSTS ARE COMMONLY SEEN IN THE DRY REGIONS WITH HIGH BASES OF CONVECTIVE CLOUDS.

(FUJITA, 1985)

2.1 Microbursts (Cont'd)

Outburst winds of outflow microbursts are mostly irrotational. This means that the streamlines of outburst winds spread out radially without rotating around the centre of the outflow. However, in a microburst accompanied by a misocyclone aloft, there is a definite sign of rotation at the height of the downflow [9], as depicted in Figure 4.

2.2 Gust Fronts

A gust front is the leading edge of a mass of cool air that has recently descended from a thunderstorm or convective cloud [13,16]. The front is marked by shifts (shear) in the wind, both in the vertical and horizontal directions.

The general shape of a thunderstorm outflow was described by Simpson [17]. Figure 5 shows a schematic vertical cross-section of the basic features of a mature outflow [13]. The bold solid line in this figure depicts the transition zone between the cool outflow and the warmer environment, while the arrows show the flow field relative to the gust front. As cold air approaches the front from within the outflow, much of it is deflected upward (counterclockwise) by a sinusoidally induced circulation. Air closer to the ground turns downward under the influence of surface friction; this is marked "backflow" in Figure 5.

A gust front may propagate in clear air many tens of kilometers away from the thunderstorm that caused it. Yet, the front may harbour shear forces that are capable of destroying an aircraft, especially when the crew of the aircraft is unaware of its presence. The wind behind the front is usually strong and turbulent, and in the vicinity of the downdraft strongly divergent.

Although a gust front does not usually pose as big a threat to aircraft as a microburst does, nevertheless, an aircraft passing through a gust front may experience turbulence and buffeting.

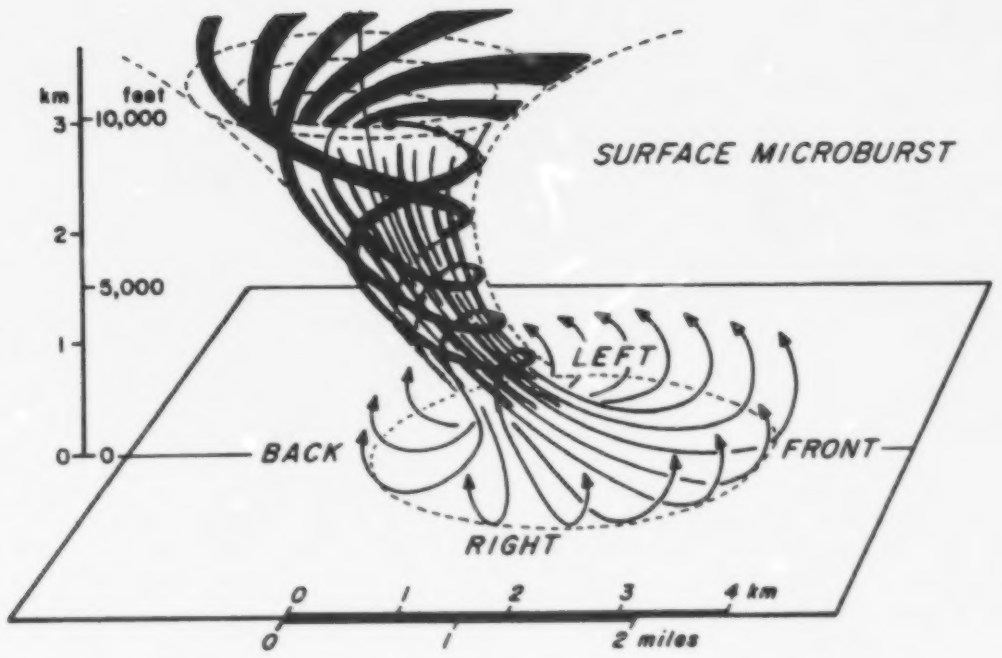

FIGURE 4: A SCHEMATIC VIEW OF A SURFACE MICROBURST ACCOMPANIED BY A MISOCYCLONE ALOFT. MOST MISOCYCLONES, LESS THAN 4 KM IN DIAMETER, ROTATE CYCLONICALLY WHILE EXCEPTIONAL ONES ROTATE ANTICYCLONICALLY.

(From Fujita)

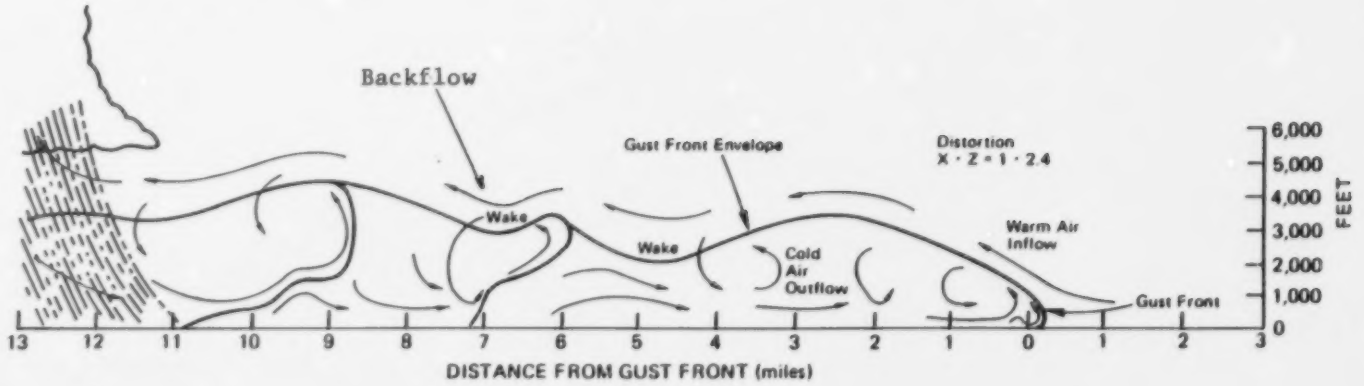

FIGURE 5

SQUALL LINE THUNDERSTORM OUTFLOW (SCHEMATIC)

(REPRODUCED FROM REPORT BY NATIONAL RESEARCH COUNCIL [13])

2.3 Laboratory and Numerical Models

Outgoing cold air is an example of a diverging three-dimensional gravity current. The flow is driven primarily by the buoyancy forces produced by the density difference between the cold air and the warmer air surrounding it. In the case of a microburst, some of the initial horizontal momentum comes from the momentum of the descending air.

According to Linden and Simpson [18], the flow may be modelled in the laboratory using aqueous salt solutions with different densities to simulate the excess density of the cold air. They have thus introduced laboratory experiments to explain some of the characteristics of observed microbursts. In particular, the experiments produce, both qualitatively and quantitatively, the properties observed in two-dimensional atmospheric gravity currents.

Numerical simulations of microburst outflows have been performed by various investigators. Recently Anderson [19] has reported on a series of numerical experiments with a three-dimensional numerical model. The work by Anderson shows that a single downdraft produces a circularly symmetric outflow. This suggests that any asymmetries observed in real-life microbursts may be caused by external environmental factors or by the superposition of individual small-scale downdrafts.

Some important results obtained from a numerical simulation of microbursts have also been reported by Droegemeier [20], Droegemeier and Davies-Jones [21]. In these studies, a two-dimensional numerical cloud model (simulated on a Cray-1 supercomputer) is used to investigate the velocity dynamics of microburst-scale downdrafts. The model efficiently solves the fully compressible equations of motion, along with appropriate equations governing the thermodynamic energy and water substance. By varying the ambient thermal stratification, relative humidity, and size and intensity of microburst draft, several parameter spaces are spanned with the model to elucidate the sub-cloud dynamics of microbursts.

2.3 Laboratory and Numerical Models (cont'd)

In another series of studies also based on a Cray-1 supercomputer, Droegemeier and Wilhelmson [22,23] have developed a two-dimensionsal numerical model and used it to investigate the dynamics of thunderstorm outflows. In Figure 6, we have reproduced two of the three photographs reported in [23]. The top photograph shows a submerged density current (salt water colored white) moving from left to right in a tank of fresh water; this photograph was obtained by Simpson using the laboratory model described in [18]. The bottom photograph shows a colour-enhanced image of the perturbation potential-temperature field from two-dimensional numerical outflow simulation; the blue shades in this photograph represent the coldest air. The closeness of these two photographs is remarkable.

In [24], Droegemeier deals with the issue of the enormous amounts of data produced by numerical models run on today's supercomputers. Specifically, this issue is addressed through examination of techniques for visualizing complex flow calculations.

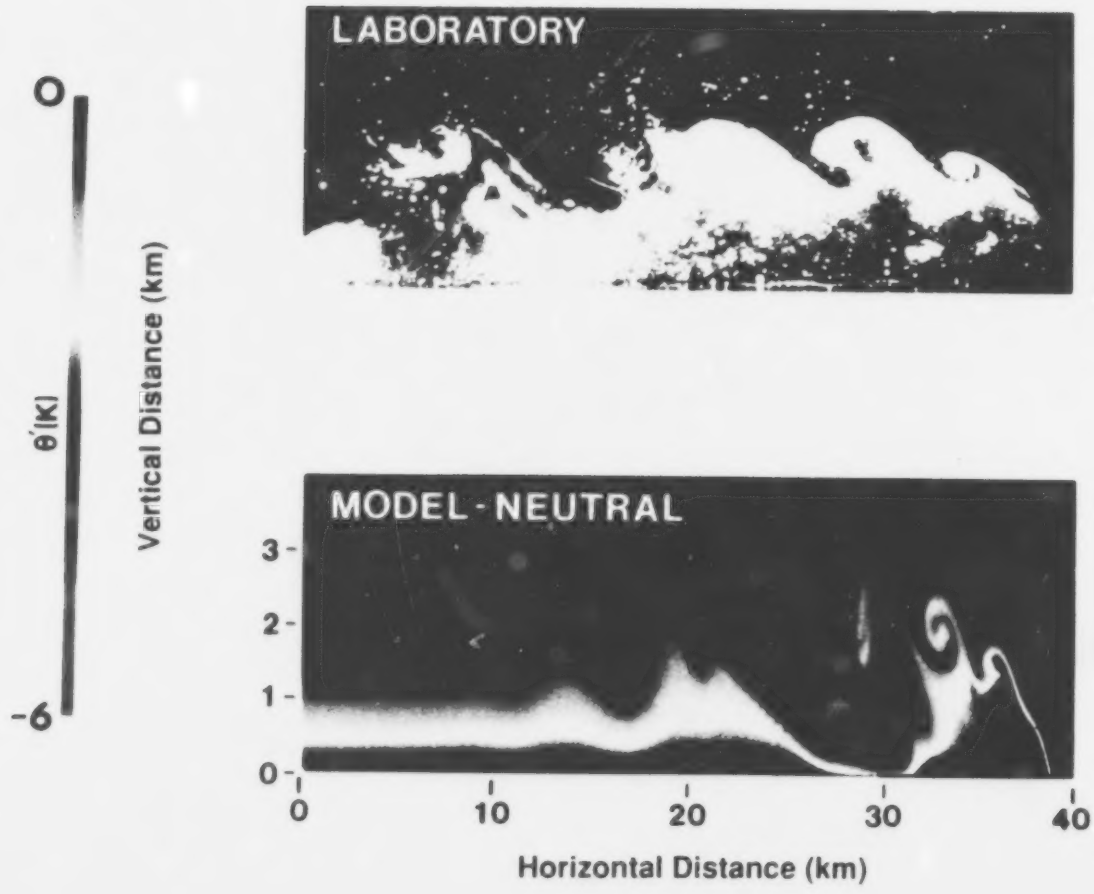

Figure 6

The top photograph shows a submerged density current (salt water colored white) moving from left to right in a tank of fresh water (photo by Prof. John E. Simpson, University of Cambridge). Shearing instabilities form at the leading edge of the current, and eventually break down into small-scale turbulence. The bottom photo shows an outflow propagating through a neutral boundary layer with a stable environment above. Note the suppression of the turbulent eddies relative to the completely neutral case above.

(Adapted from Droegemeier and Wilhelmson [23])

3.0 RADAR MEASUREMENTS AND REFLECTIVITY

This section explains the parameters that can be estimated from radar data and their interpretation for wind shear events.

3.1 Reflectivity

The **reflectivity** is general radar terminology for the scattering cross-section density of an atmospheric target. If the scattering particles that constitute the target are known to be spherical with diameters small compared to the radar wavelength λ, we may express the reflectivity η as follows:

$$\eta = \frac{\Pi^5}{\lambda^4} \left| K_w \right|^2 Z \qquad (1)$$

where K_w is the complex refractive index of water. The parameter Z, is called the **reflectivity factor**; it is defined as the summation per unit volume of the sixth power of the drop parameters, as shown by:

$$Z = \frac{1}{\Delta V} \sum_i D_i^6 \qquad (2)$$

where ΔV denotes volume of the scatterers, and D_i is the diameter of the ith scatterer. The values of Z commonly encountered in weather observations span many orders of magnitude. Accordingly, meteorologists use a logorithmic scale:

$$dBZ = 10\log_{10} Z \qquad (3)$$

where Z is in units of mm^6/m^3. Precipitation produces dBZ values ranging from near zero dBZ to values somewhere as high as 60 dBZ in regions of heavy rainfall and hail [3].

The measurement of rainfall intensity involves the determination of the radar energy, P, scattered back to the radar antenna by the populations of raindrops within a number of volumes. Each volume is defined by the antenna beamwidth and the duration of the radar pulse. In [25], it is shown that P is proportional to Z/r^2, where r is the range from the radar and Z is the reflectivity factor.

3.2 Doppler Spectrum

Where an RF pulse impinges on a target (e.g., raindrop), it induces molecular vibrations in synchronism with the time-varying electromagnetic field. For a monostatic radar (i.e., a radar for which the transmitter and receiver are co-located), the frequency of scattered radiation is Doppler-shifted by the amount [3]

$$f_d = -\frac{2V_r}{\lambda} \qquad (4)$$

where v_r is the radial component of the target velocity, and λ is the radar wavelength. The following points are noteworthy:

1) The velocity v_r is positive when the target moves away from the radar. Hence, the Doppler shift f_d is negative for a target moving away from the radar, and it is positive for a target moving towards the radar.

2) The factor of 2 in Eq. (4) is the result of a two-step change in frequency. First, the target's electric vibrational frequency is changed by v_r/λ. Second, the frequency of its radiation field in the direction of the receiver is increased by v_r/λ.

3) The Doppler shift f_d is zero if the target is stationary or moving tangentially to the radar.

The Doppler spectrum is a plot of the power spectrum (power spectral density) of the received signal as a function of the radial (Doppler) velocity v_r.

A pulsed Doppler radar supplies the three most important spectral moments [3,25]:

1) The **mean echo power** or zero moment of the Doppler spectrum (i.e., total area under the curve of the Doppler spectrum). This parameter is an indicator of liquid water content or precipitation rate in the resolution volume under study.

2) The **mean Doppler velocity** of the first moment of the Doppler spectrum normalized with respect to the zero moment. This second parameter is equal to the mean motion of scatterers weighted by their radar cross-sections. For near-horizontal antenna orientations, it is essentially an indication of air motion towards or away from the radar.

3.2 Doppler Spectrum (cont'd)

3) The spectral width or square root of the second moment about the first moment of the normalized Doppler spectrum. This third parameter is a measure of velocity dispersion (i.e., shear or turbulence) within the resolution volume.

While both coherent and noncoherent radars may be used to estimate zero and second order spectral moments of a weather echo, only a Doppler radar provides an estimate of the first spectral moment.

When performing spectral moment estimation, a large number of echo samples (acquired during a few milliseconds) must be processed in order to provide the desired accuracy. The accuracy of an estimate depends directly on the signal-to-noise ratio, distribution of velocities within the resolution volume, frequency response of the receiver, and the number of samples processed. Moreover, since the samples are collected while the antenna is rotating, we find that the desired precision determining the collection (i.e., dwell) time restricts the rotation rate of the antenna.

Let x_n denote a complex video sample with magnitude and phase corresponding to an electric field echo from some scatterers. For an estimate of the mean echo power, we may use the uniformly weighted average [3,25]:

$$\hat{P} = \frac{1}{M} \sum_{N=1}^{M} |x_n|^2 - N \qquad (5)$$

where M is the number of samples, and N is the receiver white noise power. The averaging in Eq. (5) is performed over a period MT_s where T_s is the pulse repetition time (PRT); this period must be large compared to the decorrelation time (i.e., reciprocal of the Doppler spectral width).

To estimate the mean Doppler velocity, the recommended procedure is to use the pulse-pair formula [3,25]:

$$\hat{V} = -\frac{\lambda}{4\pi T_s} \arg [R(T_s)] \qquad (6)$$

3.2 Doppler Spectrum (cont'd)

where

$$\hat{R}(T_s) = \frac{1}{M} \sum_{n=1}^{M-1} x_n^* \, x_{n-1} \qquad (7)$$

and the asterisk denotes complex conjugation. The argument of the autocorrelation function $\hat{R}(T_s)$ is in radians. Also, the negative sign in Eq. (4) signifies that a positive Doppler shift is created by negative target velocities. The pulse-pair formula was originally derived by Rummler [26]; it is an example of a blend between theoretical ingenuity (the algorithm) and technological advance (integrated digital circuits) [25].

When weather echo spectra closely follow a Gaussian shape, which is frequently the case, it is natural to estimate the spectral width from estimates of the autocorrelation function $R(T_s)$. Specifically, the pulse-pair algorithm for the estimate of Doppler spectral width reads [3,25]:

$$\sigma_v = \frac{\lambda}{2\pi T_s \sqrt{2}} \sqrt{\mathrm{Ln}\left(\frac{\hat{P}}{\hat{R}(T_s)}\right)} \qquad (8)$$

where the estimated $\hat{P}$ and $\hat{R}(T_s)$ are themselves defined by Eqs. (6) and (7), respectively.

3.3 Doppler Interpretation

The efficient use of a pulse Doppler radar by operational nowcasters/forecasters requires the physical understanding and recognition of certain meteorological signatures found in reflectivity and Doppler velocity fields. Wood and Brown [27,28] have developed an atlas of single Doppler velocity signatures (patterns) for the interpretation of nondivergent environmental winds. In particular, they provide simulated single Doppler velocity patterns for a variety of vertical wind profiles in a horizontal homogeneous environment. Patterns are produced for wind profiles that are increasingly complex. These patterns may be used to provide recognition and interpretation of wind fields.

The items that are sought in a Doppler display representation are basically three-fold:

1) Zero lines (i.e., lines of little or no Doppler velocity).

2) Pattern and gradient of isodops (i.e., lines of constant Doppler velocity).

3) Doppler velocity maxima and minima.

To develop their simulation model, Wood and Brown consider a Cartesian coordinate system in which x and y are horizontal distances from a Doppler radar site, as depicted in Figure 7. As the radar antenna rotates above a vertical axis z at a constant elevation angle, detailed displays are obtained of the Doppler component of the target velocity as a function of azimuth θ and slant range r_s (or height h). To interpret the simulation model, we may consider the example of wind field and associated Doppler velocity pattern shown in Figure 8. Part (a) of this figure shows a plan view of the wind field. It is assumed that the wind direction changes linearly from south at the radar location through southwest to west at the edge of the radar collection region; wind speed is assumed to be constant throughout. Part (b) of Figure 8 shows a plan view of the corresponding single Doppler velocity contours along an inverted conical surface (constant elevation angle) with the radar located at the apex (centre) as shown in Figure 7(a).

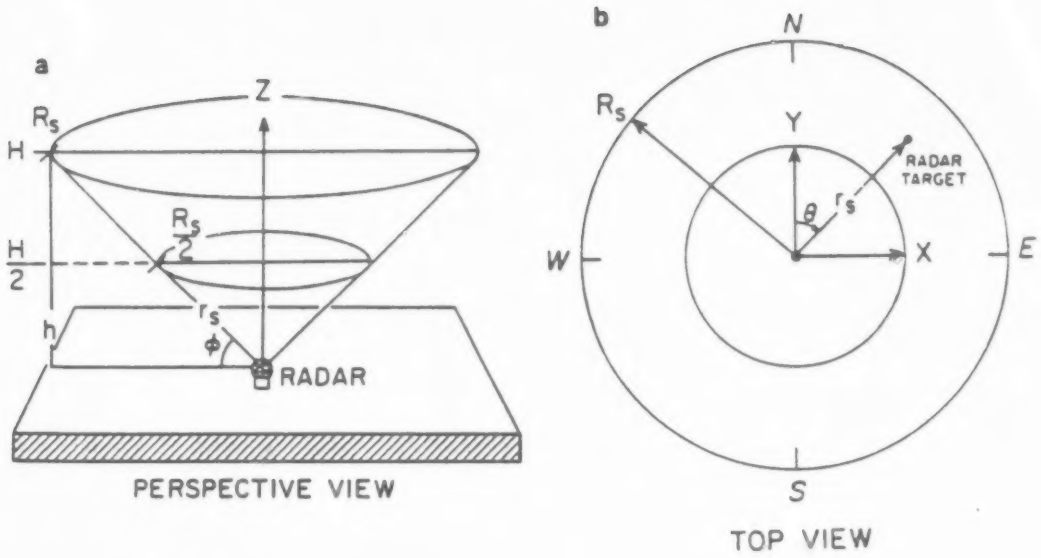

Figure 7 Doppler radar viewing configuration. (a) Radar scanning around vertical axis, z, at a constant elevation angle, ϕ; (b) view of (a) from the top, representing a PPI (plan position indicator) scope.

(Reproduced from Wood, Brown [27-28])

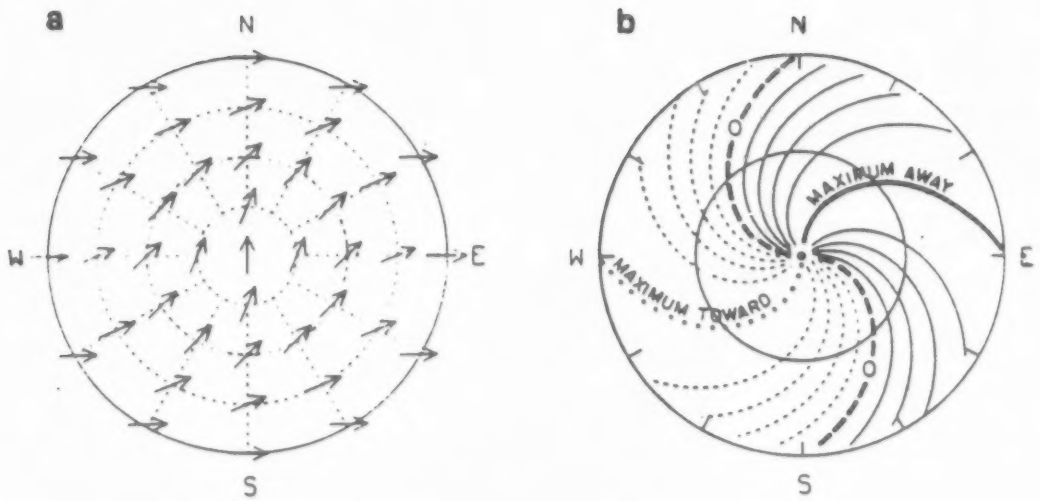

Figure 8 Plan view of (a) wind field and (b) corresponding single Doppler velocity contours along an inverted conical surface (constant elevation angle) with the radar at the apex (center) as shown in Fig. 7. The wind direction changes linearly from south at the radar location through southwest to west at the edge of the radar collection region; wind speed is constant throughout. Solid contours represent flow away from the radar, short dashes represent flow toward the radar, and heavy long dashes represent zero Doppler velocity. Heavier solid and dotted lines indicate locations of extreme Doppler velocity values within the display. The spacing between contour lines represents constant Doppler velocity intervals.

(Reproduced from Wood, Brown [27-28])

3.3 Doppler Interpretation (cont'd)

The solid contours in Figure 8(b) represent flow away from the radar; short dashed lines represent flow towards the radar, and heavy long dashes represent zero Doppler velocity. Heavy solid and dotted lines indicate locations of extreme (maximum and minimum) Doppler velocities within the display. Finally, the spacing between contour lines (isodopes) represents constant Doppler velocity intervals.

Figure 9 depicts the characteristic single Doppler radar signatures associated with the flow fields of a microburst. Specifically, the figure shows the signatures for upper-level inflow (convergence), middle-altitude rotation, and surface outflow (divergence).

Figure 10 depicts the signature associated with a gust front characterized by a region of cold air outflow converging with a warm air inflow. This convergence creates a long, thin line of negative radial shear (decrease in radial velocity with increasing radial distance) which is independent of whether the gust front is moving towards or away from the radar. Note also that the radial shear of a gust front has the opposite polarity to that of the surface outflow of a microburst.

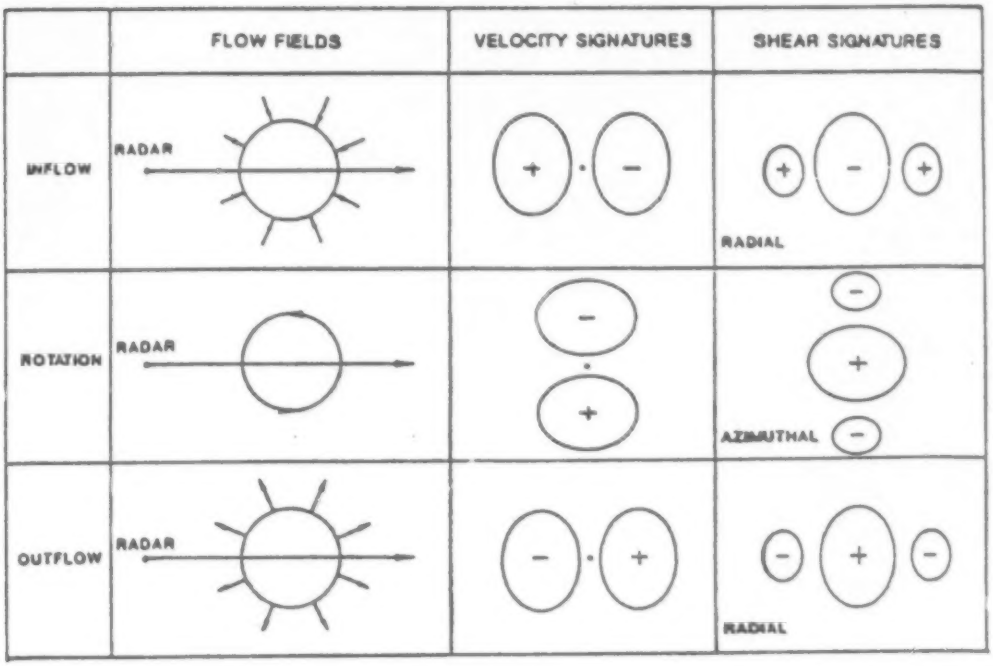

Figure 9 Single-Doppler radar signatures of a microburst

(Reproduced from Campbell and Olson [36])

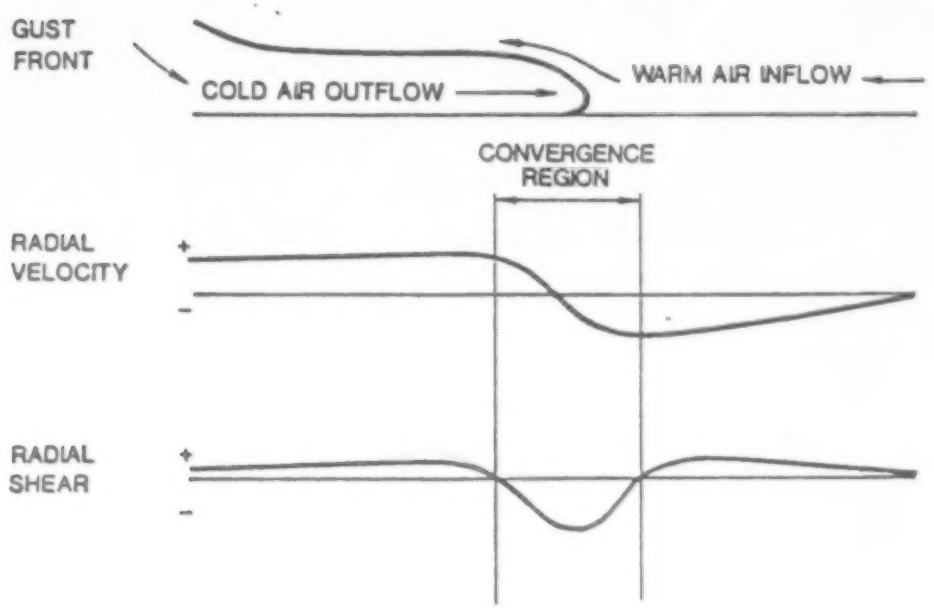

FIGURE 10 GUST FRONT CONVERGENCE SIGNATURES

(Reproduced from Campbell and Olson [36])

4.0 DETECTION AND PATTERN RECOGNITION ALGORITHMS

4.1 Automatic Detection of Microbursts

Merritt [29] describes an ad hoc algorithm for automatic detection of microbursts in Doppler weather radar displays. The detection algorithm operates in real time, extracting brief textual warning messages from the rapidly evolving radar images with high reliability. The hazardous regions are tracked by the algorithm as distributed events rather than individual point targets.

Merritt's algorithm focuses on the surface divergence formed by the downdraft in a microburst as the feature of interest. First, the surface divergence is the actual source of hazard to an aircraft flying through the microburst. Second, an image analysis procedure based on surface divergence alone minimizes complexity of the detection algorithm, and, hence, computation requirements.

Nevertheless, the algorithm has been shown to perform quite well.

The microburst surface outflow detection algorithm described by Merritt is composed of three basic stages, as illustrated in Figure 11. The three stages of the algorithm operate as follows:

(1) The first stage, labelled "shear segment identification", attempts to locate regions of divergent shear along individual radials of velocity measurements. The result is set of linear segments of detected shear.

(2) The second stage associates these linear segments in azimuth; hence, the label "azimuthal association". The association is done by joining together overlapping segments found on adjacent radials. Thus, the output of the second stage consists of a set of two-dimensional regions of shear.

(3) The third stage of the algorithm correlates these regions from one radar scan to the next. A time history is thereby computed for each region. Finally, those shear regions that exhibit adequate time continuity and sufficient outflow strength are declared as microbursts.

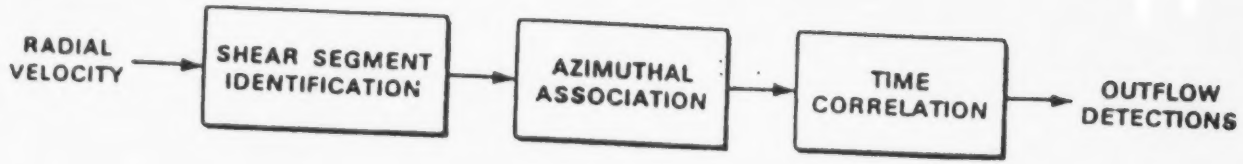

FIGURE 11 MICROBURST OUTFLOW DETECTION ALGORITHM BLOCK DIAGRAM

(Reproduced from Merritt [29])

4.1 Automatic Detection of Microbursts (cont'd)

The first stage, namely, the shear segment identification process, is the fundamental element in Merritt's algorithm. The remaining two stages are included primarily to filter out those segments and regions of the radar images that are not of adequate significance to produce microburst alarms.

Microbursts are of different sizes and shapes. Accordingly, the shear segment identification technique employed by Merritt is made scale-independent, thereby avoiding complications associated with scale-specific gradient operators. The technique is adapted from a pattern search algorithm developed by Zrnic and Gal-Chen [30].

The performance of Merritt's algorithm has been evaluated through an extensive data collection and analysis program, designed to compare the microburst alarms generated by the algorithm when applied to actual radar data with those identified by experienced radar meteorologists. To evaluate the performance of the algorithm, two basic quantities are computed: the probability of detection P_D and the probability of false alarm P_{FA}. The P_D is the ratio of the number of events detected by the algorithm to the total number of events. The P_{FA} is the ratio of the number of false alarms to the total number of alarms. The performance statistics presented in [29] are based on data collected at Huntsville, Alabama, using a Doppler weather radar. All of the microbursts used in the performance evaluation were wet in that they were associated with strong precipitation. A total of 38 microbursts (recorded during the period June 7 to September 26, 1986) were considered. However, no dry microbursts were available for the evaluation. For each of the days considered in the experimental evaluation, the outflow algorithm outputs were compared to the relevant ground truth data, and both detection and false alarms were recorded on each radar scan. The results of the evaluation are shown in Figure 12, which is broken down into several outflow strength categories. The detection threshold was set at 10 m/s. Figure 12 shows that the detection performance of Merritt's algorithm improves with the strength of the outflow, and that strong outflows (those above 20 m/s velocity change) are almost always detected. The figure also shows that microbursts are detected reliably on a scan-by-scan basis.

Date	Microbursts	Surface Scans	Timer Period (hrs)
June 7	5	40	1.7
July 1	7	75	2.2
July 25	12	67	3.8
July 31	6	144	2.2
Sept 26	8	100	3.7
Totals:	38	426	13.6

FIGURE 12 CASES USED FOR PERFORMANCE EVALUATION. ALL CASES TAKEN FROM 1986 DATA COLLECTED WITH FL2 RADAR, IN HUNTSVILLE, AL

(Reproduced from Merritt [29])

4.1 Automatic Detection of Microbursts (cont'd)

Indeed, it appears that the algorithm rarely misses a microburst over its entire lifetime. Specifically, of the 38 microbursts used for the statistical evaluation of the algorithm, only 3 microbursts were missed (92 percent detection rate). The microbursts that were missed by the algorithm were very weak (averaging a velocity difference of 13 m/s) and lasted for only a few minutes each.

4.2 Automatic Detection of Gust Fronts

Uyeda and Zrnic [31], and Sanford, Witt and Smith [32] describe a pattern recognition-theoretic algorithm for the automatic detection and tracking of gust fronts. The algorithm uses a procedure for searching through Doppler velocity data for large gradients (shears) along radials. Gust fronts propagating (at low levels) towards or away from the Doppler radar produce a well-defined line of convergent radial velocities. Except for the situation when the gust front is parallel to the radar beam, convergence is detected as a decrease in the velocities along a radial.

The gust front detection algorithm proceeds in a systematic fashion as follows:

(1) The algorithm starts by searching along a radial for runs of decreasing velocities, which characterize radial convergence. This search is done by comparing consecutive velocities. When a run terminates, a radial pattern vector is formed.

(2) For each pattern vector, the peak shear and endpoint velocity difference are computed. These features are then checked against shear and delta velocity thresholds. Runs that pass the thresholds are then formed into convergent features based upon range and azimuth overlap.

(3) Convergent features on different tilts are combined into gust fronts based upon vertical continuity.

(4) For every gust front identified by the algorithm, an estimate of wind speed and direction ahead of and behind the front is generated.

(5) Finally, after a gust front has been identified in two consecutive volume scans, predictions are made as to where the gust front will be located at future times.

The gust front detection algorithm uses radial velocity estimates collected by the Doppler radar. Owing to the fact that the processing performed by the algorithm is sensitive to rapid changes in the velocity field, it is essential that all forms of contamination resulting from ground clutter, point targets, and velocity aliasing are removed prior to application of the algorithm. Another point of interest is that the algorithm requires velocity data from two elevations tilts of the antenna (e.g., 0.5° and 1.0°).

4.3 Clutter Residue Map

Dangerous wind shears are often associated with an outflow region that is characterized by a low reflectiv-ity, occasionally as lows as zero dBZ. The detection of outflows with such low values of reflectivity is made difficult by the presence of ground clutter. In [35], Mann describes a clutter residue map editing system that removes ground clutter from those parts of the radar image where the antenna beamwidth and high-pass filters have not suppressed it adequately. Indeed, the use of a clutter residue map is called for in the TDWR (Terminal Doppler Weather Radar) specification by the FAA.

The operational function of a clutter residue editing map is to serve as a spatial threshold for weather measurements.

Ground clutter, produced by radar returns for trees and crops, may be viewed as a random (stochastic) process. Because of the statistical nature of these sources of ground clutter, it is likely that an instantaneous clutter level may exceed its respective map value. If this happens, the measured value may be falsely interpreted as a weather measurement. Such an occurrence is referred to as a clutter break-through. The rate of clutter break-through is dependent on the short-term statistical behaviour of the residual clutter. Indeed, this rate is variable in that it is subject to change due to variations in environmental conditions (e.g., wind speed).

The regulation of clutter break-through is the basic objective of the clutter residue map utilization algo-rithm. Specifically, the weather level must be X_{cr} times greater in magnitude then its corresponding clutter map cell level for the data in question to be considered valid. The use of this multiplicative factor increases the representation of each cell in the clutter map from a mean value to a higher quintile probability. The net effect is to reduce the probable occurrence of a clutter break-through. The method is effective for controlling clutter break-through due to short-term variability. In order to deal with long-term changes in the clutter environment (e.g., construction of new buildings), it may be necessary to construct a new clutter residue map.

4.4 An Artificial Intelligence Approach to Microburst Precursor Recognition

During the summer of 1984, the National Center for Atmospheric Research (NCAR) conducted a real-time operational microburst advisory service at the Denver Airport, under contract to the FAA. The effort was named the CLAWS (Classify, Locate, and Avoid Wind Shear) Project [33,34]. The principal tool for the advisory service was a single Doppler weather radar located 34 km northwest of the airport. The project was a clear demonstration of the ability of meteorologists to recognize microbursts and gust fronts by means of a Doppler radar. During the life of the CLAWS Project, 35 microburst advisories were issued, and one pilot credited a warning with saving his aircraft. The bad news, however, was that the CLAWS Project required two professionals with Master's and Ph.D. degrees in meteorology to be on duty round the clock in the airport control tower, and another two meteorologists to operate the Doppler radar [12]. Their task was to interpret the Doppler data very quickly and convert it into handwritten reports that were then read out to pilots. Needless to say, the whole operation was time-consuming, and the services of the meteorologists were expensive.

A lesson learned from the CLAWS Project is that the operational use of a Doppler radar to support air traffic control (ATC) functions will require an automated wind-shear recognition capability. The Merritt algorithm of Section 4.1 represents an important first step forward in this direction. However, the Merritt algorithm does not go far enough. Campbell and Olson [36] and Campbell [37] describe an artificial intelligence-based approach that utilizes additional microburst features aloft.

Specifically, the system described in [36,37] consists of an expert system equipped with numerical and computer vision capabilities that are designed to extract features from radar images. The overall aim is to make the system (called WX1) mimic the performance of a meteorologist in recognizing low-altitude wind-shear hazards from Doppler radar images.

For the system to emulate the performance of a radar meteorologist, it has to combine symbolic reasoning with visual processing. Accordingly, the basic requirement is to refine the massive details of the input radar data into an abstract representation of meteorological phenomena.

4.4 An Artificial Intelligence Approach to Microburst Precursor Recognition (cont'd)

An interesting feature of the WX1 system is that it does not depend on a single algorithm to interpret a given source of information. Rather, it uses a multitude of pattern recognition algorithms for extracting features from the incoming radar data. To extract wind-shear features from Doppler data, for example, the system uses two different algorithms. Neither algorithm by itself works in all cases. But by using the two algorithms together, the system is enabled to detect wind shears that would be missed otherwise.

Figure 13 depicts the block diagram of the WX1 system. It consists of two major elements:

(1) An observer that contains the numerical modelling and image processing capabilities of the system.

(2) An expert that contains the system's meteorological knowledge and symbolic reasoning capability.

The two elements of the system communicate with each other by exchanging messages, with the expert generating queries and the observer producing responses.

The observer (radar image processing element) performs numerical and computer vision operations on radar images. These operations include the processing of input radar data, the extraction of image features, and the performing of various computations on the features.

The role of the expert element is to examine and classify the results derived from lower-level pattern recognition algorithms. It contains symbolic models of weather phenomena to be recognized. In particular, the low-level features extracted by the observer from the input radar data are compared against these symbolic models. The most likely classification of each feature is thereby determined.

The results obtained on the WX1 system have demonstrated the ability of the system to recognize microburst and wind-shear gust fronts.

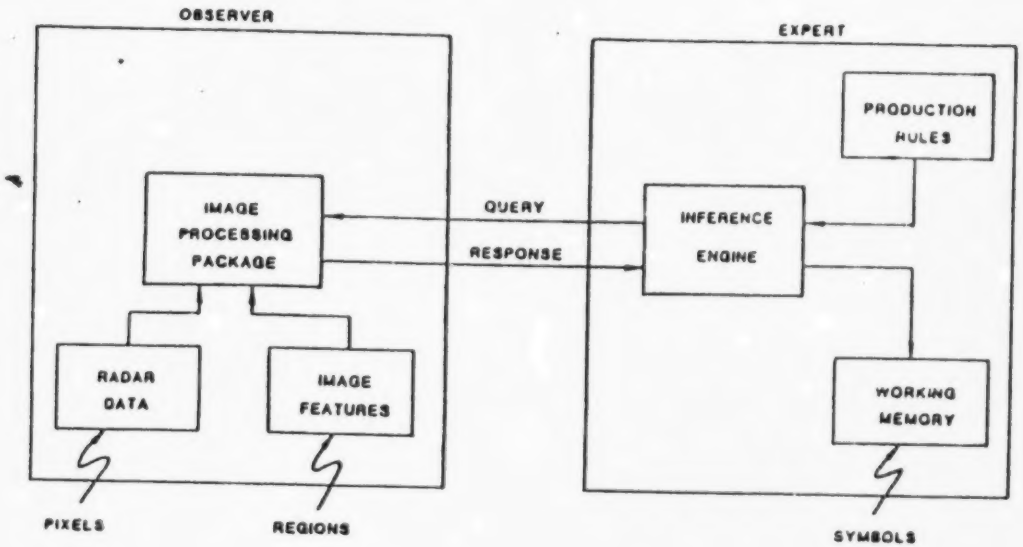

Figure 13 WX1 System Design.

(Reproduced from Campbell and Olson [36])

5.0 DATA UPDATE RATES AND LIMITATIONS

This section discusses the selection of pulse repetition frequency, antenna scanning strategies and the importance of low antenna sidelobes.

5.1 Pulse-repetition Frequency Selection

Atmospheric targets have certain physical characteristics that influence the design of a pulse Doppler radar. First, an atmospheric target may be distributed quasi-continuously over a large spatial region (tens to hundreds of kilometers). Second, the strength of a weather echo may span an 80 dB power range. Third, a weather echo is semicoherent (i.e., it is not purely sinusoidal). Accordingly, the nature of weather echoes imposes specific limitations and imposes tradeoffs on the selection of important radar parameters.

The **unambiguous range**, r_a, of a pulse Doppler radar is defined at the maximum distance over which a transmitted RF pulse can travel to a target and then echo back to the radar before the next pulse is transmitted. Let T_p denote the pulse repetition time, and c denote the speed of light. Then, the unambiguous range of the radar is defined by [38,39]

$$r_a = \frac{cT_p}{2} \qquad (9)$$

When a target of interest (e.g., storm cell) is located beyond r_a, its radar echo will actually appear at a range less than or equal to r_a. The target is then said to be **range aliased**.

The **unambiguous Doppler** velocity, v_a, measured by a Doppler radar is defined by [38,39]

$$v_a = \frac{\pm \lambda}{4T_p} \qquad (10)$$

where λ is the radar wavelength. Doppler data from a target with a radial velocity greater than v_a will appear aliased; that is, the target will appear to be at some reduced velocity that lies within the v_a interval.

5.1 Pulse-repetition Frequency Selection (cont'd)

Combining Eqs. (9) and (10), we find that for a specified radar wavelength λ the product of the unambiguous range and the unambiguous velocity is a constant, as shown by

$$r_a v_a = \pm \frac{\lambda c}{8} \qquad (11)$$

This relation presents a basic dilemma to the designer of a pulse Doppler radar. Specifically, it shows that the unambiguous range r_a or the unambiguous velocity v_a can be increased only at the expense of the other. To simultaneously collect both unambiguous range and velocity data on a target under the constraint of a specified radar wavelength Q, we get the graphs plotted in Figure 14 for the tradeoffs associated with the pulse repetition frequency ($1/T_p$) of the radar. In this figure, we have plotted the unambiguous range r_a versus the unambiguous velocity v_a for two radar frequencies: S-band and C-band [38].

We see therefore that the improper selection of the pulse repetition frequency (PRF) of a pulse Doppler weather radar may result in obscuration due to ambiguous range foldover from distant weather targets. The quality of the radar data collected may then be naturally degraded. This degradation in data quality may seriously affect the operation of automated detection algorithms. Hence, provisions must be made for proper selection of the PRF so as to ensure that the radar data processed by low-level wind-shear detection algorithms are of the highest quality possible.

One effective technique for ambiguity resolution in pulse Doppler weather radar is to use a staggered PRF scheme, which involves the staggered spacing between transmitted pulses.* Crocker [38] has developed a staggered PRF-based algorithm suitable for use in a Terminal Doppler Weather Radar (TDWR). The algorithm is designed to satisfy the following objectives:

1. Identification of distant weather targets.
2. Assessment of obscurations that may be attributed to distant weather targets as a function of frequency.

---

* Zrnic and Mahapatra [39] describe another technique for ambiguity resolution that uses a fixed PRF but with random phase shifts between transmitted pulses. According to Zrnic and Mahapatra, this second technique is superior in performance (but more demanding in complexity) than the staggered PRF technique in the context of NEXRAD.

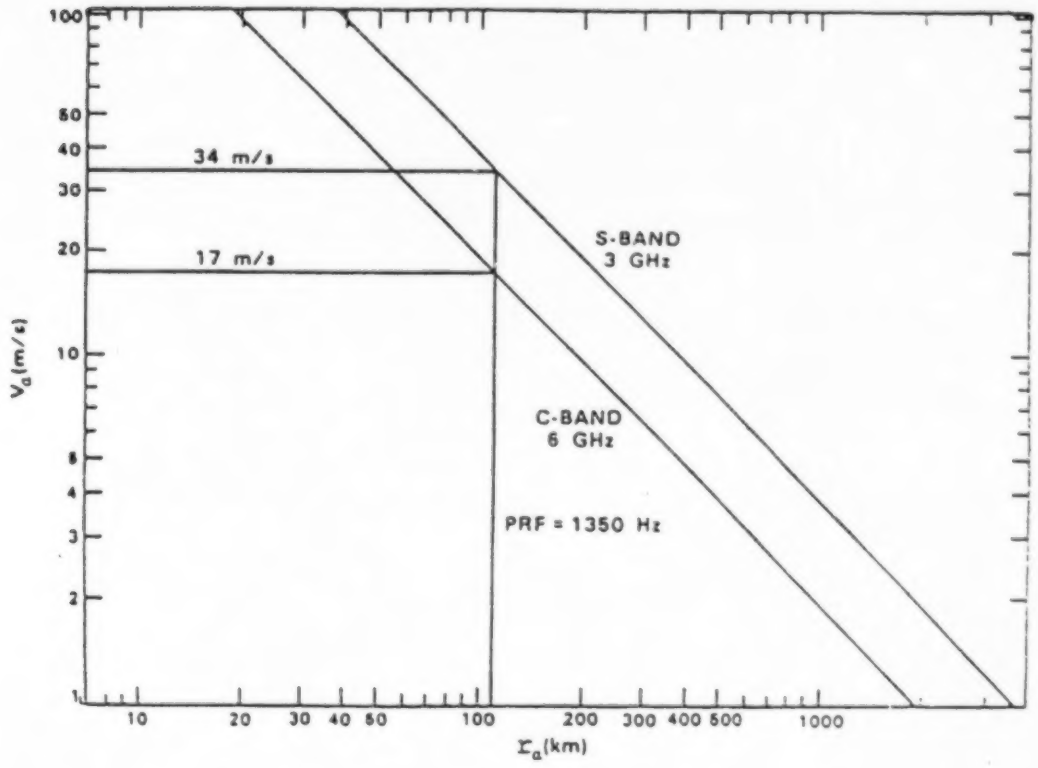

FIGURE 14 SIMULTANEOUS UNAMBIGUOUS r_a AND v_a INTERVALS

(Reproduced from Crocker [38])

5.1 Pulse-repetition Frequency Selection (cont'd)

3. Selection of a PRF that minimizes the obscuration.
4. Provision of a means for flagging any possible remaining obscured data.

According to Crocker [38], the algorithm is presently undergoing real-time tests at the test bed radar in Denver, Colorado.

5.2 Scanning Strategies

In a typical weather radar application, data concerning the weather conditions at a specific range of interest are refreshed at regular intervals corresponding to a complete scan cycle of the antenna. Another major issue in the specification of a pulse Doppler weather radar is therefore the minimum rate at which weather data collected by the radar must be updated, so that no phenomena potentially hazardous to aviation would go undetected. Campbell and Merritt [40] describe the requirements for the scanning strategy to be employed in the Terminal Doppler Weather Radar (TDWR).* The rational for the scanning strategy described therein is based on two criteria:

1. Detection of hazardous meteorological phenomena.
2. Minimization of range and velocity aliasing (folding) effects; this issue was considered in Section 13 and therefore will not be pursued further.

In the context of microbursts, the primary requirement for TDWR is the reliable and timely detection of surface outflows associated with microbursts. Since surface outflows evolve rapidly, it is necessary to perform frequent surface scans. Typically, a microburst reaches maximum intensity within five minutes from the onset of surface outflow. Hence, surface scans should be repeated once per minute in order to capture the peak outflow and permit the computation of trends in the microburst's evolution. Moreover, in order to provide for the adequate scanning of the surface outflow, the vertical beam size of the antenna should not exceed 300 m at the limit of the coverage region. Correspondingly, for a vertical beamwidth of 0.5°, the far edge of the coverage region should be no more than 34 km from the radar. Thus, in the off-airport case, the radar should be positioned no further than 23 km away from the reference point of the airport.

* Mahapatra and Zrnic [41] discuss a similar issue in the context of the Next Generation Weather Radar (NEXRAD).

5.2 Scanning Strategies (cont'd)

A secondary requirement of TDWR is to scan aloft for microburst features, which precede the initial surface outflow by about 10 minutes. The availability of microburst features can be exploited in two ways. First, the detection of a microburst feature aloft such as a descending core accompanied by convergence or rotation may be used to provide an early declaration of the microburst hazard. Second, the detection of features aloft may be used to improve the reliability of microburst detection. According to Campbell and Merritt [40], a scan sequence that repeats in 3 minutes would permit the scanning of a descending core twice before it reaches the ground surface. Note that the sequence of scans aloft is performed in order of increasing elevation angle, which ensures that a descending reflectivity core will be detected without ambiguity.

Table 1 shows the scanning sequence for the TDWR. The purpose of the individual scans listed in this table is as follows [42]:

1. The low-angle scans labelled "MB Outflow" are used to detect low-altitude divergence associated with microbursts. These scans occur once every minute.

2. The scans labelled "Wind Shift" are intended for detecting wind-shift lines such as gust fronts. Two scans at different elevations (0.5° and 1.0°) are needed for detecting the wind-shift lines.

3. The scan labelled "Low PRF" uses a low pulse repetition frequency, so that the Doppler radar can scan storms at long distances from the radar. The data thus collected are used to set the PRF for the next 5 minutes, so that second-trip echoes do not overlap the radar returns from nearby weather targets of interest.

4. The scans that are not labelled in Table 1 are used to scan above the airport environment, looking for radar features aloft that are associated with microbursts. These features, if they do exist, improve our confidence that the surface outflow is indeed microburst-related.

TABLE 1 1987 TDWR SCAN STRATEGY

Tilt #	Elevation Angle deg	Speed deg/sec	Range km	Scan Limit deg	Purpose
1	0.5	21	70	360	Wind shift/ MB outflow
2	2.2	25	44	120	
3	4.5				
4	6.7				
5	8.8				
6	11.0				
7	13.1				
8	0.4				MB outflow
9	1.0	21	70	360	wind shift
10	15.6	25	44	120	
11	18.6				
12	21.9	30			
13	25.8				
14	0.4	25			
15	30.1	30			
16	34.8				
17	1.1	25			
18	2.2				
19	4.5				
20	6.7				
21	0.4				MB outflow
22	0.6	30	460	360	Low PRF
23	8.8	25	44	120	
24	11.0				
25	13.1				
26	15.6				
27	18.6				
28	21.9	30			
29	0.4	25			MB outflow
30	25.8	30			
31	30.1				
32	34.8				
33	39.9				
34	1.2	460	360		

(Private Communication [42])

5.2 Scanning Strategies (cont'd)

Two complete volume scans are made every 5 minutes. The first volume scan is complete with tilt number 16 in the scan sequence. During tilts 1 through 16, the radar scans higher and higher above the airport, returning to low-elevation scans every minute to check for microbursts and windshifts.

In Appendix A, we present a functional block diagram of the TDWR and highlight some of its specifications of interest.

5.3 Antenna Sidelobes

The measurement capability required of a weather radar imposes a severe constraint on the antenna sidelobe level. This is mainly because of the distributed nature of weather-related scatterers and their large dynamic range (60 dB). Furthermore, the extent of solid angle covered by the scatterers may be several orders of magnitude greater than that covered by the antenna main lobe. Since the echo power is proportional to the integral of the reflectivity field weighted by the two-way antenna pattern, it follows that for weather targets of large extent, the power received through the antenna sidelobes may assume a value comparable to the power received through the main lobe [43]. This is especially true when the resolution volume resides in a weak reflectivity region.

There are no simple solutions to the antenna sidelobe problem [3]. Shrouding the antenna may help, and so may the elimination of radomes or the use of better ones.

6.0 SUMMARY AND DISCUSSION

In this report we have presented a review of the important issues involved in the use of a pulse Doppler radar for the detection of low-level wind shear due to microbursts and gust fronts.

A Doppler radar provides three important weather-related measurements:

(a) Reflectivity.
(b) Doppler velocity.
(c) Spectral width.

In the case of a wet microburst, the reflectivity provides information on the descending core. For all microbursts (wet and dry), the Doppler velocity is used to provide information on upper-level inflow (convergence), middle-altitude rotation, and surface outflow (divergence). As for spectral width, it provides a measure of turbulence. However, it appears that spectral width has not been exploited in the detection of microbursts. This may be a fruitful area for future research.

Present designs of Doppler weather radars have been based essentially on modifications of off-the-shelf radar equipment. There may be a need for a fresh look at the design of a Doppler radar optimized for the detection of microbursts and gust fronts, starting from first principles.

Canadian industry has the capability to produce radar systems and subsystems to meet the wind shear detection performance requirements. To our knowledge, suitable radar systems are not produced or available in Canada at present.

However, if we were to identify the research area with the biggest potential for payoff in the future, it would have to be that of an artificial intelligence approach to the recognition of low-altitude wind-shear hazards using data collected from a Doppler weather radar. We say this for a number of reasons. First, the use of precursors (microburst features aloft) and signature analysis to provide an early declaration of a microburst hazard is very much in its infancy; algorithms presently available represent a first stab at the problem. Second, the approach represents a multidisciplinary area for research, involving the use of numerical modelling of low-level wind-shear phenomena, radar image processing techniques, computer vision, and expert systems. Third it may well be that in the long run the perfection of an artificial intelligence approach to provide an automated wind-shear recognition capability is the only practical way in which the operational use of a Doppler weather radar can support air traffic control functions.

6.0 SUMMARY AND DISCUSSION (cont'd)

A word of caution is in order here. The perfection of an artificial intelligence approach to microburst detection is no simple task. For it to be successful, there will have to be an extensive data base encompassing wind-shear related phenomena. Moreover, it will have to integrate the multidisciplinary facets of the problem, with particular attention having to be given to phenomenology and signature analysis and classification. The final system, however successful, will naturally have to include a human interface as an integral component for final decision-making.

During the summer of 1988, tests were performed at the Denver International Airport, Colorado, involving the use of two Doppler weather radars (an X-band radar belonging to the Massachusetts Institute of Technology and a C-band radar belonging to the University of North Dakota). The aim of these tests was to evaluate the operational performance of the automatic wind-shear detection algorithms described in sections 9 and 10. If these tests proved successful, the automatic wind-shear detection algorithms will be incorporated into the TDWR design.

It should, however, be recognized that there are considerable regional differences between severe storms. In particular, the balance of thermodynamic and dynamic influences on the development of severe local storms in Canada is generally different from that in the Mid-West and South-East of the United States, which may lead to significant quantitative differences in kinematic structure. These regional differences may require that wind-shear detection algorithms developed in the United States will have to be tuned to the local meteorology in Canada. This observation is borne out by results on the evolution of mesocyclonic circulation in severe storms reported by Joe and Crozier [45]. The results reported therein were obtained using a partially coherent 5 cm

Doppler weather radar located at the King Weather Research Station of the Atmospheric Environment Service; characteristics of this radar are summarized in Appendix B. It appears that macrobursts have been observed with this radar quite frequently, but no microbursts. There may be two reasons for not having detected microbursts with this radar. First, the radar is magnetron-based and therefore only coherent on receive, thereby giving rise to phase noise. Second, the algorithm for detecting microbursts may not have been tuned properly for the local meteorology at King City.

It is therefore important that special attention be given to the tuning of wind-shear detection algorithms to suit local meteorology at Canadian Airports requiring the use of Doppler weather radar.

APPENDIX A

TERMINAL DOPPLER WEATHER RADAR

In this appendix we present aspects of the Terminal Doppler Weather Radar (TDWR) Specifications that are relevant to the study reported herein.* The primary mission of the TDWR is the timely detection and reporting of hazardous wind-shear phenomena. The secondary mission of the TDWR is the prediction of wind shifts and other hazardous weather phenomena. Thus, the TDWR products are:

1. Microburst Detection
2. Gust Front Detection
3. Wind Shift Prediction
4. Precipitation
5. Storm Movement Prediction
6. Turbulence
7. Tornado Detection
8. Microburst Precursor
9. Gust Front Enhancement
10. Convection Initiation
11. Microburst Track

Products 1 through 5 are going to be evaluated by the FAA during Summer 1988 at the Denver International Airport using two Doppler weather radars, one X-band and the other C-band.

The TDWR will have two operational modes: a Monitor mode and a Hazardous Weather mode; and a Maintenance mode.

Coverage: Basic TDWR coverage will be from ground level to 24,000 feet above ground level out to 48 nautical miles from the system. The required minimum range is 0.25 nautical miles. These requirements are derived from operational requirements for (1) hazardous wind-shear detection from ground level to 1500 feet for all areas within 6 nautical miles of the centre of the airport, and (2) detection of gust fronts within 40 nautical miles of the same airport reference point.

* Much of the material summarized in Appendix A is based on Reference [46].

Functional Requirements: The TDWR system is composed of four major functional areas, as depicted in Figure 15:

(a) Radar Data Acquisition (RDA)
(b) Radar Product Generation (RPG)
(c) Remote Monitoring Subsystem (RMS)
(d) Display Function (DF)

None of these functions is permitted to interfere with the performance of any other.

The RDA function is responsible for weather detection, clutter suppression, and primitive processing functions. The RDA function is accomplished by the antenna subsystem, the transmitter, receiver, and signal processing equipment.

The RPG function is responsible for control command generation and real-time product generation. The RPG provides the intelligence that permits the TDWR system to fulfill its tasks automatically.

The RMS function is provided for automatic fault detection and location in the system. The RMS is functionally independent of the major TDWR system functions.

The DF will display the TDWR output to controllers and supervisors.
Archiving: The TDWR will support the storage of weather products and related data.

Antenna Subsystem
The antenna is required to provide a pencil beam no more than 0.5 $\pm$0.1 degree at the half-power points in both azimuth and elevation.

In any plane, the first sidelobe is required to be below -27 dB relative to the peak gain of the main beam. In the region between $\pm$1° and $\pm$5°, the sidelobe level is required to be below the straight line connecting -27 dB at $\pm$1° and -34 dB at $\pm$5° in all planes. Between $\pm$5° and $\pm$180°, the sidelobe envelope is required to average below -40 dB relative to the peak of the main beam. In this region, the peak of an individual sidelobe may be averaged with the peaks of the two nearest sidelobes on either side, provided that the level of no individual sidelobe exceeds -34 dB and that the combined angular extent of all peaks exceeding -40 dB does not exceed 30°. A null below -40 dB relative to the main lobe is required to exist between 0° and +1° and between 0° and -1°.

In a plane, the antenna is required to maintain the cross-polarization radiation at or below the level specified for the sidelobe and backlobe levels of the co-polarized radiation within the angular regions applicable to these levels. Within the main lobe angular region, the antenna is required to maintain the cross-polarized component at least 20 dB below the peak of the main beam of the co-polarized radiation.

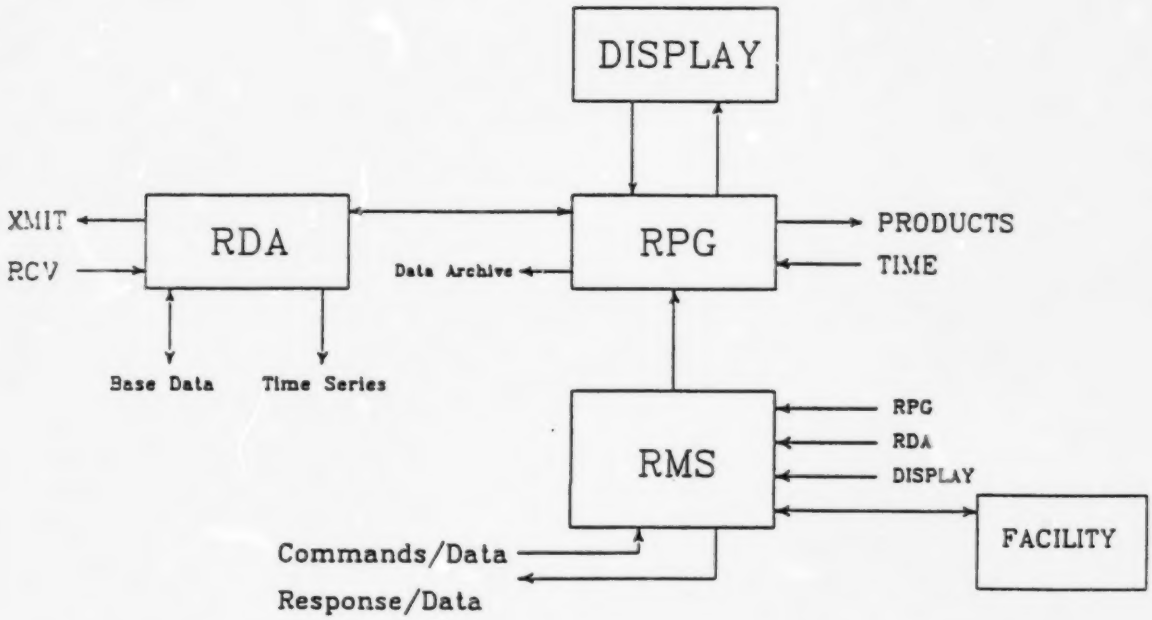

FIGURE 15 SYSTEM FUNCTIONAL RELATIONSHIPS

(Reproduced from U.S. Department of Transporation, Federal Aviation Administration [46])

The radio frequency (RF) beam position is required to be positioned to within ±0.05° of the command beam position. The resolution of the beam position measurements is required to be 0.012 or better. The RF beam positioning response to an angle input command has to be repeatable to within ±0.024° of any previous identical angle input command.

Transmitter

The TDWR is to be a C-band radar. The transmitter will use a klystron, making the TDWR fully coherent. The operating frequency will be any on of 51 possible values differing by 1 MHz in the range 5.600 to 5.650 GHz.

Receiver

The receiver accepts signals from the antenna subsystem, provides the necessary amplification, and detects microwave (radar) returns for use by the signal processor.

The receiver will have an instantaneous dynamic range of at least 100 dB.

It will provide an unambiguous estimate of the mean radial velocity from -40 to +40 meters/second with unfolding.

Accuracy

The TDWR is required to meet the following accuracies while operating over the range of dwell times compatible with a scan speed of 25 degrees/second, and with ground clutter suppression inhibited:

(a) Mean radial velocity measurement: The RDA is required to provide an estimate of the mean radial velocity with a standard deviation less than or equal to 1 meter/second, including quantization and computational errors, for a true spectral width of 4 meters/second and for signal-to-noise ratio (SNR) greater than 8 dB. The resolution of the measurements is required to be less than or equal to 0.1 meter/second. For a Gaussian spectrum, the bias (error) has to be less than 1.0 meter/second for true spectral widths between 1.0 meter/second and 4.0 meter/second and SNR greater than 10.0 dB.

(b) Reflectivity measurements: The RDA is required to provide an estimate of reflectivity with a standard deviation less than or equal to 2 dB (including quantization and computational errors) for SNR greater than 10 dB and spectral widths between 1.0 and 4.0 meters/second. The resolution of the measurements has to be less than or equal to 1 dB. For a Gaussian spectrum, the bias (error) has to be less than 2 dB for true spectral widths between 1.0 and 4.0 meters/second and SNR greater than 10.0 dB.

(c) Spectral width estimates: The RDA is required to provide an estimate of velocity spectral width with a standard deviation less than or equal to 1 meter/second (including quantization and computational errors) for true spectral widths between 1 and 4 meters/second and for SNR greater than 10 dB. The resolution of the estimate will be no greater than 0.10 meter/second. For a Gaussian spectrum, the bias (error) has to be less than 2 dB for true spectral widths between 1.0 and 4.0 meters/second and SNR greater than 10.0 dB.

(d) Range error: Due to all sources of error, the error in range measurements is required to be less than 50 meters.

(e) Signal-to-noise ratio measurement: The RDA is required to provide an estimate of the received (first trip) weather signal-to-noise power ratio with a standard deviation no greater than 2 dB (including quantization and computational errors) for true spectral widths between 1.0 and 4.0 meters/second and for SNR greater than 0 dB. The resolution of the measurements will be no greater than 1 dB. The bias (error) is required to be less than 2 dB for a true SNR greater than 0 dB.

Ground Clutter Suppression

Ground clutter suppression is described by the improvement in the ability to measure weather parameters in the presence of two different clutter models. Clutter model A is a Gaussian random (stochastic) process with a Gaussian spectrum centered a zero mean velocity. The clutter spectral width is the root mean square of 0.1 meter/second plus the root mean squared (rms) spectral width resulting from the antenna rotation at the lowest two elevation scans. Clutter model B represents a scattering echo as the antenna scans by a point target and consists of a complex waveform with an amplitude that is an approximation of the two-way antenna pattern.

Clutter suppression is defined as the signal-to-clutter power ratio at the input of a clutter suppression filter divided by the signal-to-clutter power ratio at the output of the filter. If the clutter suppression filter is linear time-invariant with unity gain in the pass band, followed by a conventional weather return parameter estimate process (e.g., pulse-pair algorithm), the clutter rejection performance is the clutter input power to filter output power for each of the two clutter models. The calculation may then proceed as indicated in Figure 16.

The RDA is required to provide at least 50 dB of ground clutter suppression for all scan strategies. When ground clutter suppression is required (e.g., high elevation angle scans), the RDA will inhibit its use with no designation in weather parameter estimation accuracy.

For each 3 km range interval commencing at the minimum detection range, the RDA is required to utilize clutter suppression level maps to select either the applicable clutter suppression level from Table 1 or no clutter suppression.

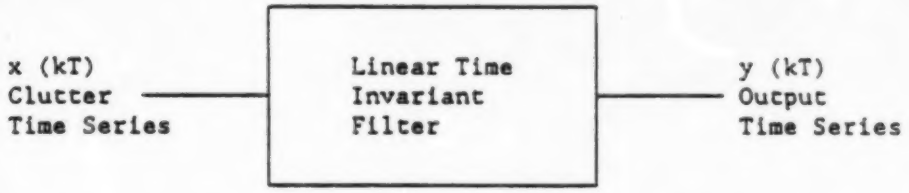

T = Pulse Repetition Time

Clutter Model	Algorithm for Computing Clutter Suppression Capability: I

Clutter Model	Algorithm for Computing Clutter Suppression Capability: I

A	$I = 10 \log_{10}(\langle \lvert x(kT) \rvert^2 \rangle / \langle \lvert y(kT) \rvert^2 \rangle)$
B	$I = 10 \log_{10}(\max\langle \lvert x(kT) \rvert^2 \rangle / \max\langle \lvert y(kT) \rvert^2 \rangle)$

$\langle\rangle$ represents the value of the time average over a moving window as the antenna ascans past a point target. The window time duration shall correspond to the appropriate weather parameter estimation interval. The scan rate assumed should be that used on the lowest two elevations.

$||$ represents absolute value.

FIGURE 16 CLUTTER SUPPRESSION CAPABILITY CHARACTERIZATION FOR LINEAR TIME INVARIANT CLUTTER FILTERING

(Reproduced from U.S. Department of Transportation, Federal Aviation Administration [46])

TABLE A-1 REQUIRED GROUND CLUTTER SUPPRESSION CAPABILITY

Minimum Usable Mean Radial Velocity in Meters/Second	Clutter Model A in dB (Distributed)	Clutter Model B in dB (Point Target)
2	20	20
3	28	30
4	50	50

APPENDIX B

KING CITY WEATHER RADAR

The Atmospheric Environment Service (AES) of Canada operates a 5-cm Doppler Weather Radar at King City, Southern Ontario, where it has been in use since late 1985 [45]. The radar is manufactured by Enterprise Electronic Corporation, Alabama. The radar uses a pulsed magnetron with partial coherence on receive. Table 2 summarizes the basic parameters of the radar.*

Custom interface hardware allows computer control of the radar and access to the raw radar returns. The radar products include severe weather, Doppler radial velocity and mesocyclone maps.

The radar operates with two sequential scanning strategies:

(a) A 24°-elevation conventional volume scan sequence from 0.3° to 24.4°.

(b) A 3°-elevation Doppler sequence, usually 0.5°, 1.4° and 3.4°.

Each sequence takes approximately 5 minutes; therefore, the radar operates on a 10-minute cycle. In the Doppler mode, the PRF alternates between 1196 and 892 pulses per second every other 0.5° of azimuth. Hence, a total of 720 radials are collected per elevation angle. The alternating PRF data is combined to unfold the radial velocity in real-time to an extended Nyquist velocity of 48 meters/second.

* The material presented in Appendix B is based on reference [45].

TABLE 2: BASIC RADAR PARAMETERS

PARAMETER	CONVENTIONAL	DOPPLER
Frequency, GHz	5.625	5.625
Wavelength, cm	5.33	5.33
Peak power, kW	260	260
Pulse duration, microsecond	2.0	0.5
Pulse length, meter	600	150
Range resolution, meter	300	75
Max. Range, kilo-meter	256	113
Pulse repetition frequency (PRF, pulse/sec.)	250	892, 1190
Scanning rate, revolutions/ minute	6.00	0.75
Antenna Gain, dB	48	48
Antenna Beamwidth, degree	0.65	0.65
Samples	8	64

REFERENCES

[1] Battan, L.J., 1973, "Radar Observation of the Atmosphere", (The University of Chicago Press).

[2] Browning, K.A. (editor), 1982, "Nowcasting" (Academic Press).

[3] Doviak, R.J., and Zenic, D.S., 1984, "Doppler Radar and Weather Observations", (Academic Press).

[4] Atlas, D., 1974, "Advances in radar meteorology", Adv. Geophysics, pp. 317-478.

[5] Skolnik, M.I. (editor), 1970, "Radar Handbook", (McGraw-Hill).

[6] Skolnik, M.I., 1980, "Introduction to Radar Systems", (McGraw-Hill).

[7] Seliga, T.A. and Bringi, V.N., 1978, "Differential reflectivity and differential phase shift: Applications in radar meteorology", Radio Science, pp. 271-275.

[8] Stewart, O., 1958, "Danger in the Air", (William Clowed and Sons).

[9] Fujita, T.T., 1985, "The Downburst: Microburst and Macroburst", (The University of Chicago Press).

[10] McCarthy, J., Wilson, J.W., and Fujita, T.T., 1982, "The Joint Airport Weather Studies Project", Bull. Amer. Meteorological Soc., pp. 15-22.

[11] Bedard, A.J. Jr., and LeFebvre, T.J., "The JAWS Project", Wave Propagation Laboratory, Boulder, Colorado, Report No. 01-86.

[12] Zorpette, G., "The Menacing Microburst", 1986, IEEE Spectrum, pp. 50-56.

[13] National Research Council, 1983, "Low-Altitude Wind Shear and its Hazard to Aviation", (National Academy Press).

[14] McCarthy, J., 1984, "Recommendations for coping with microburst Wind Shear: An Aviation Hazard", J. of Air Law and Commerce.

[15] Wakimoto, R.M., 1985, "Forecasting Dry Microburst Activity over the High Plains", Monthly Weather Review, pp. 1131-1143.

[16] Goff, R.C., 1980, "Low-Level Wind Shear Alert Systems (LLAWS)", Report No. FAA-RD-80-45, Federal Aviation Administration.

[17] Simpson, J.E., 1969, "A comparison between laboratory and atmospheric density currents", Quart. J.R. Met. Soc., pp. 758-765.

[18] Linden, P.F., and Simpson, J.E., 1985, "Microbursts: A Hazard for Aircraft", Nature, pp. 601-602.

[19] Anderson, J.R., 1987, "Numerical simulation of thunderstorm microburst outflows", submitted to Monthly Weather Review.

[20] Droegemeier, K.K., 1988, "Simulation of Microburst vorticity dynamics", Conf. on Severe Local Storms, Baltimore, Maryland.

[21] Droegemeier, K.K., and Davies-Jones, R.P., 1987, "Simulation of Thunderstorm Microbursts with a supercompressible numerical model", in book entitled "Numerical methods in laminar and turbulent flow", edited by G. Taylor, W. G. Habash, and M.M. Hafez (Pineridge Press).

[22] Droegemeier, K.K. and Wilhelmson, R.B., 1987, "Numerical Simulation of Thunderstorms Outflow Dynamics, Part I: Outflow Sensitivity Experiments and Turbulence Dynamics", J. Atmospheric Sciences, pp. 1180-1210.

[23] Droegemeier, K.K. and Wilhelmson, R.B., 1986, "Kelvin-Helmholtz instability in a numerically simulated thunderstorm outflow", Bulletin of Amer. Meteorological Spc., pp. 416-417.

[24] Droegemeier, K.K., 1987, "The use of realtime animation graphics in the analysis of meteorological model data", Workshop on Meteorological Operational Systems, Reading, England.

[25] Zrnic, D.S., and Lee, J.T., 1982, "Pulsed Doppler radar detects weather hazards to aviation", J. Aircraft, pp. 183-190.

[26] Rummler, W.D., 1968, "Introduction of a new estimator for velocity spectral parameters", Bell Telephone Laboratories (Whippany, N.J.), Tech. Memo. MM-68-4121-5.

[27] Wood, V.T., and Brown, R.A., 1986, "Single Doppler velocity signature interpretation of nondivergent environmental winds", J. Atmospherical Oceanic Tech., pp. 114-128.

[28] Wood, V.T., and Brown, R.A., 1983, "Single Doppler velocity signatures: An atlas of patterns in clear air/widespread precepitation and convective storms", National Severe Storms Laboratory (Norman, Oklahoma), Tech. Memo. ERL-SSL-95.

[29] Merritt, M.W., 1987, "Automated detection of microburst Wind Shear for terminal Doppler weather radar", Digital Image Processing and Visual Communications Technologies in Meteorology, Cambridge, MA.

[30] NEXRAD Program Office, 1985, "Divergence detection algorithm description", NX-DR-03-042/10.

[31] Uyeda, H., and Zrnic, D.S., 1985, "Automatic detection of gust fronts", National Severe Storms Laboratory, Norman, Oklahoma, DOT/FAA/PM-85/11.

[32] Sanford, J.P., Witt, A., and Smith, S., 1987, "Gust front wind shift detection algorithm description (PDL)", MIT Lincoln Laboratory and National Severe Storms Laboratory.

[33] McCarthy, J., Wilson, J.w., and Helmjfelt, M.R., 1986, "Operational Wind Shear detection and warning: The CLAWS experience at Denver and future objectives", 23rd Conference on Radar Meteorology.

[34] Roberts, R.D., and Wilson, J.W., 1986, "Nowcasting Microburst events using single Doppler radar data", 23rd Conference on Meteorology.

[35] Mann, D.R., 1987, "TDWR clutter residue map generation and usage", MIT Lincoln Laboratory, LL ATC-148, DOT/FAA/PM-87-26.

[36] Campbell, S.D., and Olson, S.H., 1987, "Recognizing low-altitude Wind Shear hazards from Doppler weather radar: An artificial intelligence approach", J. Atmospheric and Oceanic Tech., pp. 5-18.

[37] Campbell, S.D., 1988, "Microburst precursor recognition using an expert system approach", Conf. Interactive Information and Processing Systems for Meteorology, Oceanography and Hydrology, Anaheim, California.

[38] Crocker, S.C., 1987, "TDWR PRF Selection Criteria", MIT Lincoln Laboratory, LL ATC-147, DOT/FAA/PM-87-25.

[39] Zrnic, D.S., and Mahapatra, P., 1985, "Two methods of ambiguity resolution in pulse Doppler weather radars", IEEE Trans. Aerospace and Electronic Systems, pp. 470-483.

[40] Campbell, S.D., and Merritt, M.W., 1987, "TDWR scan strategy requirements", MIT Lincoln Laboratory, ATC-144.

[41] Mahapatra, P., and Zrnic, D.S., 1984, "A physical basis for NEXRAD data update rates", J. Aircraft, pp. 840-850.

[42] Biter, C.J., 1988, private communications.

[43] Sachidananda, M., Dorviac, R.J., and Zrnic, D.S., 1985, "Whitening of sidelobe powers for pattern switching in radar array antenna", IEEE Trans. Antennas and Propagation, pp. 727-735.

[44] Litva, J., 1988, Wind Shear Study: Meteorological Review", Communications Research Laboratory, McMaster University, Report No. 184.

[45] Joe, P.J., and Crozier, C.L., 1988, "Evolution of Mesocyclonic Circulation in Severe Storms", to be published in Preprints of the 10th International Cloud Physics Conference, Bad Homburg, FRG, August 1988.

[46] U.S. Department of Transportation, Federal Aviation Administration, "Specification: Terminal Doppler Weather Radar", FAA-E-28060, February 19, 1988.

PART C

CONCEPTUAL DESIGNS AND COST ESTIMATES

1.0 INTRODUCTION

The aim of this latter part of the report is to crystalize the main outcomes and recommendations of the study in terms of preferred solutions to the wind shear detection problem and associated order of magnitude costs. Since much of this information has already been discussed earlier in the report, some repetition is unavoidable.

It is the opinion of the authors that two key technologies used as an integral part of operational equipments can provide Canadian airports with reliable warning of hazardous low-level wind shear conditions. The technologies relate to anemometers and pulse-Doppler radars. Specifically two systems have been identified:

a) A network of anemometers for low-density airports and
b) A network of anemometers combined with a single pulse-Doppler radar.

Each of these systems will now be discussed.

2.0 ANEMOMETER SYSTEM

A system which comprises an array of wind-velocity measuring instruments located on the ground and placed within, or on, the airport perimeter can provide detection of large-scale wind shear activity. Wind shear activity such as gust fronts, sea breezes and macrobursts are amenable to detection with a relatively small number of anemometers placed around the airport. The location of the anemometers must be chosen such that they monitor all runways used. No precise guidelines are given here to where the anemometers should be placed, however two examples of airports employing anemometer systems are presented, Hong Kong and Denver Stapleton International. The former airport has one runway NW-SE the latter 4 runways: 2 running EW and 2 running NS.

Figures 1.1 and 1.2 show the location of the anemometers and as can be seen by comparing Figure 1.1 with either Figure 1.2(a) or 1.2(b) the distribution of the anemometers is clearly different for each airport. A brief description of the system utilized at Stapleton is given below, if familiar to the reader this section, section 2.1.1, may be skipped.

2.1 LLWAS

For the Denver Stapleton airport installation there were 5 wind sensors and one centrefield sensor, the spacing between sensors being approximately >2.5km.

Typically a LLWAS system consists of a centrefield wind sensor and 5 outlying sensors normally about 3km from the center site, located on the basis of meteorological factors, terrain considerations, logistical constraints, and to favor the Instrument Landing System (ILS). The sensors have propeller vanes on standards that rise about 10 to 60 feet above the ground as necessary to obtain clear airflow above terrain or other obstructions. Each site is polled once every 10 seconds. The centrefield site is considered a reference site, for which a 2-minute running average of wind velocity is maintained.

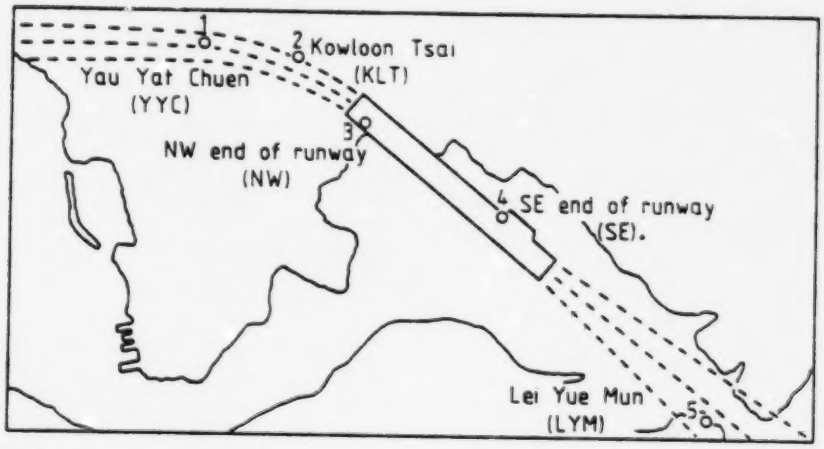

FIGURE 1.1: LOCATIONS OF THE FIVE ANEMOMETERS FOR HONG KONG LOW-LEVEL WIND SHEAR DETECTION SYSTEM

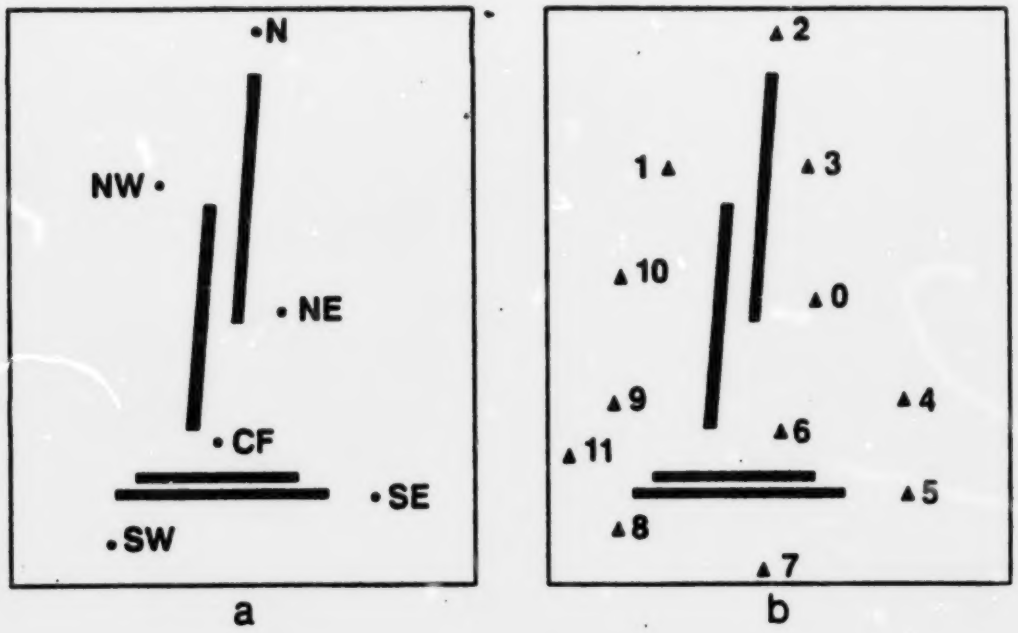

FIGURE 1.2:

Illustration of the LLWAS at Denver Stapleton International Airport, showing a generalized array of wind sensors spaced around airport. Note that spacing is wider than typical microburst, resulting in many microbursts slipping through the "net." The system was originally designed to detect gust fronts rather than microbursts. (a) Shows the spacing prior to 1985, while (b) shows the spacing as enhanced to better detect microbursts. This improved spacing (b) is available at both Denver Stapleton International Airport and New Orleans International Airport. (Source: FAA, 1987a).

LLWAS is controlled by a central miniprocessor (usually located in the control tower), which maintains the 2-minute running average of the centrefield wind. This information is continuously displayed in the tower, is used by controllers, and is relayed to pilots.

In addition, once every 10 seconds, the miniprocessor compares the 10-second wind at outlying sites to the 2-minute average at the center site. A vector difference computation is made and, if a 15-knot threshold is reached or exceeded, an alert is given to tower controllers. The computer normally displays only the centrefield average wind velocity, plus a gust factor,* if appropriate. But if the wind shear threshold is exceeded, the wind velocity at the appropriate peripheral anemometer also is displayed. Controllers may, however, choose to display any or all sectors at one time.

The wind shear calculation is designed to detect the sudden onset of a gust front at an outlying site by comparing the wind discrepancy at the outlying site with that at the centrefield site. The centrefield site, because of its long averaging period, cannot effectively detect wind shears.

LLWAS has been installed in many U.S. airports. LLWAS is the only operational means currently in use excluding some on-board sensors for detecting low-level wind shear. Nevertheless, the system has several limitations. These include the following:

- The system cannot measure winds above the sensors on the ground. This may not be a big problem for gust fronts or sea breezes, but it limits the detection of wind shear that may not be present at the surface.

- There are temporal and spatial resolution limitations that may present serious problems for detecting the smallest-scale events. Although LLWAS sensors are located an average of about 3km between the centrefield and remote sites, the effective wind shear resolution is near 6km because of the long averaging period at the centrefield site. Likewise, the temporal resolution is comprised by the long averaging at the centrefield site; a brief high-wind encounter at centrefield would probably not be identified. This effectively eliminates the centrefield site as a high-resolution wind-shear sensor.

---

* A gust factor is also calculated and displayed for the centrefield site, this factor being the difference between the peak and mean values of the wind velocity during the 2-minute averaging period.

- o Surface wind events outside of the perimeter of the anemometer field would not be detected.

- o Vertical wind motions are not sensed directly; only horizontal ones are detected, and these, of course, may have been initiated by downdrafts.

- o Sensors do not directly measure wind along flight paths and are thus susceptible to reporting events that may not reflect wind shear or lack of one on an airplane's flight path.

2.2 Anemometer Based System For Microburst Detection

The previous section highlighted some of the deficiencies of the LLWAS system, in particular resolution is relevant to the microburst detection problem. To provide improved performance against small scale wind shear events, such as microbursts, future systems, such as those that could be installed at Canadian airports, should:

- o utilize sufficient measuring stations close to the runways to provide a spatial resolution to capture small scale events. This could mean up to 12 stations at a large multi-runway airport or less (say 6) for a single runway airport.

- o be equipped with locally tuned algorithms to specifically detect microbursts.

- o have a good man-machine interface.

- o perhaps utilize pressure sensors.

2.3 Technical & Environmental Constraints

An anemometer system must conform to the requirements and standards detailed in "General Specifications for Procurement of Electronic Equipment" , DFS 1000 (TP 3131).

Further, any operating equipment must not interfere with other airport/aircraft equipment. Table 2.1 supplied by Aviation Group of Transport Canada: Facility Engineering Systems Development Branch, presents the equipments and their respective frequency bands of operation. Also, any installed airport equipment must conform to zoning requirements as detailed in the Transport Canada publication T.P.1247 "Land Use in the Vicinity of Airports".

TABLE 2.1: OPERATIONAL EQUIPMENT

9 - 14 kHz	Omega
90 - 110 kHz	Loran-C
190 - 1750 kHz	Automatic Direction Finder (ADF)
2850 - 3025 kHz	H.F. Air Ground Communications
3400 - 3500 kHz	H.F. Air Ground Communications
4650 - 4700 kHz	H.F. Air Ground Communications
5450 - 5680 kHz	H.F. Air Ground Communications
6525 - 6685 kHz	H.F. Air Ground Communications
8815 - 8965 kHz	H.F. Air Ground Communications
10005 - 10100 kHz	H.F. Air Ground Communications
11275 - 11400 kHz	H.F. Air Ground Communications
13260 - 13560 kHz	H.F. Air Ground Communications
17900 - 17970 kHz	H.F. Air Ground Communications
75 MHz	ILS - Marker Beacon
108 - 118 MHz	ILS - Localizer, VOR
118 - 137 MHz	VHF Air Ground Communications
121.5 MHz, 243 MHz	ELT
328.6 - 335.6 MHz	ILS - Glide Path
406 - 406.1 MHz	Possible new band for ELT
890 - 902 MHz	Airphone - airborne telephone
942 - 960 MHz	Airphone - airborne telephone
960 - 1215 MHz	DME, TACAN
1030 MHz, Rx; 1090 MHz Tx	SSR Transponder
1215 - 1240 MHz	Future Band for Navstar Satellite System
1250 - 1350 MHz	Ground Based Primary Radar
1545 - 1559 MHz	Future Aeronautical Mobile Satellite (space to earth)
1559 - 1610 MHz	Future band for Navstar Satellite System
1610 - 1626.5 MHz	Proposed for Radio Determination Satellite System (earth to space)
1646.5 - 1660.5 MHz	Future Aeronautical Mobile Satellite (earth to space)
2483.5 - 2500 MHz	Proposed for Radio Determination Satellite System (space to earth)
2700 - 2850 MHz	Ground Based Primary Radar
4200 - 4400 MHz	Radio Altimeter
5030 - 5090.7 MHz	MLS
5350 - 5460 MHz	Airborne Weather Radar
8750 - 8850 MHz	Airborne Doppler Navigator
9300 - 9500 MHz	Airborne Weather Radar
13.25 - 13.4 GHz	Airborne Doppler Navigator
15.4 - 15.7 GHz	National MLS
15.7 - 16.6 GHz	Ground Based Airport Surface Detection Equipment
24.25 - 25.25 GHz	Ground Based Airport Surface Detection Equipment

2.4 Technology Risk

The anemometer systems described in the previous section do not require new technology. The sensors required are anemometers and possibly microbarographs, the system will also require a basic computer to carry out integration of sensor data. Data rates are slow and can be handled with most commercially available microcomputers. The algorithms need development and fine tuning. There is little risk in this area and much can be learnt from the work done by F. Wesley Wilson, J and John A. Flueck at NCAR, Boulder, Colorado.

2.5 Cost

The cost of the total installation of these systems is primarily dependent on the number of sensors used. For a sensor system a total cost of between $500K to $750K is expected which includes algorithm development work.

3.0 RADAR SYSTEM

The second sensor technology is radar or more precisely groundbased Doppler radar. There is a significant amount of evidence to demonstrate that Doppler radar can reliably detect and give early warning to both large and small scale wind shear events. The most recent data coming from the pulse Doppler TDWR radar system under test at Stapleton International airport. This radar can provide many products including detection of gust fronts, thunderstorms, macrobursts and microbursts.

The aim of this subsection is not to reiterate the rationale for using Doppler radar as a wind shear detection system in the U.S., this is discussed in Part B of the report, rather to try and address some of the following issues:

- Is Doppler radar a suitable sensor for the detection of wind shear in and around Canadian airports?
- If suitable, what is the radar design and what information could it provide?
- What are the technical risks associated with the development of such radar?
- What is the total cost of the radar?

These issues will now be addressed in turn and form the remainder of the text for Part C of this report.

3.1 Canadian Doppler Radar

A Doppler radar which possesses suitable characteristics will detect wind shear events in and around Canadian airports. The general key characteristics the radar requires are as follows:

- Coherence
  - ideally fully coherent
  - coherent-on-receive as a minimum
- Fine Resolution
  - spatial (range and angle)
  - spectral (Doppler)

- o Low Antenna Sidelobes
- o Coverage
  - azimuth
  - elevation (small angles)
- o Tuned Algorithms
  - optimized for different wind shears
  - adjusted to local conditions
- o User Interface
  - friendly

All of these characteristics are realizable and can be implemented into several radar concepts or configurations.

3.1.1 Options

There are a number of options for the Doppler radar configuration and include:

a) Existing radar e.g. TDWR.

b) Modified radar e.g. enhanced version of the King city radar.

c) New radar - design from scratch.

All of these configurations have merit and deserve further consideration.

The use of TDWR is appealing because the technical risk is reduced since much of the development has already been carried out. Note however, TDWR is not optimized to wind shear detection close to the airport and it is required to perform many other weather data functions. In this respect, TDWR may be more sophisticated, and therefore more costly, than necessary to fulfill a different set of requirements, such as those for Canada. Reduced sophistication or complexity can be achieved by assessing the specific Canadian requirement and designing a new radar. A new design offers many desirable features, but technical risk is very high for a completely new radar. Also, it must not be forgotten that any radar, new or existing, designed to produce automatic detection and recognition must employ locally tuned software which will be extremely costly, perhaps half the price of the total radar system.

The current estimated cost for TDWR is $5M Cdn.

In many respects a modified "King City" radar may be a good compromise solution in the short term. Currently, an installation similar to that used at by Atmospheric and Environmental Services (AES), Ontario, King City would cost $700K Cdn. but it has limitations particularly with regards to detecting microbursts. Enterprise Electronics of Alabama, who supplied the AES radar, can readily supply modified versions which would be better suited to the Canadian requirements, for example, a short range version. This version would have 75m range resolution over a 17 km range, ideal for microburst detection. The radar signal processing of this system is no different to that employed at King city i.e. same number of range bins.

On the debit side, the Enterprise radars at 5cm (C-band) wavelengths are partially coherent resulting in unwanted levels of phase noise - typically 5 times that of a klystron. However, Enterprise estimates a 1-2 year development cycle for a C-band Klystron with a final radar system cost of $1.4-2m Cdn.

Opinion is varied on phase noise and its effect on wind shear detection. Compared to a partially coherent radar, a fully coherent radar will better represent the Doppler signature and offer higher signal to noise ratios of received echoes. The degree of coherency required for a radar operating in the shorter range Canadian context has not been addressed and needs investigation.

3.1.2 Technical & Environmental Constraints

The radar options discussed in this report operate or would operate at C-Band. Specifically, TDWR operates between 5.60 and 5.65 GHz as does the AES radar made by Enterprise Electronics Corporation.

Inspection of Table 3.1, presenting operating frequency bands for operational airport equipments, reveals that a radar could operate in the frequency ranges 5.2 - 5.25 GHz and 5.6 to 5.65 GHz for example without interfering with other airport equipments and other things in the area; this needs to be confirmed. Also, any installed equipment must conform to zoning requirements as detailed in the transport Canada publication T.P. 1247 "Land Use in the Vicinity of Airports".

TABLE 3.1: OPERATIONAL EQUIPMENT

9 - 14 kHz	Omega	
90 - 110 kHz	Loran-C	
190 - 1750 kHz	Automatic Direction Finder (ADF)	
2850 - 3025 kHz	H.F. Air Ground Communications	
3400 - 3500 kHz	H.F. Air Ground Communications	
4650 - 4700 kHz	H.F. Air Ground Communications	
5450 - 5680 kHz	H.F. Air Ground Communications	
6525 - 6685 kHz	H.F. Air Ground Communications	
8815 - 8965 kHz	H.F. Air Ground Communications	
10005 - 10100 kHz	H.F. Air Ground Communications	
11275 - 11400 kHz	H.F. Air Ground Communications	
13260 - 13560 kHz	H.F. Air Ground Communications	
17900 - 17970 kHz	H.F. Air Ground Communications	
75 MHz	ILS - Marker Beacon	
108 - 118 MHz	ILS - Localizer, VOR	
118 - 137 MHz	VHF Air Ground Communications	
121.5 MHz, 243 MHz	ELT	
328.6 - 335.6 MHz	ILS - Glide Path	
406 - 406.1 MHz	Possible new band for ELT	
890 - 902 MHz	Airphone - airborne telephone	
942 - 960 MHz	Airphone - airborne telephone	
960 - 1215 MHz	DME, TACAN	
1030 MHz, Rx; 1090 MHz Tx	SSR Transponder	
1215 - 1240 MHz	Future Band for Navstar Satellite System	
1250 - 1350 MHz	Ground Based Primary Radar	
1545 - 1559 MHz	Future Aeronautical Mobile Satellite (space to earth)	
1559 - 1610 MHz	Future band for Navstar Satellite System	
1610 - 1626.5 MHz	Proposed for Radio Determination Satellite System (earth to space)	
1646.5 - 1660.5 MHz	Future Aeronautical Mobile Satellite (earth to space)	
2483.5 - 2500 MHz	Proposed for Radio Determination Satellite System (space to earth)	
2700 - 2850 MHz	Ground Based Primary Radar	
4200 - 4400 MHz	Radio Altimeter	
5030 - 5090.7 MHz	MLS	Possible
5350 - 5460 MHz	Airborne Weather Radar	allocations
8750 - 8850 MHz	Airborne Doppler Navigator	for windshear
9300 - 9500 MHz	Airborne Weather Radar	radar
13.25 - 13.4 GHz	Airborne Doppler Navigator	
15.4 - 15.7 GHz	National MLS	
15.7 - 16.6 GHz	Ground Based Airport Surface Detection Equipment	
24.25 - 25.25 GHz	Ground Based Airport Surface Detection Equipment	

3.2 Doppler Summary For Risks and Costs

For ease of presentation, risks and order of magnitude costs for the recommended Doppler technology are given in the Table below.

Radar Option	Technical Risk	Cost	Figure of Merit*
TDWR	Low for radar hardware	High $5M Cdn	4
Enterprise - modified[3] - revised[2] - existing[1]	 Medium Very low Very low	Low $2M Cdn $1M Cdn $1M Cdn	 3 1 2
New design	High	High	5

* A low Figure of Merit represents a preferred option.

1: As per current King City installation.
2: As per 1 with optimized range.
3: As per 2 with fully coherent source.

The figure of merit is traded by that information supplied in the table and radar performance expectations such as spectral purity.

The costs are based on figures supplied by Enterprise Electronics and the TDWR Project Office. Spar does not commit to build or supply these radars at the quoted prices.

PART D

RECOMMENDATIONS

THIS PAGE INTENTIONALLY LEFT BLANK

PART D: RECOMMENDATIONS

Two systems are recommended for a low-level wind shear detection system: the first an anemometer system suitable for low traffic airports; the second a radar with an anemometer system for a high density traffic airport e.g., Toronto.

The radar provides long range detection and warning but is more expensive. Of that expense approximately 50% could be for the purchase of the equipment and the remainder on software development and testing.

Different software will be required for the various wind shear phenomena and in particular, software for microburst detection requires detailed attention. At present, microburst detection and recognition can only be reliably provided by meteorologists, clearly in an operational system an automatic process is required.

To achieve robust automatic recognition of low-altitude wind shear, much work is required on pattern recognition. The fundamental pre-requisite for the development of pattern recognition techniques is real data. For it to be applicable it must be representative of the weather phenomenon in Canada.

This need, of course, brings us to the nub of the wind shear question:

> Is there Canadian wind shear data to measure? or, more generally, "Do wind shear events such as microbursts occur in and around Canadian airports"? It is a fact, that no major incidents have been attributed to microbursts concerning large commercial aircraft in Canada, but how long will this remain to be true? It is recommended that a planned measurement program be undertaken as soon as possible to try and quantify the risks. The type and scope of this program needs to be defined at the earliest possible time.

Measurement Program

The detailed objectives, schedule, implementation and cost for a measurement program is beyond the scope of this study. However, the major objectives of the program must be to answer some of the most fundamental questions concerning microbursts in Canada.

- Do they occur? and if so
- What is the likelihood of their occurrence at Canadian airports?

RECOMMENDATIONS (cont'd)

Measurement Program (continued)

Assuming they occur:

- What are the processes involved in the initiation of microbursts?
- What is their fine structure?
- How applicable are the Stapleton results to Canada?
- What are their physical and occurrence differences across Canada?

To answer these and other questions there is an overwhelming need for Doppler radar measurements. Doppler radar is an essential, although not the sole component of the wind shear measurement system. It is a fact that it can detect both large and small scale wind shear events.

Two locations for a measurement program could form the kernel of a future program. The Atmospheric and Environment Service facility at King City near Toronto could be one location, utilizing the existing radar equipment. It is expected that for microburst detection the radar software would need to be modified to provide finer range resolution (~75m). This radar is not fully coherent and may prevent the detection of some microburst activity - as yet this is unknown and needs study. Such a study should be carried out as soon as possible in collaboration with AES.

A new facility could be set up at or close to Calgary airport. Being a new facility a fully coherent radar would be preferred for ensuring the best possible target sensitivity. The choice of Calgary is commensurate with the Alberta maximum for the incidence of tornadoes which are suspected to having some relationship to microburst activity. Further the experience of the Alberta Hail project suggests that microbursts occur in central and southern Alberta.

If, and we strongly recommend it, a measurement program is initialized, the data and wealth of knowledge residing in the U.S. much not be ignored. Indeed it should be reviewed further to see how it can complement a Canadian measurement program. Also expertise should be built up in Canada on developing software for the recognition of wind shear, particularly microbursts. This is important since conditions from one airport to another are not alike and a good understanding of all aspects of the wind shear problem is essential.

RECOMMENDATIONS (cont'd)

Measurement Program (continued)

In conclusion, it is the opinion of the authors that

- microbursts are likely to occur in Canada,
- there is a danger to aviation due to wind shear at Canadian airports,
- pulse Doppler radar will provide detection of wind shear events, particularly microbursts,
- much more information is needed on microbursts in Canada,
- a measurement program is required, using existing or modified facilities at AES King City and/or a new facility in Alberta,
- a follow on stage to the current study is required to define detailed objectives and scope of the measurement program.